OCS Study
BOEM 2012-108

Integrated Bio-Physical Modeling of the Louisiana-Texas (LATEX) Shelf

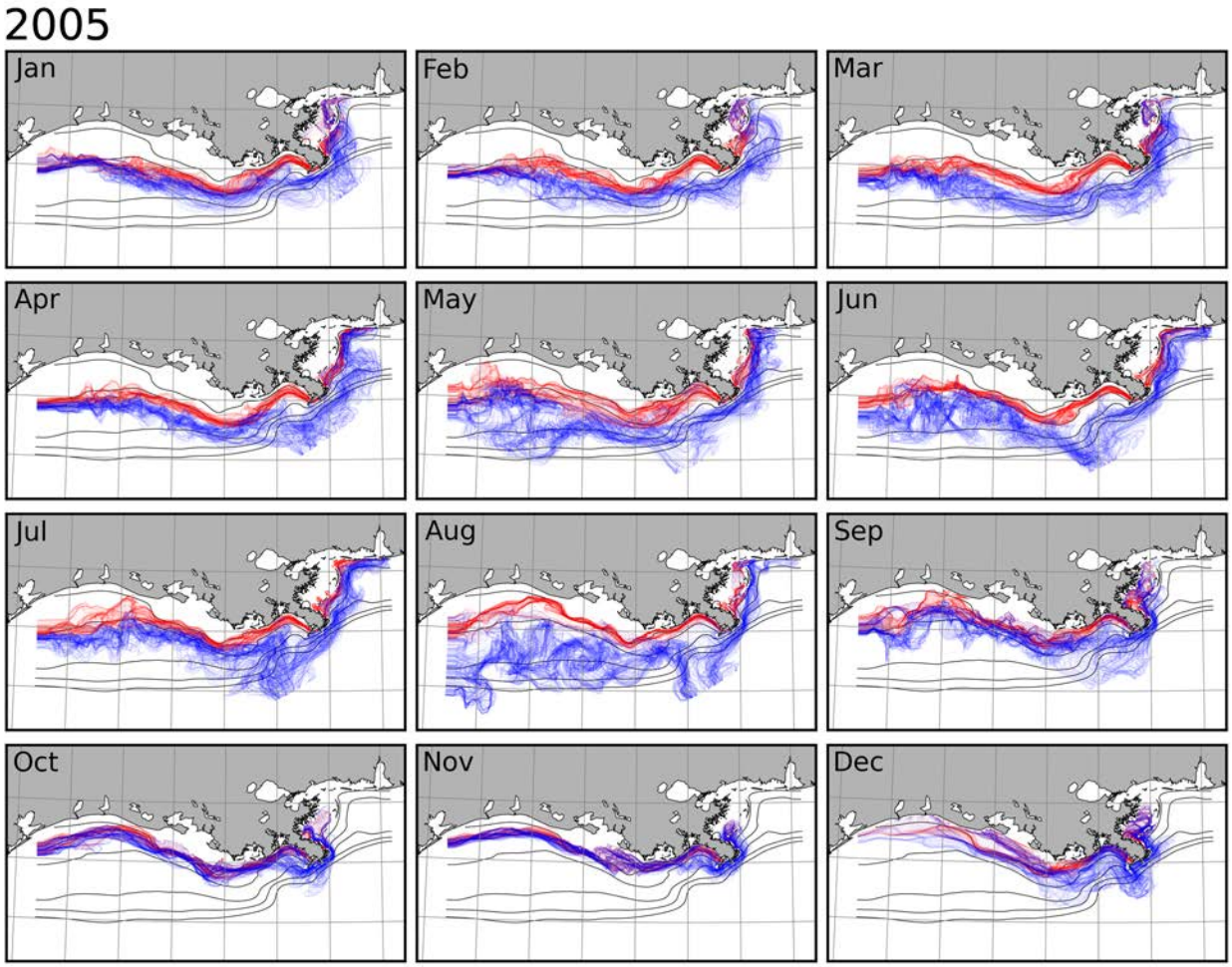

U.S. Department of the Interior
Bureau of Ocean Energy Management
Gulf of Mexico OCS Region

BOEM
Bureau of Ocean Energy Management

OCS Study
BOEM 2012-108

Integrated Bio-Physical Modeling of the Louisiana-Texas (LATEX) Shelf

Authors

R.D. Hetland
K. Fennel
C.K. Harris
J. Kaihatu
K. Xu
S.F. DiMarco

Prepared under BOEM Contract
M07AC12922
by
Texas A&M University
Department of Oceanography
602AA Eller O&M Building
College Station, TX 77843-3146

Published by

U.S. Department of the Interior
Bureau of Ocean Energy Management
Gulf of Mexico OCS Region

New Orleans
December 2012

DISCLAIMER

This report was prepared under contract between the Minerals Management Service (MMS, now the Bureau of Ocean Energy Management [BOEM]) and the Texas A&M Research Foundation. This report has been technically reviewed by BOEM, and it has been approved for publication. Approval does not signify that the contents necessarily reflect the views and policies of BOEM, nor does mention of trade names or commercial products constitute endorsement or recommendation for use. It is, however, exempt from review and compliance with BOEM editorial standards.

REPORT AVAILABILITY

This report is available on CD from the Bureau of Ocean Energy Management, Gulf of Mexico OCS Region, for $15.00, and free of charge as a pdf file downloaded from the BOEM Web site. Copies can also be viewed at selected Federal Depository Libraries. The addresses are listed below.

To order a CD, use the Gulf of Mexico OCS Region contact information below and reference OCS Study BOEM 2012-108. To download a pdf copy, use the Environmental Studies Program Information System (ESPIS) and search on the study report number. In the near future, you will also be able to get this report also from the National Technical Information Service.

U.S. Department of the Interior
Bureau of Ocean Energy Management
Gulf of Mexico OCS Region
Public Information Office (MS 5034)
1201 Elmwood Park Blvd.
New Orleans, Louisiana 70123-2394
Phone: (504) 736-2519, 1-800-200-GULF
Fax: (504) 736-2620

U.S. Department of Commerce
National Technical Information Service
5301 Shawnee Rd.
Springfield, Virginia 22312
Phone: (703) 605-6000, 1-800-553-6847
Fax: (703) 605-6900
Web site: http://www.ntis.gov/

CITATION

Hetland, R.D, K. Fennel, C.K. Harris, J. Kaihatu, K. Xu and S.F. DiMarco, S. **2012**. Integrated bio-physical modeling of Louisiana-Texas (LATEX) Shelf. U.S. Dept. of the Interior, Bureau of Ocean Energy Management Gulf of Mexico OCS Region, New Orleans, LA. OCS Study BOEM 2012-108, 128 pp.

ABOUT THE COVER

The cover illustration shows surface (blue) and bottom (red) contours of the 33 psu isohaline displayed at four-hour intervals for each month in 2005.

ACKNOWLEDGEMENTS

This report would not have been possible without the contributions of several entities who contributed observational data, and numerical output from ocean circulation models. The principal investigators of this study and their responsibilities are:

Program Manager: Dr. Steven F. DiMarco, Department of Oceanography, Texas A&M University;

Lead Physical Modeling: Dr. Robert Hetland, Department of Oceanography, Texas A&M University

Lead Biological Modeling: Dr. Katja Fennel, Dalhousie University;

Lead Sediment Modeling: Dr. Courtney Harris, Virginia Institute for Marine Sciences;

Lead Surface Gravity Wave Modeling: Dr. James M. Kaihatu, Zachry Department of Civil Engineering, Texas A&M University.

We thank Dr. Kehui Xu for his contributions to the sediment modeling element of this investigation. We acknowledge the contributions of Drs. Valeria Kiselkova and Xiaoqian Zhang and Ms. Yang Feng for their efforts in the circulation and biological modeling elements.

We thank the BOEM Contracting Officer's Representative, Dr. Alexis Lugo-Fernandez, for his enthusiasm and guidance, which contributed greatly to this study's success, throughout this investigation.

The Integrated Modeling Team

CONTENTS

LIST OF FIGURES

LIST OF TABLES

1 EXECUTIVE SUMMARY

The Bureau of Ocean Energy Management (BOEM), formerly known as Minerals Management Service (MMS) of the U.S. Department of the Interior funded the "Integrated bio-physical modeling of the Louisiana-Texas (LATEX) Shelf" Study. The contract was awarded to the Texas A&M Research Foundation in July 2007 and the work was performed by scientists at Texas A&M University (TAMU), the Virginia Institute for Marine Science (VIMS), and Dalhousie University (DU). Dr. Steven F. DiMarco was Program Manager; Principal Investigators were Dr. Robert D. Hetland (TAMU), Dr. Katja Fennel (DU), and Dr. Courtney Harris (VIMS). The study objectives were: 1) to produce a realistic coupled physical-biological-geochemical numerical model of the LATEX shelf and runs scenarios of interest to MMS through leveraging with the ongoing NOAA-funded MCH study and 2) to continue and expand the numerical modeling component developed earlier using a realistic high-resolution hydrodynamic model of the region that is driven by local winds and river discharge.

The study substantially leverages an ongoing and concurrent effort by the Principal Investigators that is funded separately by the National Oceanic and Atmospheric Administration, National Ocean Service, Center for Sponsored Coastal Ocean Research.

A realistic numerical simulation of the northern Gulf of Mexico is described. The model contains three components: a hydrodynamic base model, a water column biogeochemical model, and a sediment transport model. Additionally, a surface gravity wave model was implemented to provide input wave properties for sediment transport calculations. The model was integrated from Spring 1992 to 2008, in order to better understand and characterize inter-annual variability. The model resolution is approximately 2 km in the interior of the model domain, with an internal timestep of 20 seconds. As such, the model resolves flow features that are the scale of the deformation radius, and temporal variability from hours to decades. This report discusses in detail the skill of the model at reproducing observed hydrodynamic, biogeochemical and sediment transport phenomena. The model is shown, reliably reproduces large-scale, seasonal circulation and associated biogeochemical distributions. There is considerable noise at smaller spatial scales, approximately 20-50 km, due to an active eddy field along the boundary of the Mississippi/Atchafalaya plume. The model is able to reproduce these features in a statistical sense, but cannot predict the exact details of the flow. Additionally, the coupled hydrodynamic and sediment transport model provides reasonable estimates of sediment dispersal and reworking within a model year representing calendar year 1993, thus laying the groundwork for later coupling of sedimentary and biogeochemical processes.

2 INTRODUCTION

An integrated, multidisciplinary investigation of the physical and biogeochemical processes of the middle and western Louisiana shelf, funded by the National Atmospheric and Oceanic Administration (NOAA) includes shipboard, moored and remote sensing real-time multidisciplinary observations designed to complement a coupled physical-biogeochemical numerical modeling element. This study is entitled *Mechanisms Controlling Hypoxia* (MCH); a project website is maintained at http://hypoxia.tamu.edu. The project was first funded in 2003 to investigators at Texas A&M University (TAMU) and Louisiana State University (LSU). In 2006, the MCH project was refunded to involve eight principal investigators from five institutions: TAMU, TAMU-Galveston, LSU, Virginia Institute of Marine Science (VIMS), and Dalhousie University, Canada. The project was expanded to target process-oriented high spatial resolution hydrographic surveys, multidisciplinary moored observations, and to develop the coupled model to resolve small (order 10 km) temporal and spatial scales of variability of hypoxia on the middle and eastern Louisiana shelf.

In 2007, the Minerals Management Services funded the "Integrated bio-physical modeling of the Louisiana-Texas (LATEX) Shelf" Study to leverage the realistic MCH modeling component of the realistic coupled physical-biological-geochemical numerical model of the LATEX shelf and to simulate scenarios of interest to BOEM.

2.1 BACKGROUND AND PROGRAM OBJECTIVES

In October 2002, the Mississippi River/Gulf of Mexico Watershed Nutrient Task Force (henceforth Task Force) held a monitoring, modeling and research workshop in St. Louis, MO. The report of this workshop (USDOI, GS, 2004), describes a framework for research activities that is expected to provide a sound scientific basis for future management actions. A thrust of the Task Force is to improve the physical, chemical and biological modeling capability to better understand and quantify the rates of the particular processes that contribute to hypoxia. During MCH, we developed a three-dimensional circulation model of the Louisiana-Texas continental shelf based on the Regional Ocean Modeling System (ROMS).

This NOAA-funded study extended the canonical ideas about the processes creating and controlling hypoxia on the Louisiana-Texas continental shelf. We believe that in locations where hypoxia is most variable (west of Terrebonne Bay) processes controlling hypoxia are sensitive to local winds, shelf-scale circulation features, and benthic biogeochemical processes in addition to inputs of nutrients and fresh water.

Basic numerical experiments illustrate the importance of the location of respiration in determining the vertical structure of oxygen in the water column (Hetland and DiMarco 2008). A tracer representing oxygen was added to the basic physical model. Oxygen was initialized using saturated values (in turn dependent on the local temperature and salinity), and saturation concentrations were maintained at the surface and for the inflowing river water, while being nudged toward saturation along the open boundaries.

Two types of respiration were then applied that reduced the oxygen in the model. First, benthic respiration was applied, based on measurements by Rowe et al. (2002). Second, respiration was applied throughout the water column, higher where surface salinities were lower. The second scenario was based on the idea that the organic material necessary for respiration, and ultimately hypoxia, is highest near the fresh water sources due to enhanced nitrogen introduced to the coastal ocean through the river water. Both cases created hypoxic conditions within the model. Water column respiration produced hypoxia east of Terrebonne Bay, where hypoxia is observed often. Benthic respiration produced hypoxia west of Terrebonne Bay, where the presence of seasonal hypoxia is more sporadic. Comparisons with vertical profiles of oxygen in this region confirm that benthic respiration appears to be the driving factor controlling the western limb of seasonal hypoxia.

There have been a variety of studies investigating hypoxia that use simple box models (e.g., Justic et al. 2002, Scavia et al. 2003). While simple box models are common in work on rivers, it is not clear how they relate to the dynamics of the buoyant river plume; for instance, neither the changing dimensions of the plume itself nor wind forcing were included in the model. Thus, we believe that the results of these studies are limited. *The need for a more realistic model incorporating local forcing functions was specifically recommended by Brezonik et al.* (1999). Our ROMS model provides three-dimensional capability that can follow changes in local forcing functions.

2.2 OBJECTIVES

The objectives of the study are:

1. To produce a realistic, coupled physical-biological-geochemical numerical model of the LATEX shelf and run scenarios of interest to BOEM through leveraging with the ongoing NOAA-funded MCH study.
2. To continue and expand the numerical modeling component developed earlier using a realistic high-resolution hydrodynamic model of the region that is driven by local winds and river discharge. The physical model is currently coupled to a NPZ-type biological component, however, this component was substantially enhanced and a new sediment component added.

Several activities were identified to achieve these goals. These activities are divided into physical, biological, and sediment modeling components. Tasks are then identified to gauge the study's progress.

Through analysis of the MCHI-developed coupled biological-physical circulation model using parameterized respiration we developed a number of intriguing hypotheses that need to be tested further using more advanced models, that include biogeochemistry and sediments. For example, an implicit assumption in the parameterized respiration model is that there is ample organic material present for the parameterized respiration to occur. Preliminary numerical

simulations using an NPZD (nitrogen, phytoplankton, zooplankton, detritus) model suggest that, although surface fields are quite patchy (i.e., phytoplankton is very abundant near the river mouths), the near-bottom detritus field is relatively continuous, and supplies the shelf inshore of 50 m depth with organic material.

Physical modeling focused on improving weather-band and seasonal scale model skill by enhancing the numerical setup of the model, forcing and boundary information, and data assimilation. The largest numerical errors are due to strong advection near the Southwest Pass outflow of the Mississippi River Delta and parameterizations of turbulent mixing. Examining different numerical algorithms and comparing these to observations improved these aspects of the model. Hetland has performed similar model analysis in simulations of the Gulf of Maine (Hetland and Signell, 2005).

The primary goal of the *biological component* of the modeling study was to identify the contributions of various factors (e.g., nitrogen loads, biogeochemical feedbacks, climatic and hydrographic conditions) to biogeochemical processes through the inclusion of a nitrogen-based biological module for the water column. An NPZD-type biological model was implemented in ROMS (Fennel et al. 2006). It included nitrate, ammonium, small and large particle detrital pools, phytoplankton, chlorophyll, and zooplankton. This model configuration captured the spatial and temporal patterns in chlorophyll dynamics and primary production on the North Atlantic east coast shelves (Fennel et al. 2006). Denitrification in the water column under low DO conditions depends on the concentrations of organic matter and nitrate. The biogeochemical model parameters were defined based on rate measurements performed in this and other ongoing projects and published measurements. In addition to nitrate concentration, phosphate concentration was included as a target modeling parameter.

Consistent temporal and spatial distribution of the measurements of fluxes into and out of the sediments allows a comparison of the input of organics into the traps, the response of SCOC, the concurrent regeneration of inorganic nutrients back into the water column, and the response of these exchanges to variations in oxygen and temperature. The variation in oxygen consumption and the re-supply of nutrients are important variables in the model. Original (e.g., NECOP) versions considered the bottom a simple boundary with a constant or zero order flux of oxygen out of the water and a constant return of N from the sediments into the bottom water. This gross over simplification is now being replaced with second-order equations that define what the rates might be in response to POC input or under different oxygen states and temperature. SCOC ranged from 2 to 4 mmoles $m^{-2} \cdot d^{-1}$ in August 2004 to 4 to 10 mmoles $m^{-2} \cdot d^{-1}$ in April 2004, suggesting that the sediment system had either run out of energy, carbon, etc., by late summer, or that respiration was inhibited by low oxygen conditions, sulfide, etc. Production rates were on the order of 30 mg C m^{-2} d^{-1} in late summer and about 100 mg C $m^{-2} \cdot d^{-1}$ in the spring. The mean POC flux rates measured into traps were approximately 500 to 600 mg C $m^{-2} \cdot d^{-1}$, i.e., much larger than production would indicate. The difference could be attributed to sulfate reduction at depth in the sediments (Rowe et al. 2002), which is likely the case here when oxygen is not available to oxidize the sulfide produced, but it does not explain the disparity when oxygen is available, as in the April rates. The metazoan biota, in the samples analyzed to date, is of low density, biomass and diversity consistently throughout the study area and time periods, with little

evidence of recovery during the winter but never totally destroyed during long periods of hypoxia.

Suspended sediment impacts regional euphotic layer biological processes by limiting light penetration and redistributing sediment-associated nutrients, and benthic processes by interacting with seabed sediments and the associated geochemical constituents. Both resuspension from the seafloor and input of new sediment are important in this region. The resuspension signal dominates away from the river plumes, but advected fluvial material may be important for light limitation. Therefore, a sediment transport element was added to the LATEX model. A set of open-source routines developed for ROMS that estimate sediment transport rates and erosion and deposition (see Warner et al., 2008) was developed and added. Noncohesive (sands) and cohesive (muds) sediment transport modules within ROMS have been applied to study dispersal of fluvial sediment within the Adriatic Sea (see Bever et al. 2009, Harris et al. 2008), and within the Hudson River Estuary (Warner et al. 2005). ROMS also includes bottom boundary representations that account for shear stress by combined wave-and-current flows (e.g., Styles and Glenn, 2000), particularly important for sites within the study area where energetic waves influence resuspension.

Model calculations of suspended sediment concentration and sediment flux will be linked to geochemical and biological models. To this end, a dynamic sediment model is being formulated to account for accumulation and remineralization of organic matter at the bottom and allows organic matter to be resuspended by bottom boundary layer shear associated with storms or upwelling jets. Benthic grazing losses will be imposed. An attractive feature of ROMS is the model's ability to track Lagrangian particles. This feature enables us to map the 3D paths of a large number of particles and their biogeochemical modifications helping us to identify the origin of the organic material that is oxidized in the oxygen minimum zones.

A number of process-oriented hindcast simulations were performed that focus on 1) understanding the complex interactions between nitrogen inputs and cycling, and organic matter transport in affecting bottom DO conditions, and 2) improving our biogeochemical model formulation. This process-oriented stage is followed by a set of hindcast simulations and scenarios in which we will 1) determine the current spatial and temporal extent of hypoxia, 2) forecast changes through a range of possible scenarios, and 3) assess the feasibility to nowcast/forecast DO conditions and quantify the model's uncertainty. Specifically, the process-oriented hindcast simulations indicate the degree to which our model reproduced the observed spatial distribution of the hypoxia/anoxia centers. They also helped us to investigate the relative importance of advective import versus local production of POC.

Based on these validated hindcasts we simulated scenarios where forcing conditions and internal model features were varied in a systematic way to quantify the sensitivity of bottom DO. In particular, we assessed the effects of 1) changes in nitrogen loading from both point and non-point sources, 2) variability in physical forcing and hydrographic conditions, and 3) model parameters and parameterizations.

Guiding questions for this investigation were: How will a *reduction or increase* in nitrogen load affect primary production, nitrogen cycling, and bottom DO? Do the effects differ for non-

point and point sources of nitrogen? How does the presence/absence of benthic suspension feeders affect primary production and bottom DO? Does the pre-conditioning of the system with a larger than average spring bloom (with higher accumulation of POC at the bottom that can be resuspended) determine the outcome in terms of bottom DO? Is the aggregation of particles crucial for export of POC below the pycnocline and bottom DO depletion? Will an increase in thermal stratification that can be anticipated due to global warming lead to more severe depletion in bottom DO?

This study has improved our understanding of the linkages between physical and biogeochemical processes on the shelf. The model proposed here includes both riverine and atmospheric forcing. Based on fundamental physical and biogeochemical processes, our model, therefore, promises to provide better predictive ability than a purely statistical model under unusual forcing conditions.

2.3 STUDY TASKS

Using coupled existing numerical models; the following tasks were assigned:

Task 1. Develop 3-D maps of hindcast hypoxia region depicting aerial and vertical extent at a frequency of 4 maps per months or weekly to capture temporal evolution during the hypoxia season.

Task 2. Use the model to estimate the dispersion/transport of material released at the Flower Garden Banks 7 days after the August full moon or closest to this date; and from 3 selected oil and gas platforms provided by the MMS for a period of 30 days for the four seasons of the year.

Task 3. Use the model to produced monthly maps of the 30-33 PSU water mass in 3-D.

Task 4. Use the model to produced monthly maps of suspended particulate matter (SPM) associated with the 30-33 PSU water mass.

Task 5. Provide to MMS in printed and digital format the numerical model hindcast results and fields after completion of the **Tasks 1-4**.

2.4 STUDY PRODUCTS

Based on the above tasks, the following study products were assembled for this project:

1. Maps of the hindcast hypoxia region depicting aerial and vertical extent at a frequency of 4 maps per months or weekly to capture temporal evolution during the hypoxia season (shown in Appendix A)
2. Tracking dispersion/transport of material from the Flower Garden Banks 30 days after each day in August for each of the physical simulation years (shown in Appendix B)
3. Monthly maps of depth average suspended particulate matter (shown in Appendix C)

4. Monthly maps of the surface and bottom 33 PSU isohaline (shown in Appendix D)

2.5 REPORT ORGANIZATION

Section 3 presents descriptions of the circulation of the Louisiana-Texas shelf and the configuration of the hydrodynamical, wave, water column biogeochemical, and sediment transport models. Section 4 presents results of the numerical simulations from the model years 1990 to 2008, model skill assessment, biogeochemical simulations, sediment and wave model output and observation comparison, case studies of the 1993 Storm of the Century and Fairweather conditions, physical and sediment controls on hypoxia. Section 5 briefly describes of the study conclusions. The Appendix contains monthly horizontal plan view maps of the 33 psu isohaline for the years 1992–2007. A digital appendix accompanying this report contains animations of surface and bottom salinity fields, bottom dissolved oxygen fields, surface nitrate concentration fields, and surface chlorophyll concentrations for the years 1992—2007.

3 DESCRIPTION OF CIRCULATION AND NUMERICAL MODEL

This chapter consists of a brief introduction to the circulation on the Louisiana-Texas continental shelf, and a detailed description of the numerical model configuration.

3.1 CIRCULATION ON THE LOUISIANA-TEXAS CONTINENTAL SHELF

Variability in circulation on the Louisiana-Texas continental shelf is dominated by two controlling factors: the fresh water introduced to the shelf by the Mississippi and Atchafalaya Rivers, and by changes in the seasonal wind-stress patterns. These two factors interact such that the fresh water tends to pool over the shelf in summer, and flow downcoast (southwestward) along Texas toward Mexico. As discussed in more detail below, the water over the Louisiana-Texas shelf tends to be more stratified in summer than during the rest of the year. These circulation patterns have been observed previously (Cochrane and Kelly 1986, Cho et al. 1998, Nowlin et al. 2005). However, these studies have focused primarily on relating the flow to regional wind forcing. The model described here allows us to start to examine the combination of buoyancy forcing from the rivers, and how that is modulated by differences in seasonal wind patterns.

3.2 HYDRODYNAMIC MODEL CONFIGURATION

The Regional Ocean Modeling System (ROMS, Shchepetkin and McWilliams, 2005) was configured for a domain covering the Louisiana-Texas continental shelf from approximately Port Arthur, TX, to Mobile, AL, and extending from the coast to just past the shelf break. The domain and topography are shown in Figure 1. The model is configured to use fourth-order horizontal advection of tracers, third-order upwind advection of momentum, conservative splines to calculate vertical gradients, and Mellor and Yamada (1974) turbulence closure with the Galperin et al. (1988) stability functions. The model had a higher horizontal resolution of slightly greater than 1 km near the inner shelf and a relatively lower resolution (up to ~20 km) on the southern boundary in the deep sea. Twenty layers were stretched on an s-coordinate vertical grid to have a higher resolution near the water surface and sea-bed. Water depths resolved by the model ranged from a minimum of 5 m to a maximum of 410 m.

The model is initialized on February 1, 1991, with an averaged climatological profile of temperature and salinity, horizontally uniform, based on historical hydrographic surveys. Monthly climatologies based on the same hydrographic surveys are also used to provide information on the open boundaries during the simulation. The climatological profiles were modified slightly by clipping the salinity values to be no fresher than 36.0 g kg^{-1}, and were applied as boundary conditions for the model in order to maintain oceanic salinity values for inflows at the open boundaries. The monthly climatology contains the signal of freshwater from the two large rivers within the domain being exported from the shelf, and as such represents *outgoing* information with regard to the model boundary conditions. The boundary conditions

should represent the *incoming* information of offshore oceanic conditions during the periods when offshore information is flowing into the domain, and thus should not contain the fresh water signal from the two river plumes. Finally, the unmodified monthly climatology was also used as a reference when calculating model skill. We note that simulations were run using both the clipped and unclipped versions of the climatology, and model skill increased when using the clipped climatological boundary conditions.

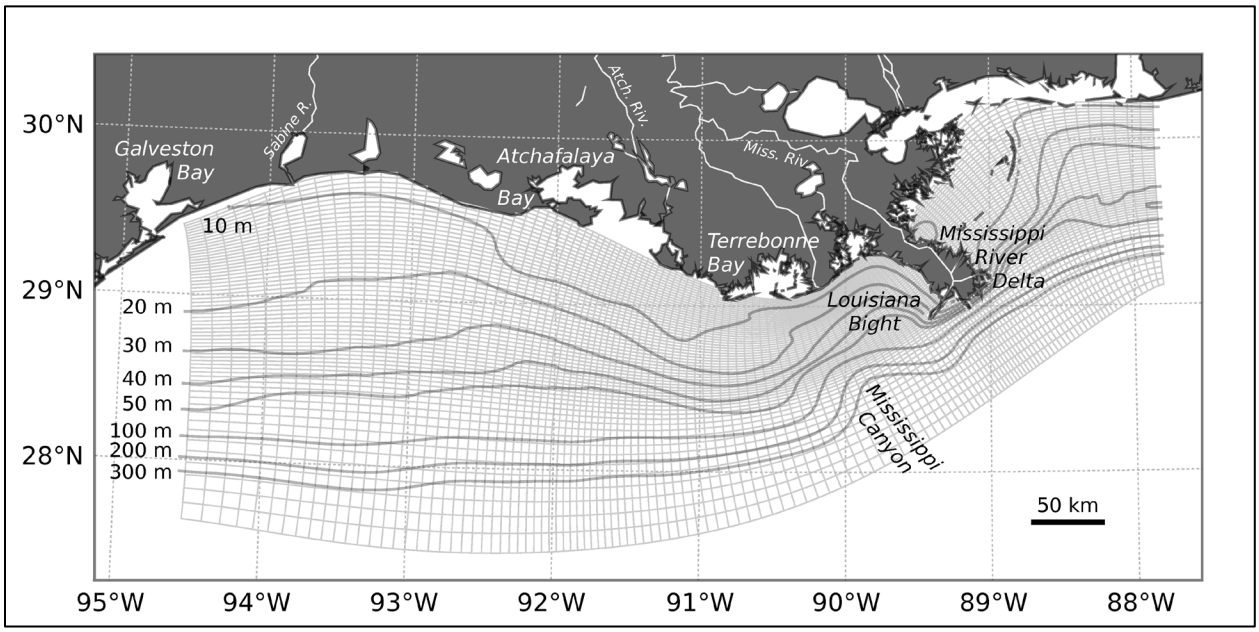

Figure 1: Model grid, showing grid resolution, model bathymetry, and notable features.

The temperature and salinity boundary conditions use an adaptive nudging technique (Marchesiello et al., 2001); tracers are relaxed to the horizontally uniform monthly climatology throughout the integration with a timescale of ten days for outgoing information, one day for incoming information. The western boundary (downcoast, in the direction of Kelvin wave propagation), however, uses no-gradient conditions for three-dimensional velocity and tracer information. This allows information to leave the domain with little impedance. The other open boundaries use radiation conditions are used for the three-dimensional velocities and tracers. A Flather (1976) condition with no mean barotropic background flow is used for the two-dimensional velocities and free surface at all open boundaries.

The model is forced with spatially uniform but temporally varying winds, measured every three hours at the BURL 1 C-MAN weather station (28˚54'18"N~89˚25'42"W), near the mouth of Southwest Pass, (the major pass of the Mississippi Delta). This is appropriate given the spatial and temporal scales of the local wind field (Wang et al, 1998). Data gaps were filled using neighboring buoys (first station 42040 located at 29˚12'19" N 88˚12'19" W, then station 42007 located at 30˚5'25" N 88˚46'7" W). Fresh water inputs from the Mississippi and Atchafalaya rivers are specified using daily measurements of Mississippi River Transport at Tarbert Landing by the U.S. Army Corps of Engineers. Surface heat and fresh water fluxes are

specified using climatological measurements (da Silva et al., 1994a, b). Tides were not included, but are known to be small in the region (DiMarco and Reid, 1998).

3.3 WAVE MODELING

The wave model SWAN (Booij et al. 1999) was used to estimate the wave generation and transformation for the Gulf of Mexico and the shelf-wide LATEX region. Two grids were used for the model (see Figure 2). A grid with 2 min. resolution was used for the Gulf of Mexico region, spanning 80°W-98°W and 18°N – 30.5°N. The higher resolution grid was located over the LATEX region, and spanned 87.5°W – 95°W and 27°N – 30.5°N with a resolution of 15 seconds. Bathymetric data for both regions were taken from the National Geophysical Data Center. All waves were assumed to be generated within the Gulf of Mexico; incoming swell propagating through the Straits of Florida and the Yucatan Channel were assumed to be negligible.

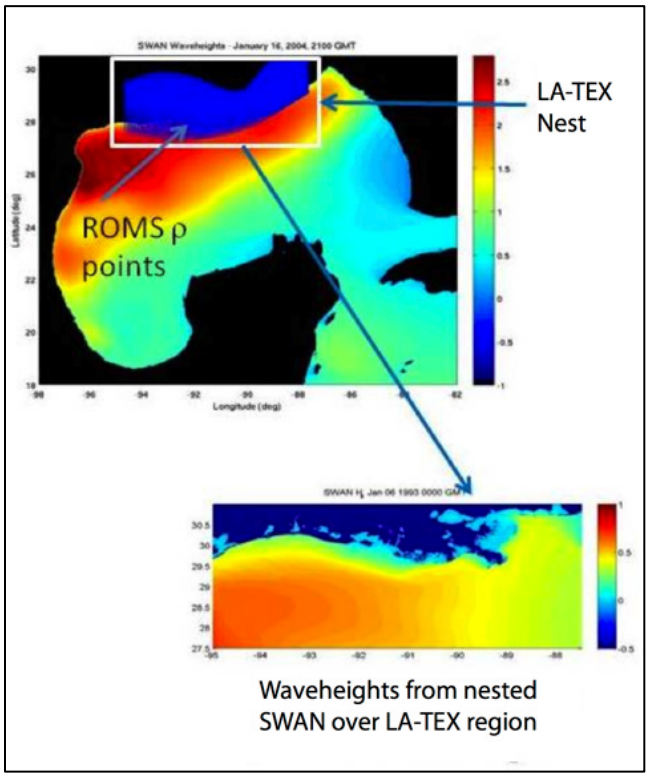

Figure 2: The model grid used for the SWAN model covers the entire Gulf of Mexico, with a nested region over the Louisiana-Texas continental shelf used for forcing the ROMS hydrodynamic model.

Wind data used for the Gulf of Mexico simulations came from the forty-year reanalysis database developed by National Centers for Environmental Prediction (NCEP) and the National Center for Atmospheric Research (NCAR). The 10 meter level winds were used, which was input directly into the SWAN model. These winds had a resolution of 1.875°W by 1.905°N. Wind data for the LATEX simulations were identical to those used for the hydrodynamic model, i.e. taken from the National Data Buoy Center (NDBC) wind measurement station at Southwest Pass, LA, and assumed to be spatial homogeneous for the nearshore domain.

The Gulf SWAN model was run in nonstationary mode with a one-hour time step. Information, in the form of wave spectra, was saved along the boundaries of the inner grid. The LATEX SWAN model was then run, also with a one hour time step, and output saved on the grid points for the coupled circulation/sediment transport model. This output included hourly information on significant wave height, mean wave direction, peak period, root-mean-square value of the maximum bottom orbital velocity, and mean wavelength. The model was run for calendar year 1993 for initial integration with the sediment transport model (Section 2.4). The model will be integrated from 1990 to near present later in the course of the project.

3.4 WATER COLUMN BIOGEOCHEMICAL MODEL CONFIGURATION

The biogeochemical component of our model uses the nitrogen cycle model described in Fennel et al. (2006), but was extended by including dissolved oxygen as a state variable and a parameterization of the air-sea flux of oxygen as described below. The nitrogen cycle model is a relatively simple representation that includes two species of dissolved inorganic nitrogen (nitrate (*NO3)*, and ammonium, (*NH4*)), one functional phytoplankton group, *Phy*, chlorophyll as a separate state variable, *Chl*, to allow for photoacclimation, one functional zooplankton group, *Zoo*, and two pools of detritus representing large, fast-sinking particles, *LDet*, and suspended, small particles, *SDet*. The representation of nitrogen cycling in the water column is similar to other coupled models (e.g., Oschlies 2001; Gruber et al., 2006); however, the model's treatment of sediment remineralization, which is critical for model application to continental shelf regions, is unusual.

The model uses an empirical parameterization of sediment denitrification. Specifically, organic matter that reaches the sediment is remineralized in fixed proportions through aerobic and anaerobic remineralization. The fractions are determined using the linear relationship between sediment denitrification and oxygen consumption that Seitzinger and Giblin (1996; their Figure 1) calculated for a compilation of published measurements (note that their relationship includes production of N_2 gas through anammox; the term denitrification is used here to denote canonical denitrification sensu Devol (2008) and includes all processes that produce N_2 gas). This empirical relationship was based on fifty data points. Fennel et al. (2009) compiled a larger data set including 648 data points across a range of aquatic environments, including from the coastal Gulf of Mexico, and reevaluated the linear regression. This new relationship deviates little from the previously published one, although the coefficient of determination for the larger data set is smaller than that of Seitzinger and Giblin (1996).

The details of the nitrogen formulation are given in Fennel et al. (2006) and are not repeated here for the sake of brevity, except for minor modifications of the aerobic remineralization and nitrification terms in order to account for low or missing availability of oxygen.

The new model equation describing the biochemical dynamics of oxygen, *Ox*, is

$$\frac{\partial Ox}{\partial t} = \mu_{\max} \cdot f(I) \cdot \left(L_{NO3} \cdot R_{O2:NO3} + L_{NH4} \cdot R_{O2:NH4}\right) \cdot Phy - 2 \cdot nhat \cdot NH4 - R_{O2:NH4}\left(r_{graz} \cdot Zoo - rhat_{SD} \cdot SDet - rhat_{LD} \cdot LDet\right), \quad (1)$$

where μ_{max} is the maximum growth rate of phytoplankton, *f(I)* is a non-dimensional light-limitation term, L_{NO3} and L_{NH4} correspond to nutrient-limitation due to nitrate and ammonium, respectively, $R_{O2:NO3}$ and $R_{O2:NH4}$ are stoichiometric ratios corresponding to the oxygen produced per mol of nitrate and ammonium assimilated during photosynthetic production of organic matter, *nhat* is the nitrification flux, r_{graz} is the grazing rate, and $rhat_{SD}$ and $rhat_{LD}$ are the remineralization rates of small and large detritus, respectively. The first term on the right-hand-side (rhs) of equation (1) corresponds to the production of oxygen during photosynthesis, the second term represents the consumption of oxygen during oxidation of ammonium to nitrate (2 mol of O_2 are consumed per mol of ammonium oxidized), and the last terms corresponds to oxygen sinks due to respiration by zooplankton and heterotrophic bacteria that degrade detritus. The hats in equation (1) indicate that terms have been modified compared to Fennel et al. (2006) to account for low oxygen concentrations. Specifically,

$rhat = r \cdot Max\left(\frac{Ox_{off}}{k_{Ox} + Ox_{off}}, 0\right)$, where k_{Ox} is an oxygen half-saturation concentration and Ox_{off} = Ox-Ox_{th} with Ox_{th} as oxygen threshold below which no aerobic respiration or nitrification occur. The same formulation is used for remineralization of large and small detritus and for nitrification.

In addition to the biochemical sources and sinks of oxygen there is gas-exchange across the air-sea interface, which directly affects the top layer of the model and is parameterized as

$F = \frac{vk_{O2}}{\Delta z}(Ox_{sat} - Ox)$, where F is in units of mmol O_2 m^{-3} and only applied to the top layer, vk_{O2} is the gas exchange coefficient for oxygen, Δz is the thickness of the respective grid box, and Ox_{sat} is the saturation concentration of oxygen. The gas exchange coefficient is parameterized following Wanninkhof (1992) as

$vk_{O2} = 0.31 \cdot u_{10}^2 \cdot \sqrt{\frac{660}{Sc_{Ox}}}$. Here u_{10} is the wind speed 10 m above the sea surface, and Sc_{Ox} is the Schmidt number, which we calculated as in Wanninkhof (1992). Ox_{sat} was calculated based on Garcia and Gordon (1992).

In combination with the freshwater discharge described above the model receives inorganic and organic nutrients, specifically nitrate, ammonium and particulate nitrogen, which are assumed to enter the small detritus pool in the model. Monthly nutrient flux estimates from the U.S. Geological Survey (Aulenbach et al. 2007) are used. Particulate organic nitrogen fluxes are determined as the difference between total Kjeldahl nitrogen and ammonium. To account for light attenuation in the river plume we introduced a salinity-dependent attenuation term in the calculation of the photosynthetically active radiation I at depth z as follows

$$I = I(z) = I_0 \cdot par \cdot \exp\left\{-zK_w - zK_{salt} - K_{chl}\int_z^0 Chl(\zeta)d\zeta\right\},$$

where I_0 is the incoming light just below the sea surface, and par is the fraction of light that is available for photosynthesis, K_w, K_{salt} and K_{chl} are the light attenuation coefficients for water and chlorophyll, respectively. The salinity-dependent attenuation is

$K_{salt} = Max(-0.024 + 0.89 * S, 0)$, where S is salinity.

Here we present an 8-year simulation starting on January 1, 1990. The biochemical variables *NH4, Phy, Chl, Zoo, SDet* and *LDet* were initialized with small constant values. *NO3* and *Ox* were initialized with horizontally homogenous mean winter profiles based on available in situ data. At the open boundaries *NO3* and *Ox* were prescribed using horizontally homogenous profiles based on measurements from the LATEX cruises. All other biochemical state variables at the boundary are set to small positive values.

3.5 SEDIMENT TRANSPORT MODEL CONFIGURATION

The physical oceanographic model described in Section 3.2 was coupled within ROMS to a three-dimensional sediment transport model, based on the Community Sediment Transport Modeling System (CSTMS; http://www.cstms.org/). Warner et al. (2008) describes in detail the CSTMS sediment transport routines. This section summarizes the implementation of the ROMS-CSTMS for the study site, which has focused on calendar year 1993. In addition to fair-weather conditions, 1993 contained a large flood and several wind and wave events. Moreover, extensive oceanographic observations (including CTD casts, buoys, and tetrapods) were collected that year for the LATEX projects (DiMarco et al. 1997; Wright et al. 1997). The availability of this data has enabled comparisons between the model estimates and observations.

The model was initialized on January 1, 1993, with an averaged climatological profile of temperature and salinity based on historic hydrographic surveys. Time steps of 60 s were used. Wave orbital velocity and period, calculated using the SWAN model as described in Section 3.3, provided the model input for the estimate of wave shear stress. Within the CSTMS combined wave–current bottom boundary layer (BBL) calculations were based on Styles and Glenn (2000) along with moveable bed routines proposed by Wiberg and Harris (1994) and Harris and Wiberg (2001).

A total of six sediment classes were used in the model, each treated as an individual tracer (Table 1). Two classes each represented Mississippi River sediment, Atchafalaya River sediment, and seabed sediment. The model required specification of a settling velocity (w_s) and

critical shear stress for erosion (τ_{cr}) for each sediment class; both of which remained constant. Specifically, the model neglected aggregation and disaggregation of flocs; there was no exchange between the six sediment tracers; and bed consolidation and swelling were neglected. Hydrodynamic properties were chosen based on past modeling studies (e.g., Bever et al. 2009; Harris et al. 2008) and comparison of model estimates to data described in more detail below.

Table1:

Sources and Sediment Properties Used for the Six Sediment Types included in Model Calculations

Sediment	**Type**	**t_{cr} (Pa)**	**w_s (mm/s)**	**Fraction**
Mississippi	Large flocs	0.11	1.0	50%
	Small flocs	0.11	0.1	50%
Atchafalaya	Large flocs	0.03	1.0	10%
	Small flocs	0.03	0.1	90%
Seabed	Sand	0.13	10.0	Spatially variable; See Figure 5
	Mud	0.11	1.0	

Fluvial Sediment Input: As mentioned previously, fresh water input from the Mississippi and Atchafalaya Rivers was specified using daily measurements from the Tarbert Landing and Simmsport gauging stations (see Figure 3) maintained by the U.S. Army Corps of Engineers and U.S. Geological Survey (USGS). The USGS sampled sediment at both stations approximately once every two weeks, and used those measurements to estimate daily sediment discharges (data from Dr. Charles Demas). These provide the best available estimate of the total amount of sediment delivered by the combined Red and mainstem Mississippi Rivers to coastal Louisiana (Meade and Moody, 2008).

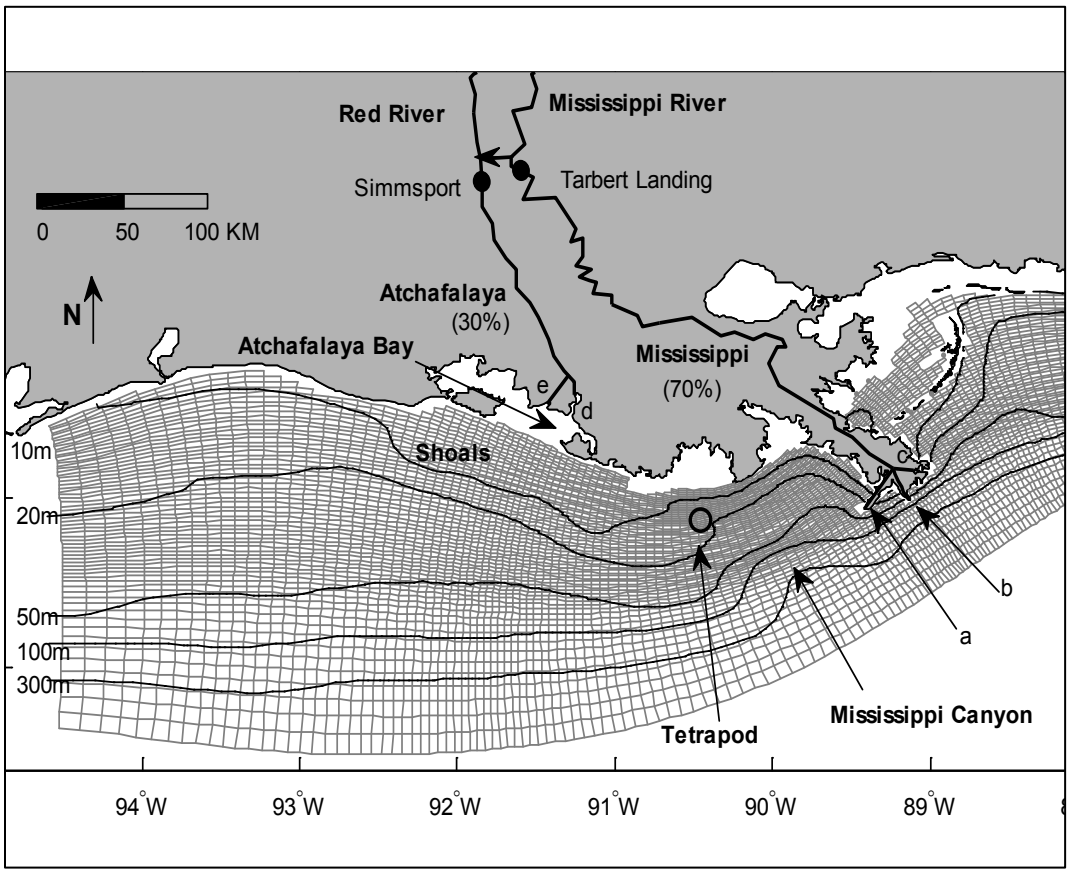

Figure 3: Curvilinear model grid for the Louisiana-Texas shelf. Isobaths contoured at 10, 20, 50, 100, 300 m. The open circle shows the tetrapod location for the LATEX sediment transport observation during summer 1993 (Wright et al., 1997). Shown on the Mississippi Delta are Southwest Pass (a), South Pass (b) and Pass a Loutre (c). Both Atchafalaya (d) and Wax Lake (e) deltas are being built in Atchafalaya Bay.

Mississippi River Discharge: Tarbert Landing, long the representative station of continuous discharge of the Mississippi River, is 525 km upstream of the mouth of Southwest Pass (Figure 3). It takes about 3-7 days for the suspended sediment to be transported from this station to the sea, depending on the flow and antecedent conditions (Demas, 2007, per. comm.). In our model we neglected this time-lag because (a) the timescale of temporal variability of discharge from these two rivers is long compared to the ~week transit time from the gauge to river mouths (Figure 4, panels C and D), and (b) calculations seem insensitive to the timing of arrival of fluvial discharge based on our model experiments. For the Mississippi sediment discharge, we specified 50% as large flocs with a settling velocity of 1 mm/s, and 50% as small flocs with a slower settling velocity of 0.1 mm/s. Critical shear stress for both types was 0.11 Pa, a value derived by Wright et al. (1997) based on near-bed measurements over somewhat-consolidated Mississippi sediment (Table 1). Like the freshwater discharge, Mississippi River sediment discharge was delivered to the model grid as forty-four point sources along the bird's foot delta.

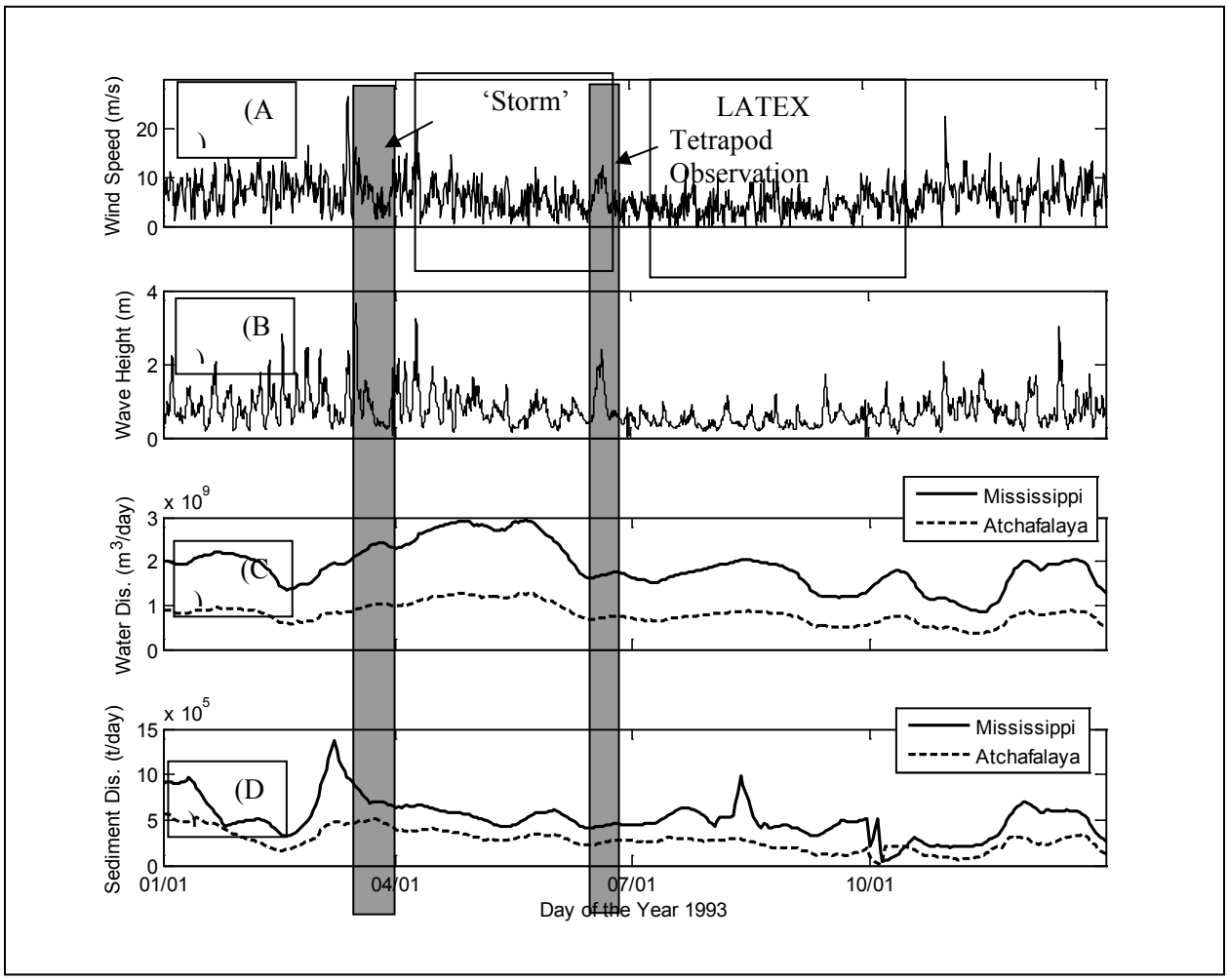

Figure 4: (A) Observed wind speed from BURL 1 C-MAN weather station on the Southwest Pass of the Mississippi Delta. (B) SWAN-modeled wave height at the LATEX tetrapod location (See Figure 1). (C and D) Water and sediment discharge from the Mississippi and Atchafalaya Rivers.

Atchafalaya Bay Discharge: Data from Simmsport represent discharge diverted from the Mississippi and Red Rivers to Bay (Figure 1). In 1993, on average 30% of sediment passing Simmsport Station was sand and 70% was mud (data from USGS). Because of the shallowness of Atchafalaya Bay (average depth of 2 m), most of the sand deposits on the Wax Lake and Atchafalaya Deltas, leaving finer sediment to be resuspended and exported to the inner shelf (Wells et al., 1984; Allison et al., 2000). Sand content, for example, exceeded 50% on the Atchafalaya and Wax Lake deltas (Roberts, 1998), and decreased rapidly to <5% at the 5-m isobath south of Atchafalaya Bay (Neil and Allison, 2005). Volumetric calculations based on bathymetric data imply that Atchafalaya Bay retains about 27% of sediment delivered to it (Wells et al. 1984; Draut et al., 2005). Our model neglected processes in Atchafalaya Bay, but we adjusted the measured Simmsport sediment discharge by 73% and delivered that in a line source at the bay mouth. Atchafalaya sediment was portrayed differently from Mississippi sediment

because it likely undergoes several cycles of resuspension before leaving the bay. Assuming a settling velocity at 0.1 mm/s, a mean depth of 2 m, and mean current at 0.2 m/s, sediment from the Atchafalaya and Wax Lake deltas would only travel 4 km before initial deposition, much less than the 20 km distance from the deltas to the bay mouth. These repeated cycles of resuspension imply that sediment discharging from Atchafalaya Bay mouth is likely finer than that passing the Simmsport Station, and composed of smaller flocs than sediment discharged from the Mississippi Delta. For sediment delivered from Atchafalaya bay, the model therefore assumed that 10% was large flocs with a settling velocity of 1 mm/s, while the remaining 90% was small flocs with a settling velocity of 0.1 mm/s (Table 1), and a reduced critical shear stress of 0.03 Pa was assumed.

Seabed Sediment: Four 10-cm thick vertical layers were used to represent the initial sediment bed. The usSEABED project (Williams et al., 2006) archived more than 50,000 historical surficial grain-size data (fraction of sand, silt, and clay) from the study site. These data were interpolated to generate the initial bed fractions of sand and mud for the model, where the mud fraction was assigned the sum of the silt and clay fractions (Figure 5). Seabed sediment included fast-settling mud (1 mm/s) and very-fast-settling sand (10 mm/s). Their critical shear stresses were assumed to be 0.11 and 0.13 Pa, respectively. Most sediments are muddy (>80% mud) in the inner and middle shelf, except the sandy Trinity and Ship Shoals (20-30% mud) between 5- and 10-m isobaths south of Atchafalaya Bay. Along the southern boundary where water depth exceeds 300 m, the seabed is mainly consolidated muds. This area was represented as sands in the model to prevent unrealistic erosion there. This was appropriate given (a) in this model we focused on the shelf area shallower than 100 m, and (b) the probable frequency of sediment movement by significant wave surge in deep water is only once every five to twenty years (Curray, 1960). Sediment density was set to be 2650 kg/m3 and porosity was 0.8 based on measurements by Draut et al. (2005) and Allison et al. (2007).

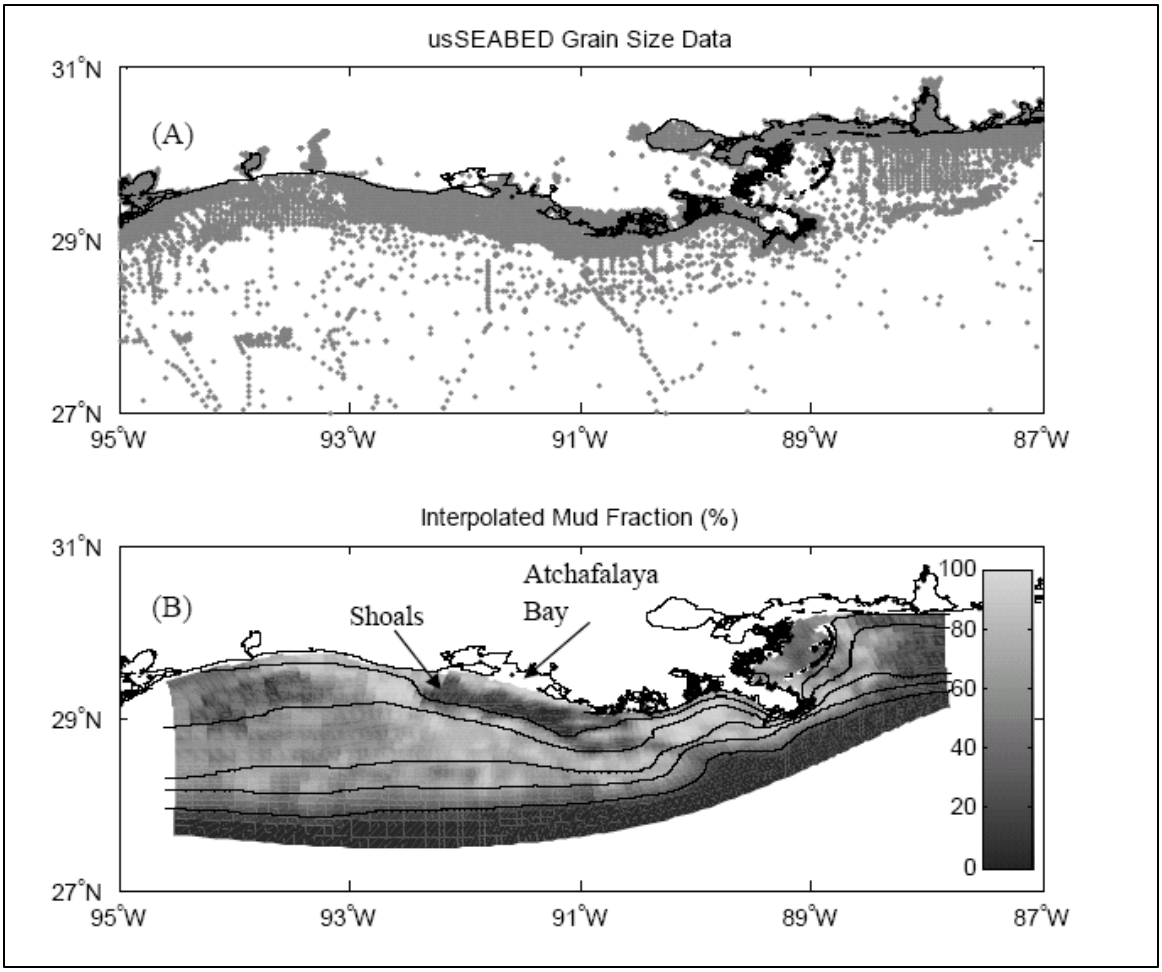

Figure 5: (A) Locations of >50,000 usSEABED grain size data points from Williams et al. (2007). (B) Interpolated mud fraction within the model grid based on usSEABED data. Isobaths contoured at 10, 20, 50, 100, 300 m. The shoals shallower than 10m south of Atchafalaya Bay are sandy. Area deeper than 300 m was modeled as sand to minimize southern boundary effects.

4 RESULTS

4.1 PHYSICAL MODEL

4.1.1 Long-term Physical Simulations Covering 1990 to 2008.

The multi-year simulations span the period from 1990 in late winter to Fall 2008. We focus on the period 1992 and beyond to allow the model to spin up for slightly over one year. This period was chosen because of the availability of local measured winds used to force the model. Animations of sea surface salinity and surface currents are available online at http://pong.tamu.edu/~rob/mch. Figure 6 shows an example frame from one these animations; surface salinity on July 28, 1993, late summer is when annual bottom hypoxia over the Louisiana-Texas shelf is typically at its largest areal extent.

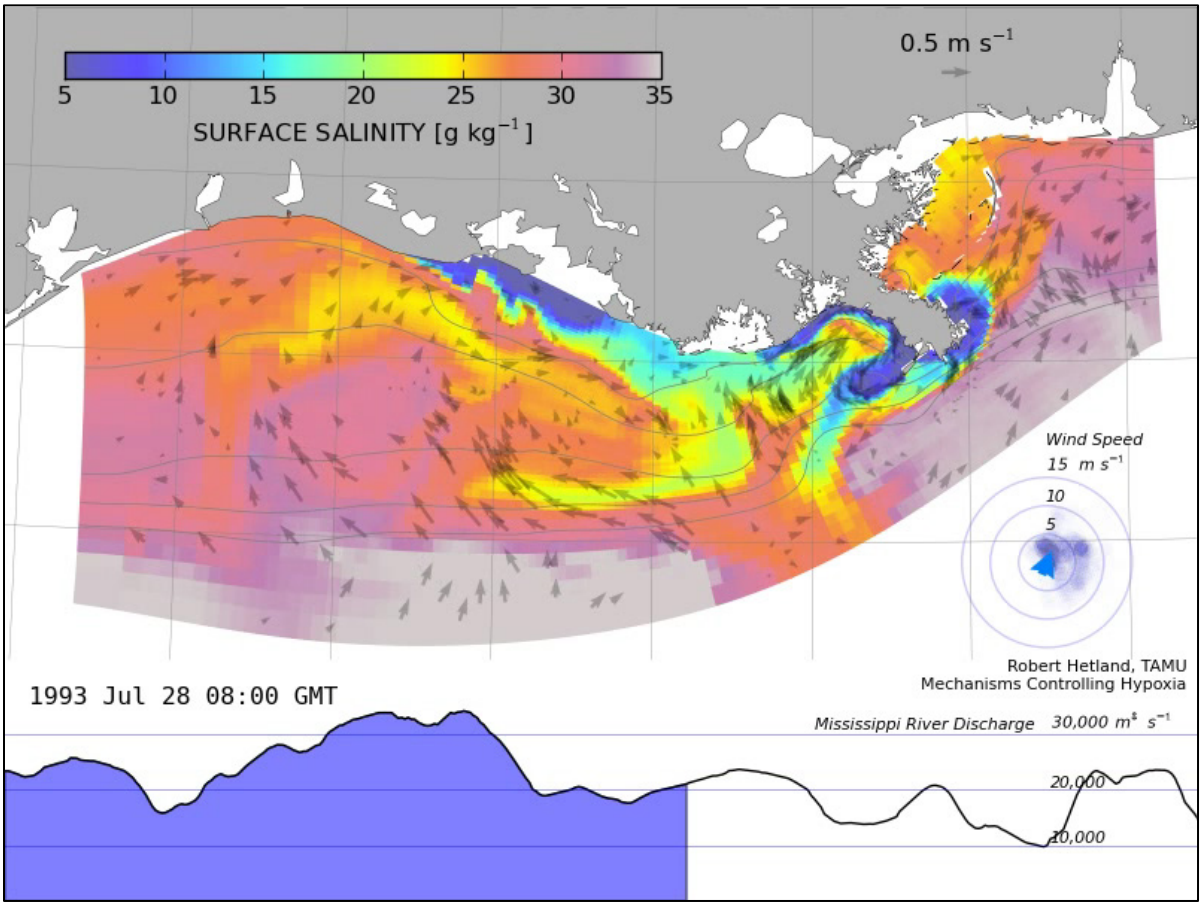

Figure 6: Surface salinity July 28, 1998 is shown in color shading according to the colorbar. The Mississippi River discharge is shown in the timeseries below for the whole year; the filled portion before July 28, 1993. The instantaneous wind is shown by the arrow within the circle, the shading represents the location of the arrowhead over the previous week to give an idea of the wind variability.

Figures D-1 through D-16 (shown in Appendix D) show contours of the surface and bottom 33 psu isohaline for each month in the years 1992 to 2007. These figures show clearly that the foot of the front, the location of the 33 psu isohaline along the bottom, does not change much between seasons. There is evidence of a slight onshore motion in summer, consistent with seasonal upwelling winds that typically occur between June and August. The surface 33 psu, on the contrary, undergoes large seasonal shifts as it moves offshore in summer months, and onshore during the rest of the year. It is apparent that stratification, here represented by the separation of the surface and bottom isohaline surfaces, is greatest in summer as observed.

Also apparent in the surface 33 psu isohaline contours are many persistent sub-mesoscale eddies, discussed further in the model skill section below. Measoscale activity is stronger in the summer months, when the 33 psu isohaline is pushed further offshore under upwelling winds. During winter, the water column is well mixed at the location of the 33 psu isohaline, and this adds to the stability of the front, such that the meanders associated with this mesoscale activity are not present.

4.1.2 Model Skill

The skill of the numerical simulations was investigated by comparing the simulated salinity field to hydrographic observations. Skill is defined as

$$\text{skill} = 1 - \frac{\sum (m_i - d_i)^2}{\sum (c_i - d_i)^2}$$

where d_i are the data, m_i are the simulated values at the observation points, and c_i are the climatological values at the observation points. This equation can be interpreted as the error variance normalized by the data variance relative to the climatology (Hetland 2005). A skill of one, therefore, implies a perfect model; the model and data have identical values. A skill of zero means that the model error variance is the same size as the variance of the data relative to climatology. It is possible for skill to be negative if the simulated field actively disagrees with observations. Thus, a model with positive skill means that the model is providing useful information beyond the previously known system state (the climatology). For this study, average monthly vertical profiles of salinity based on all available historical data were used to define the climatology. Thus, the climatology was a function of month and depth, but not a function of horizontal position on the shelf. This requires the model to accurately simulate the horizontal dispersion of fresh water over the shelf, and reduces the dependence of the skill on simply getting a fresher upper water column.

To gain a more detailed understanding of what aspects of the salinity field the model is capturing, and what aspects the model is not representing, a histogram of model error, normalized by the standard deviation of the data, is shown in Figures 7 and 8. Thus, in this figure, an error of one means that the model has an error equal to the standard deviation of the observations minus the climatology. Negative values mean that the model is too fresh, positive values mean the model is too salty.

Typically, the error is well within one standard deviation of the observations relative to the climatology. There are a few exceptions where the tails of the distribution are large. For example, the November 8–14, 1993, cruise shows that there was an intrusion of salty water onto the shelf that was not reproduced in the model (i.e., the model is too fresh). This is likely due to the fact that the model does not have any influence from the Loop Current, and thus energetic deep water flows that would push deep ocean water up onto the shelf are not present in the simulations.

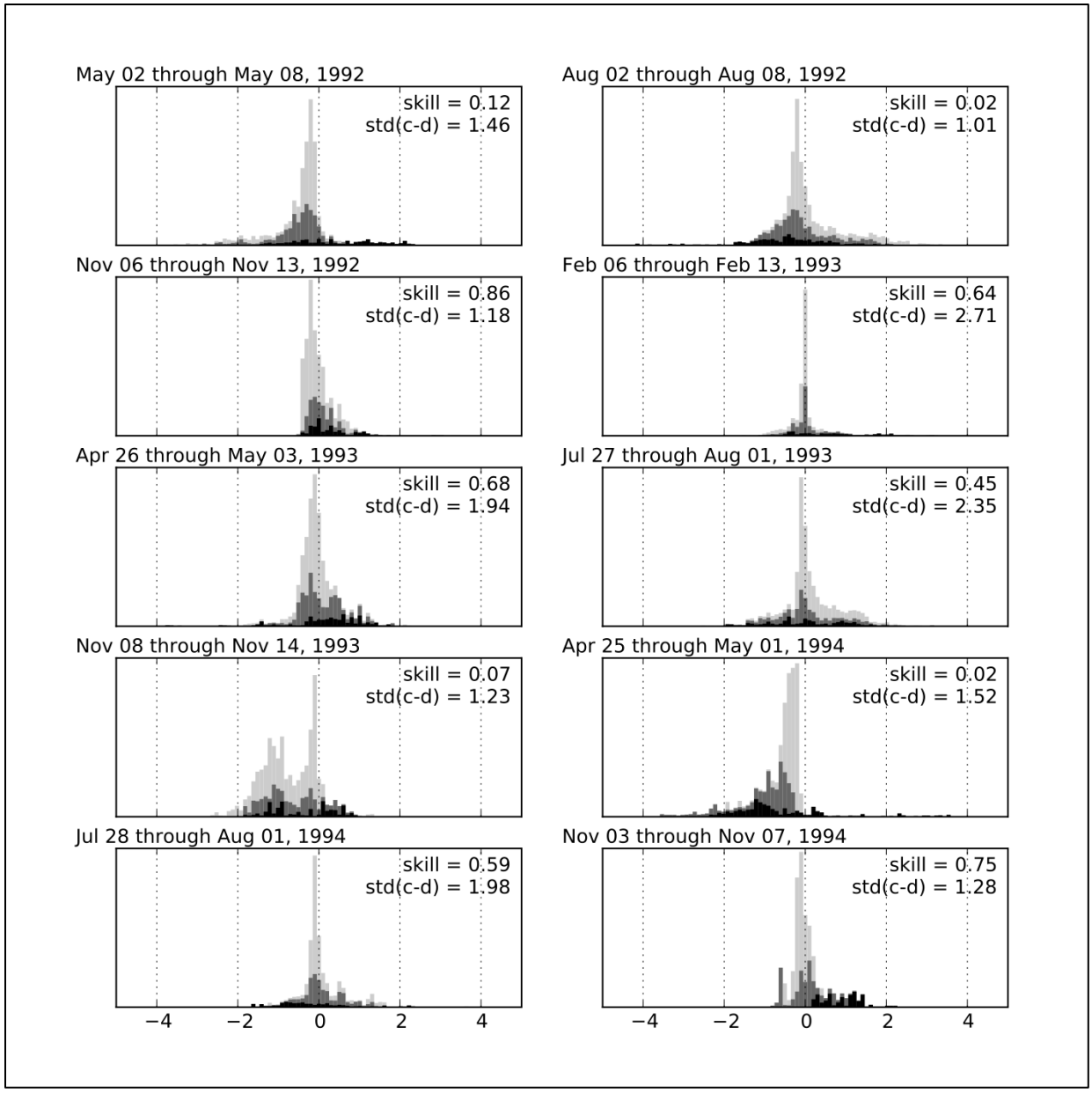

Figure 7: Histograms showing normalized error in model predictions of salinity during the LATEX field effort period. The colors correspond to observations taken at different depths, shallower than 20, 50 and 100 m for progressively lighter shades of grey. The model error is normalized by the standard deviation of the observed salinity distribution for a particular cruise, and is given in each panel. Model skill at reproducing each survey is also given in each panel.

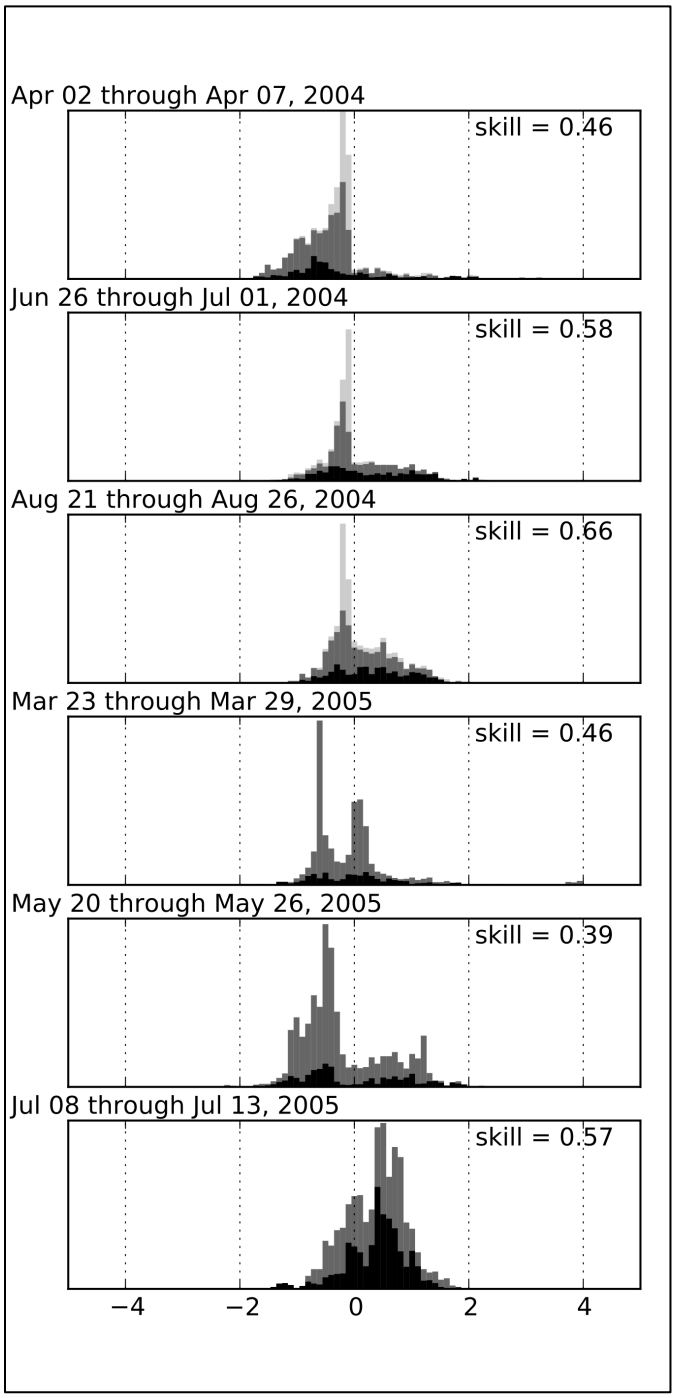

Figure 8: Same as for Figure 7 except for the Mechanisms Controlling Hypoxia hydrographic surveys.

To gain an understanding of the horizontal distribution of model error, the model error normalized by the standard deviation of the observed salinity field relative to the climatology was plotted for each cast. Note that although the climatology does not contain any information about lateral property distributions, both the observations and numerical results do. In this way, it is possible to determine regions that may be consistently under- or over-predicting salinity, and allows us to get an estimate of the horizontal spatial scales of the model error. Figures 9 and 10 show that the model error has horizontal spatial scales that are approximately 10 to 50 km. Also, it appears that the distribution of the error is random between the hydrographic cruises, indicating that there are no systematic errors in predicting the horizontal structure of salinity.

Mean velocities and variance ellipses for the observed and simulated flow structure are shown in Figure 11. The model simulation reproduces the general downcoast flow associated with the buoyancy-driven, far-field Mississippi River plume. One exception is the eastern offshore mooring, 14, that has a mean upcoast flow over the duration of the record. This is attributed to the presence of an offshore Loop Current Eddy. In all cases, the variance is larger than the mean currents in both the simulation and observations. The variance is oriented along-shore, and decreases with depth, as expected for surface-trapped, buoyancy-driven coastal flow. In all cases, the skill of the model at reproducing the currents is negative – even when the time-series is low-pass filtered up to a week – which is attributed to the dominance of small-scale variability.

Comparisons between climatological, observed and simulated temperature are shown in Figure 12. The temperature structure varies primarily vertically, so that both the observations and the simulation closely follow the seasonal pattern of the climatology. Even taking this into account, the model skill at reproducing the observed temperature timeseries is positive for all moorings, indicating that the model is also able to reproduce observed deviations from climatology. However, there are many short-lived variations in temperature, with a duration of approximately one week, that are not reproduced in the model. The fact that the skill is positive indicates that variance in these short-lived features is smaller than that associated with successfully simulating the seasonal-scale offset from the seasonal pattern.

The model was also compared to long-term, moored observations of temperature, salinity, and velocity. The locations of the moorings within the model domain, deployed during the LATEX program are shown in Figure 13.

Comparisons between climatological, observed and simulated salinity are shown in Figure 14. Error histograms for the timeseries of salinity are shown in Figure 15. The model generally reproduces the seasonal pattern in the climatology, but in this case, there is much more variance at higher frequencies. As such, the skill is negative for many of the moorings. Notably, the model skill is very low at reproducing surface salinity at the two offshore moorings 14 and 19, and the eastern mid-shelf mooring 15. Inspection of these timeseries shows that there are periods approximately 1-3 months long during which the observations differ significantly from the seasonal cycle, and these differences are not accurately reproduced in the model. Given the location of these three moorings, it is clear that these differences come from offshore, a feature of the real flow field that is not reproduced in the numerical simulation because this information is not present in the open boundary conditions. Also, the shelf is narrower to the east, so that the

mid-shelf mooring 15 is more affected by offshore currents than mooring 18, moored at the same isobath further to the west where the shelf is broader.

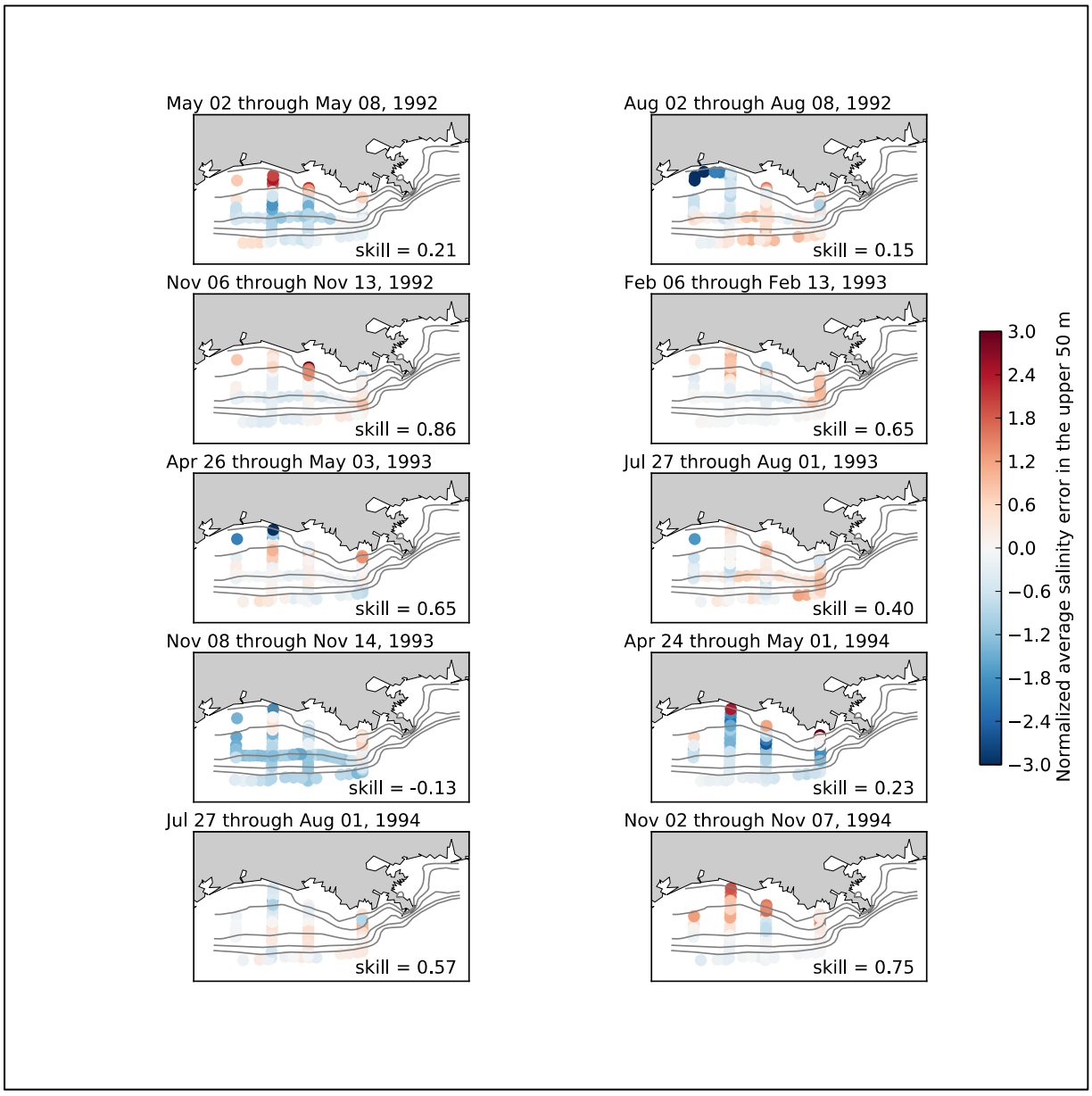

Figure 9: Normalized salinity error in the upper 50 m of the water column at LATEX hydrographic stations. The skill of the simulation at reproducing the observed hydrographic structure is given in the lower right corner of each panel.

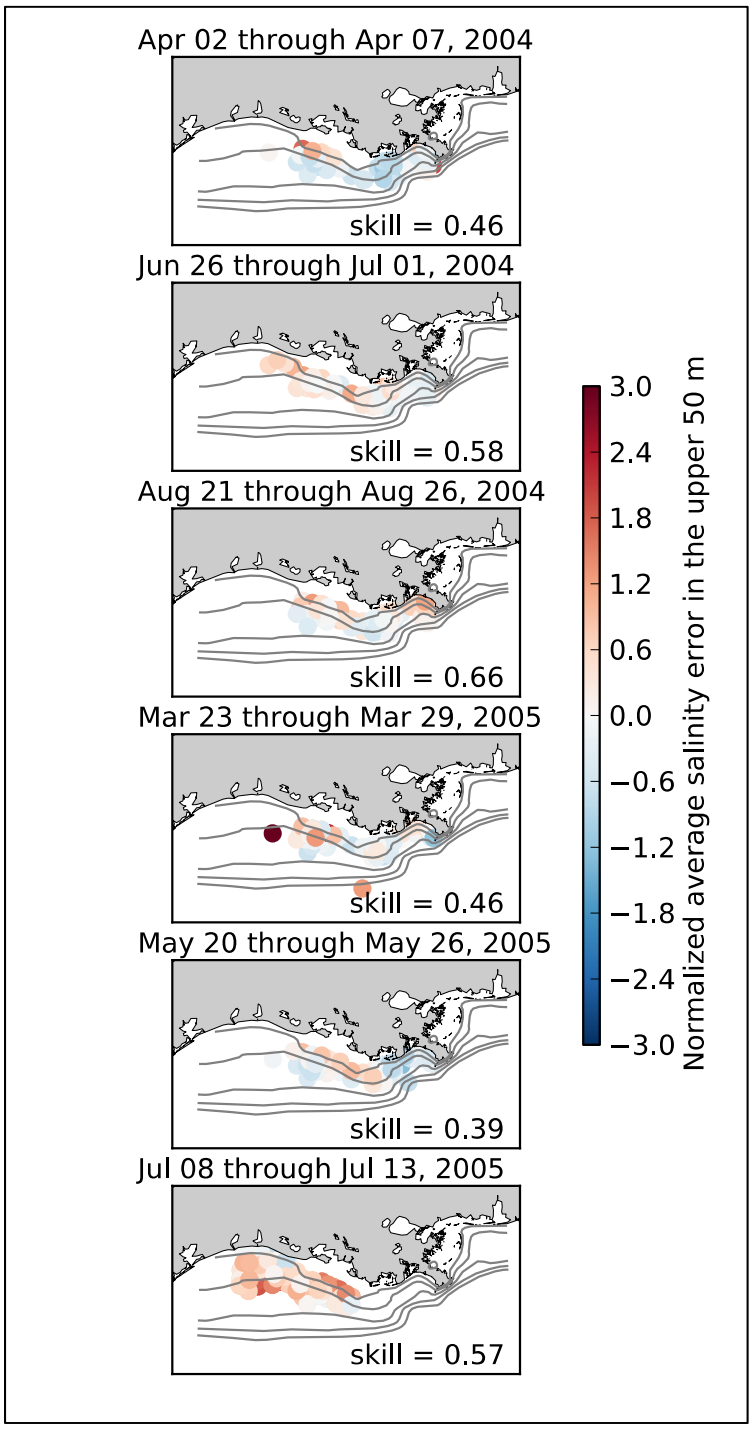
Apr 02 through Apr 07, 2004
skill = 0.46
Jun 26 through Jul 01, 2004
skill = 0.58
Aug 21 through Aug 26, 2004
skill = 0.66
Mar 23 through Mar 29, 2005
skill = 0.46
May 20 through May 26, 2005
skill = 0.39
Jul 08 through Jul 13, 2005
skill = 0.57
3.0
2.4
1.8
1.2
0.6
0.0
−0.6
−1.2
−1.8
−2.4
−3.0
Normalized average salinity error in the upper 50 m

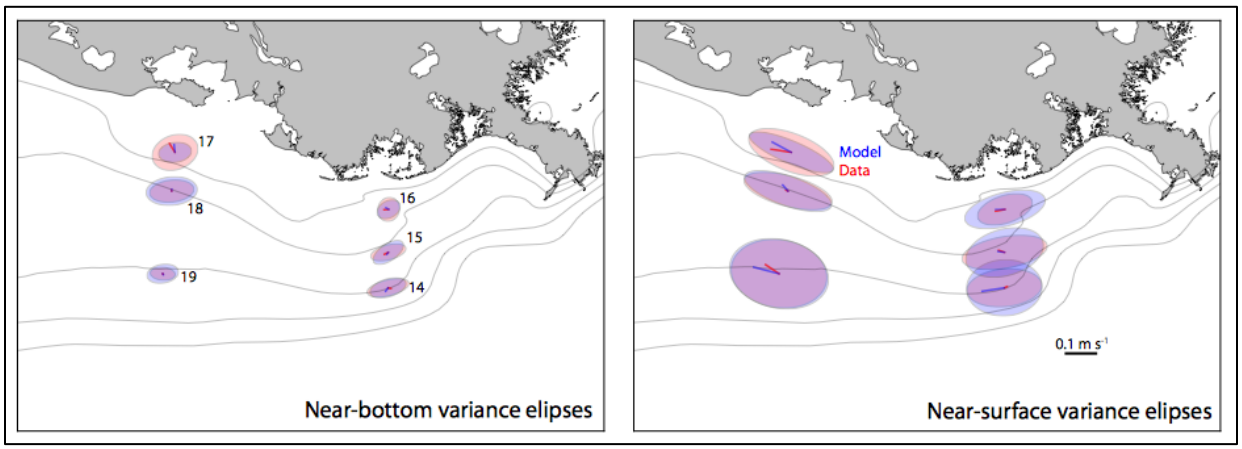

Figure 11: Near bottom and near surface current means (lines) and variance ellipses are compared over the LATEX observational period; both are defined relative to the velocity scale. Model results are in blue, observations in red.

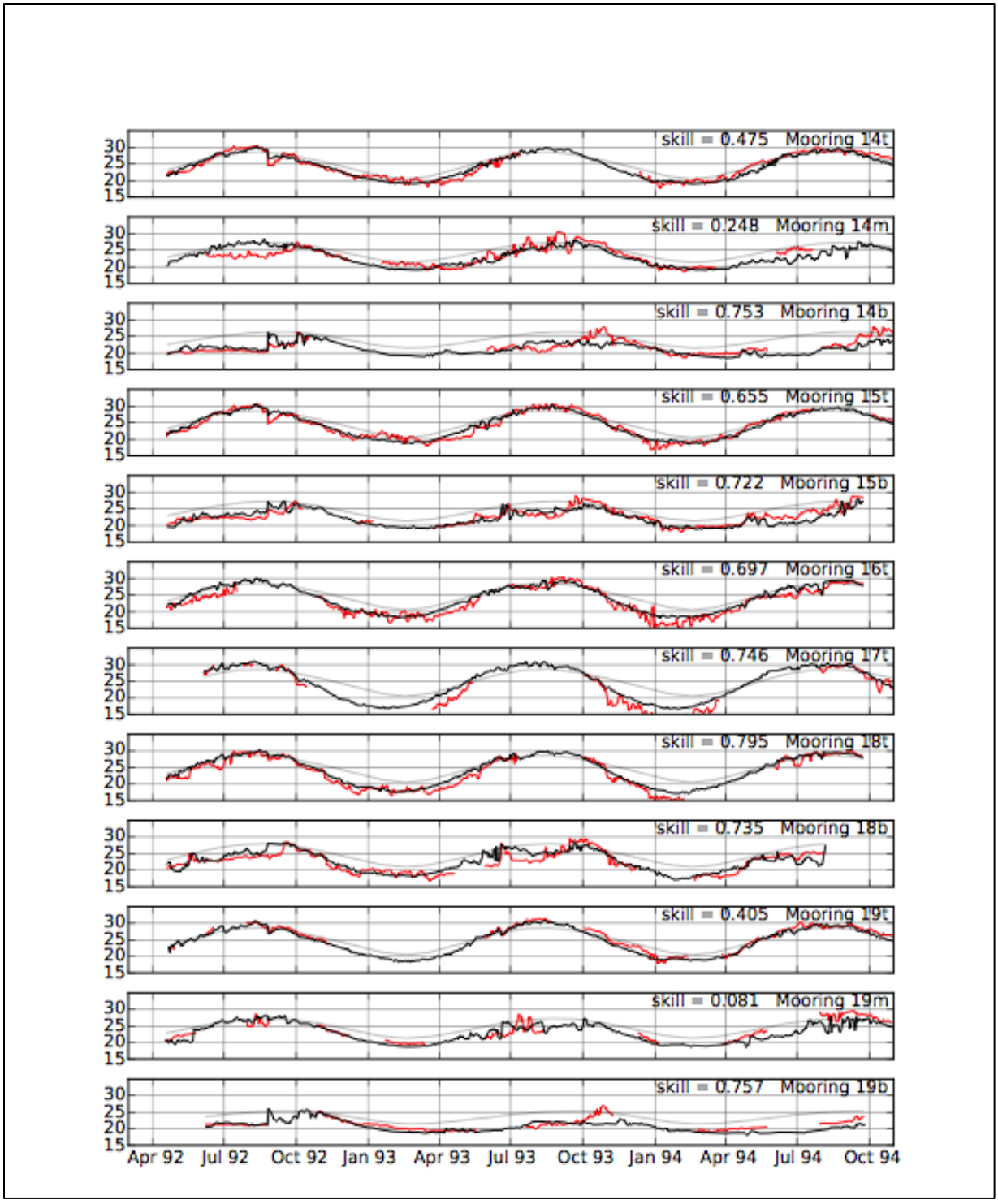

Figure 12: Comparison of climatological (grey), observed (red), and simulated (black) temperature at the mooring locations.

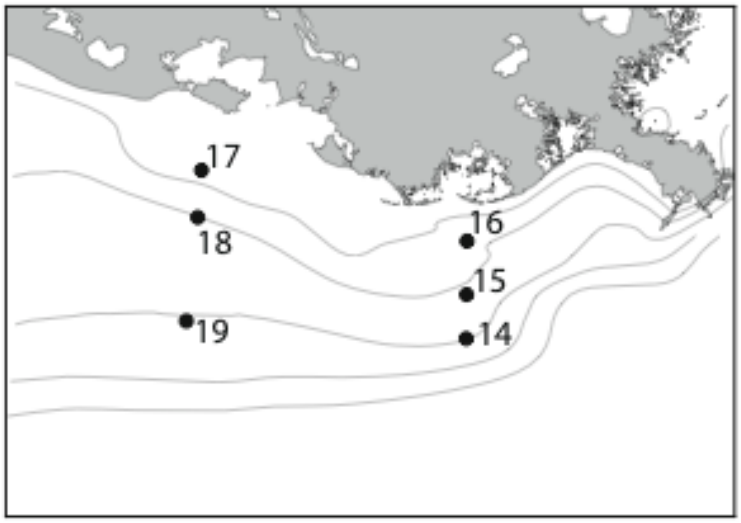

Figure 13: LATEX mooring locations used for model/data comparison.

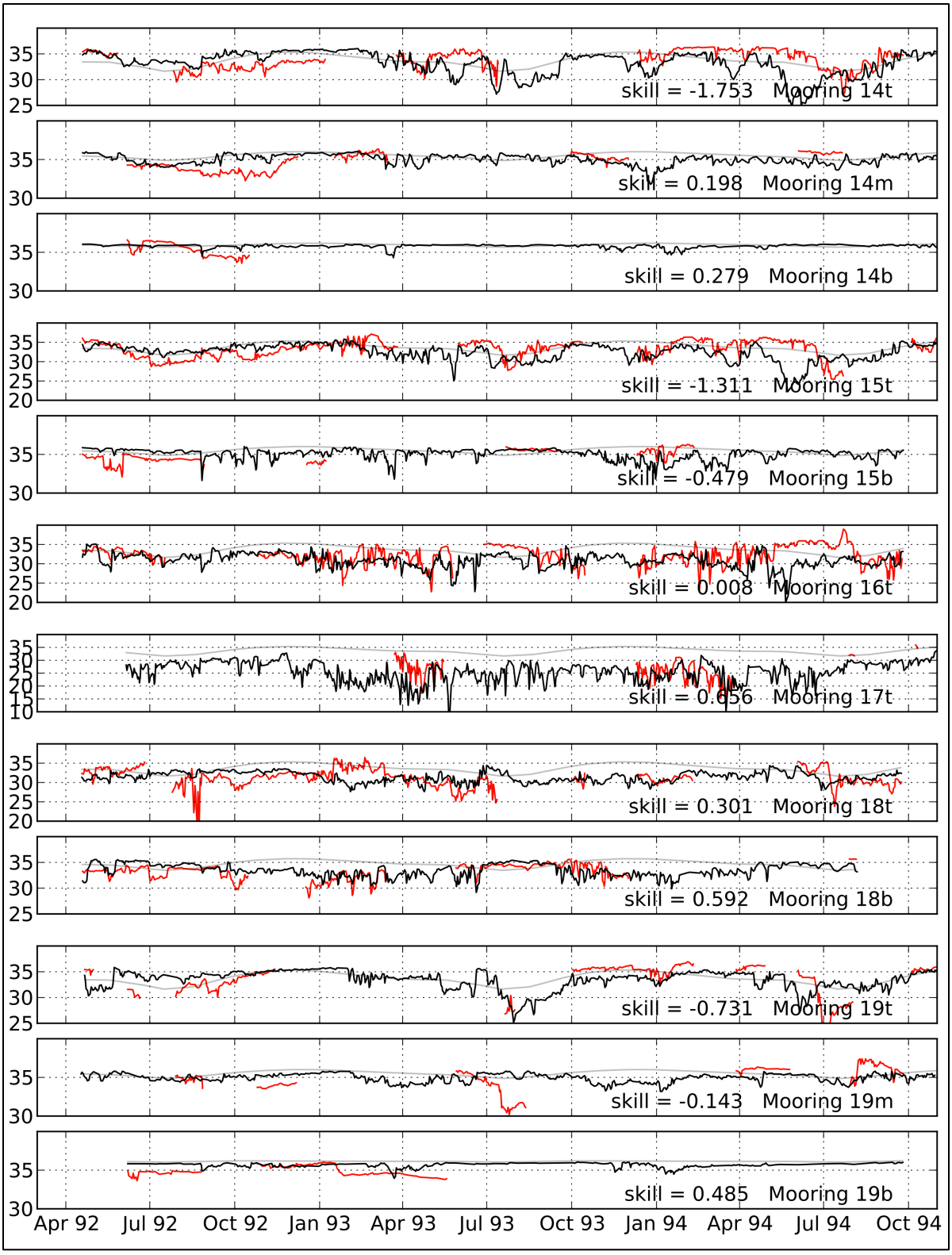

Figure 14: Comparison of climatological (grey), observed (red), and simulated (black) salinity at mooring locations.

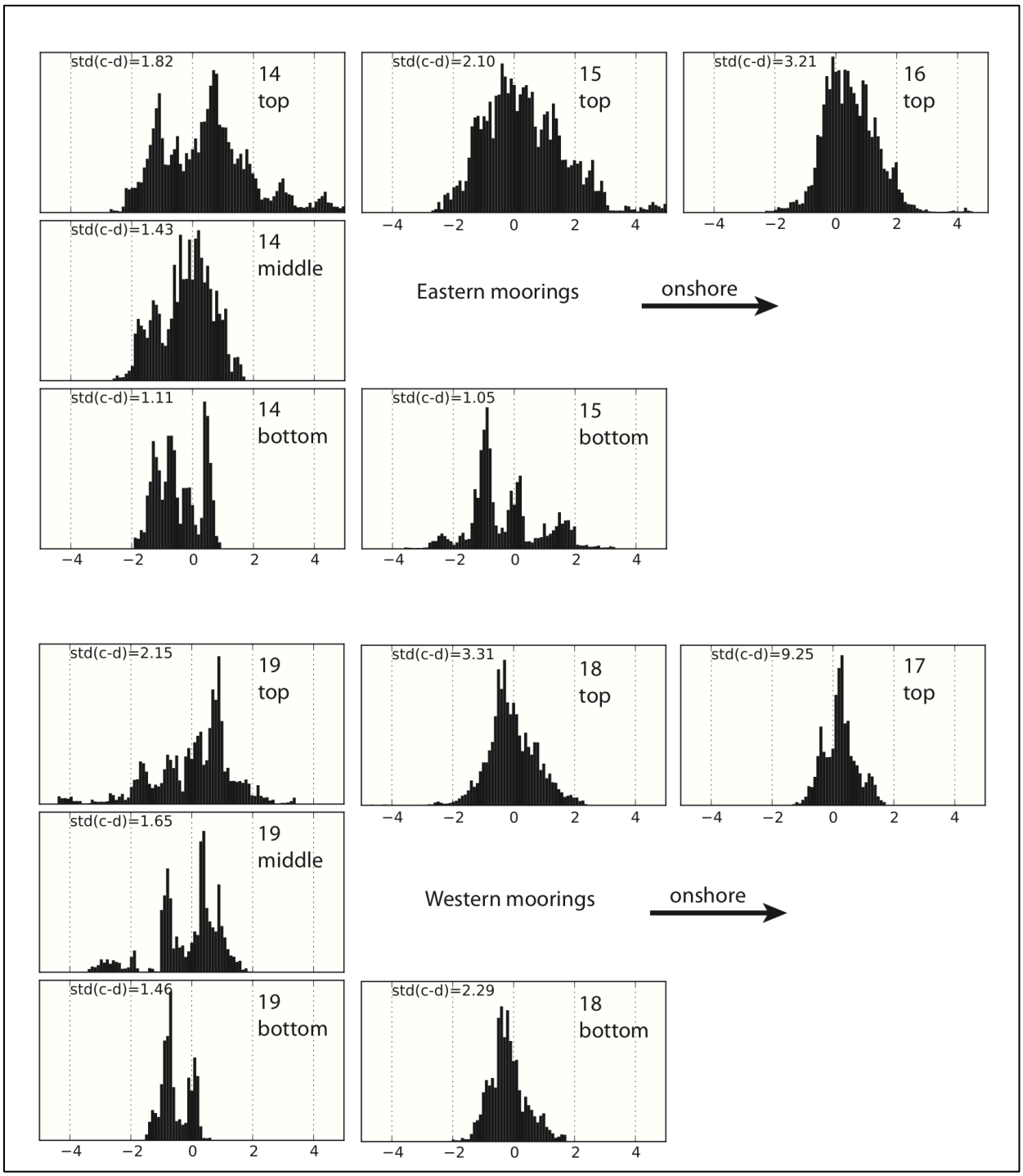

Figure 15: Histograms showing normalized model error in predicting salinity at the six mooring locations.

Error decorrelation timescales were estimated by calculating the decay rate of a lagged correlation of the model error timeseries. The error decorrelation timescales for near- surface temperature and salinity (not shown) are between 5 and 12 days, except for salinity at moorings

14, 15, and 19, which had error decorrelation timescales of approximately 3-4 weeks. Moorings 14 and 19 are the two offshore moorings, and 15 is the eastern midshelf mooring. These three moorings were also identified as moorings with particularly low skill at predicting near-surface salinity. Thus, the longer error decorrelation timescales are again attributed to persistent (1-3 months) modifications to the shelf flow field by offshore currents that are not included in the open boundary condition.

4.2 BIOGEOCHEMICAL MODEL

4.2.1 Multiyear Simulations

We performed a multi-year simulation with our coupled physical-biological model for the 1990s. As one step in model validation we compared simulated surface chlorophyll values with the monthly SeaWiFs chlorophyll climatology (Figures 16 and 17). The monthly SeaWiFS climatology was calculated by averaging all SeaWiFS SMI fields from September 1997 to December of 2007 by month (note that this period does not coincide with our simulation period). The qualitative comparison in Figure 7 suggests a generally favorable agreement between model and climatology, with highest chlorophyll concentrations near the coast, a pronounced on-shore/off-shore gradient in surface chlorophyll concentrations, and highest chlorophyll in the river plumes from May to September. It should be noted that we do not expect perfect agreement of individual features when comparing an individual model year to the 10-year SeaWiFS climatology.

Quantitative measures of model-data agreement are given in the pair-wise match-ups shown as 2-dimensional histograms and given as correlation coefficients in Figure 5. Here we interpolated the SeaWiFs monthly mean fields onto the model grid and, for each model pixel, plotted the log-transformed climatology over the corresponding log-transformed model value. The color indicates the number of model-data pairs per 2-dimensional bin (corresponding to the height of the bar in a 1-dimensional histogram). In the case of perfect agreement all point would cluster along the 1-to-1 line (white line). The black line is a linear regression to the mode-data pairs with slope and intercept given to the right of each panel. The correlation coefficients (also given to the right of each panel) are high ranging between 0.7 and 0.85.

4.2.2 Biogeochemical Model Extensions

Motivated by recent findings by Sylvan et al. (2006), who observed P-limitation of phytoplankton growth on the Louisiana-Texas shelf in May and July of 2001, we have expanded our biogeochemical model to predict inorganic phosphate concentrations in the water column in addition to the inorganic nutrients nitrate and ammonium. This allows the model to switch between N- and P-limitation of phytoplankton and was done by defining phosphate as an additional state variable (an active tracer) in ROMS, and required the following additions/modifications to our model:

- specification of phosphate concentrations in the river inputs and along the model's open boundaries,

- inclusion of phosphate limitation in the parameterization of phytoplankton growth,
- inclusion of phosphate remineralization processes in the water column, and
- specification of a benthic remineralization term for phosphate.

Our model assumes that phosphate cycles through the food web in Redfield ration in other words, the internal N:P ratios of phytoplankton, zooplankton and detritus are assumed to be 16:1 in the water column. In our specification of the benthic phosphate remineralization term we followed the established paradigm by assuming efficient phosphate return to the water column. This is in contrast to benthic nitrogen remineralization, which represents a net sink for fixed nitrogen due to denitrification. Benthic remineralization in our model thus introduces a differential recycling term that drives the system toward N-limitation.

We performed a multi-year simulation (from 1990–1995) of the expanded model with phosphate. Simulated monthly mean DIN:PO_4 ratios (Figure 18) suggest that a large portion of the Louisiana-Texas shelf is limited by phosphorus in May, and that the size of the phosphorus limited region is significantly reduced by September. This is in agreement with the observations reported by Sylvan et al. (2006) who found P-limitation in May and July of 2001, and N-limitation in September of the same year. While a significant decrease in the size of the P-limited region from May to September is predicted for all years of the simulation, the model suggests interannual differences, e.g., most widespread P-limitation in the high discharge years 1993 and 1994.

4.3 SEDIMENT AND WAVE MODELS

This section summarizes the SWAN and ROMS-CSTMS model results used to represent calendar year 1993. These are presented together because the wave estimates critically impact model estimates of resuspension. Based on model estimates for 1993, a year that included a large storm in March, high discharge, and a typical fair-weather period during the summer we concluded the following:

(A) For 1993, the model reproduced both hydrodynamic conditions and sediment dispersal and deposition on the Louisiana-Texas shelf. The model estimated that most fluvial sediment was deposited near the Mississippi Delta and Atchafalaya Bay mouths. Due to high settling velocities assumed for Mississippi flocs and shallow bathymetry offshore the Atchafalaya Bay, most sediment only traveled a short distance (20 to 40 km) before initial deposition.

(B) On the Louisiana-Texas shelf, short – term sediment accumulation rates (1 year) vary by at least two orders of magnitude, from >5 cm/yr near the sediment sources, to 0.1 cm/yr offshore, and to less than 0.01cm/yr in other areas. Although sediment from both the Mississippi and Atchafalaya Rivers accumulated southeast the Atchafalaya Bay, their contribution appeared to be insignificant in terms of annual sediment budget, accounting for less than 1% of the fluvial supply.

(C) During fair-weather conditions the two freshwater plumes spread seaward and helped stratify the water column. Model calculations indicated that at these times bed shear

stress episodically reached the critical level sufficient to resuspend sediment only at depths shallower than 10 m.

(D) During large storms, such as occurred in March 1993, the water column was well-mixed over almost the entire continental shelf. Sediment flux peaked near the Mississippi subaqueous delta and Atchafalaya Bay mouth. Most resuspension occurred in areas where wave shear stresses dominated total bed stresses.

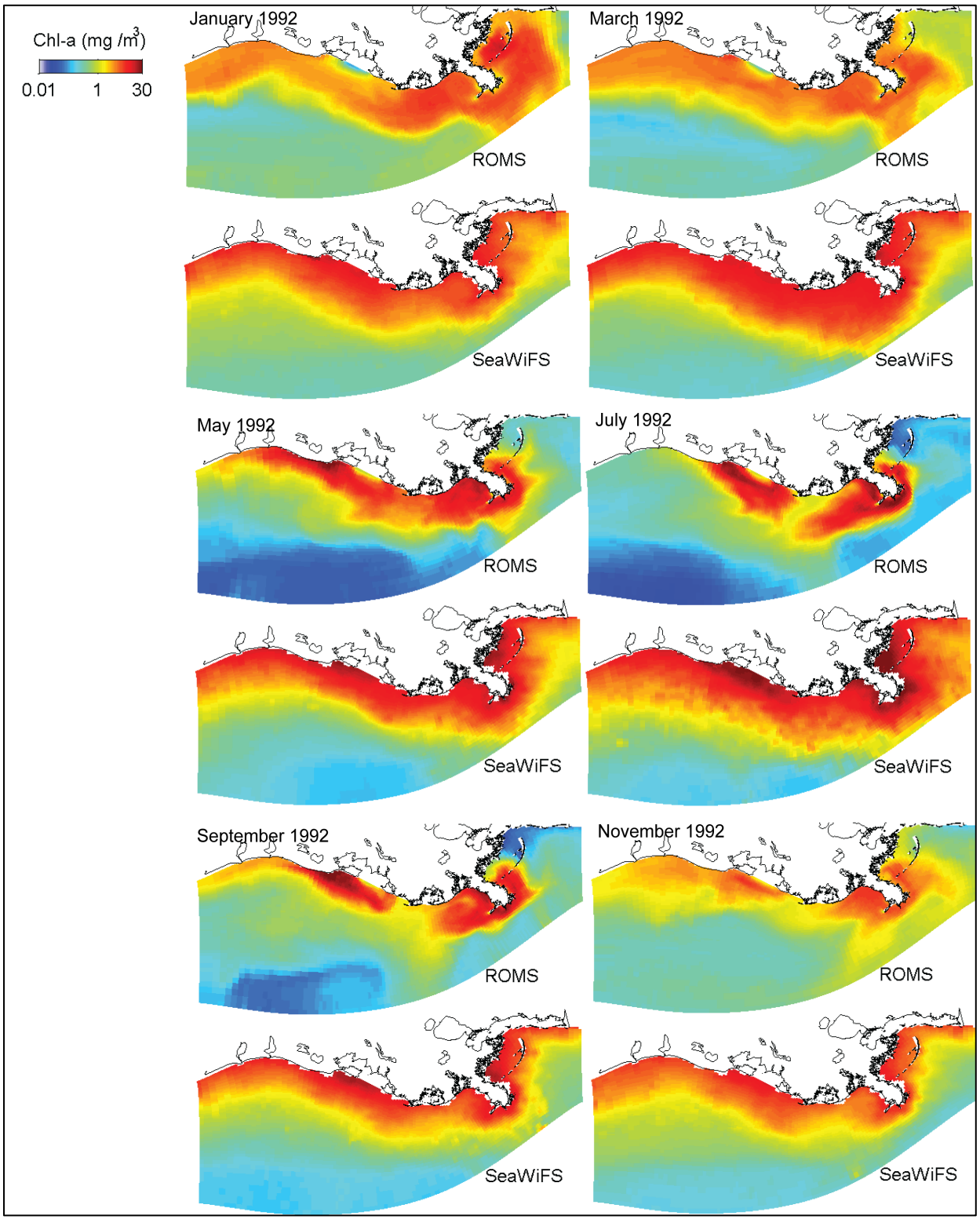

Figure 16: Comparison of model-simulated monthly mean surface chlorophyll with the monthly SeaWiFS chlorophyll climatology.

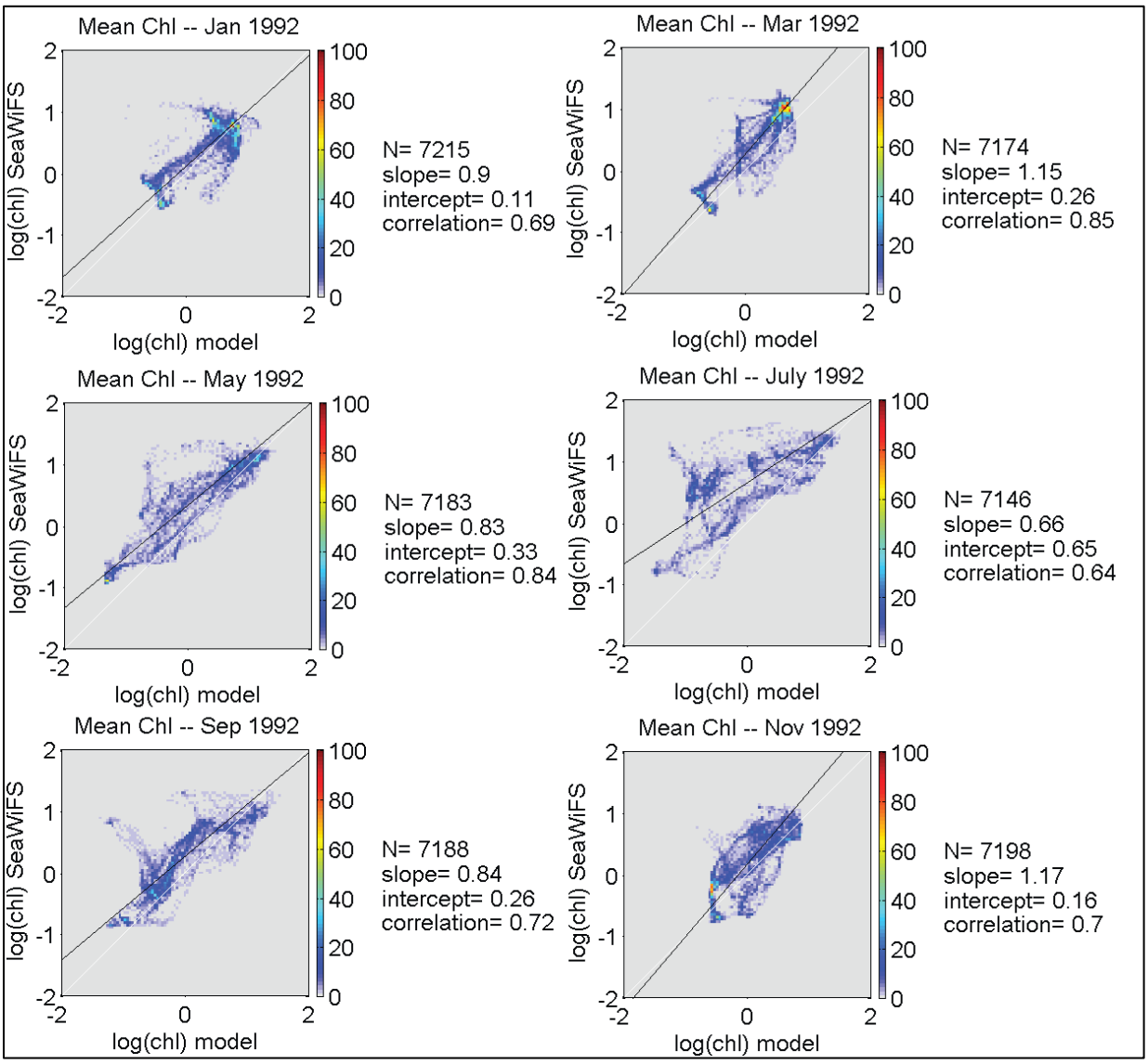

Figure 17: One-to-one match ups of monthly mean surface chlorophyll concentrations for each model grid point with monthly SeaWiFs chlorophyll climatology, which was interpolated onto the model grid. The total number of data pairs (N), the slope and intercept of a linear fit to the data pairs and the correlation coefficient are given for each panel.

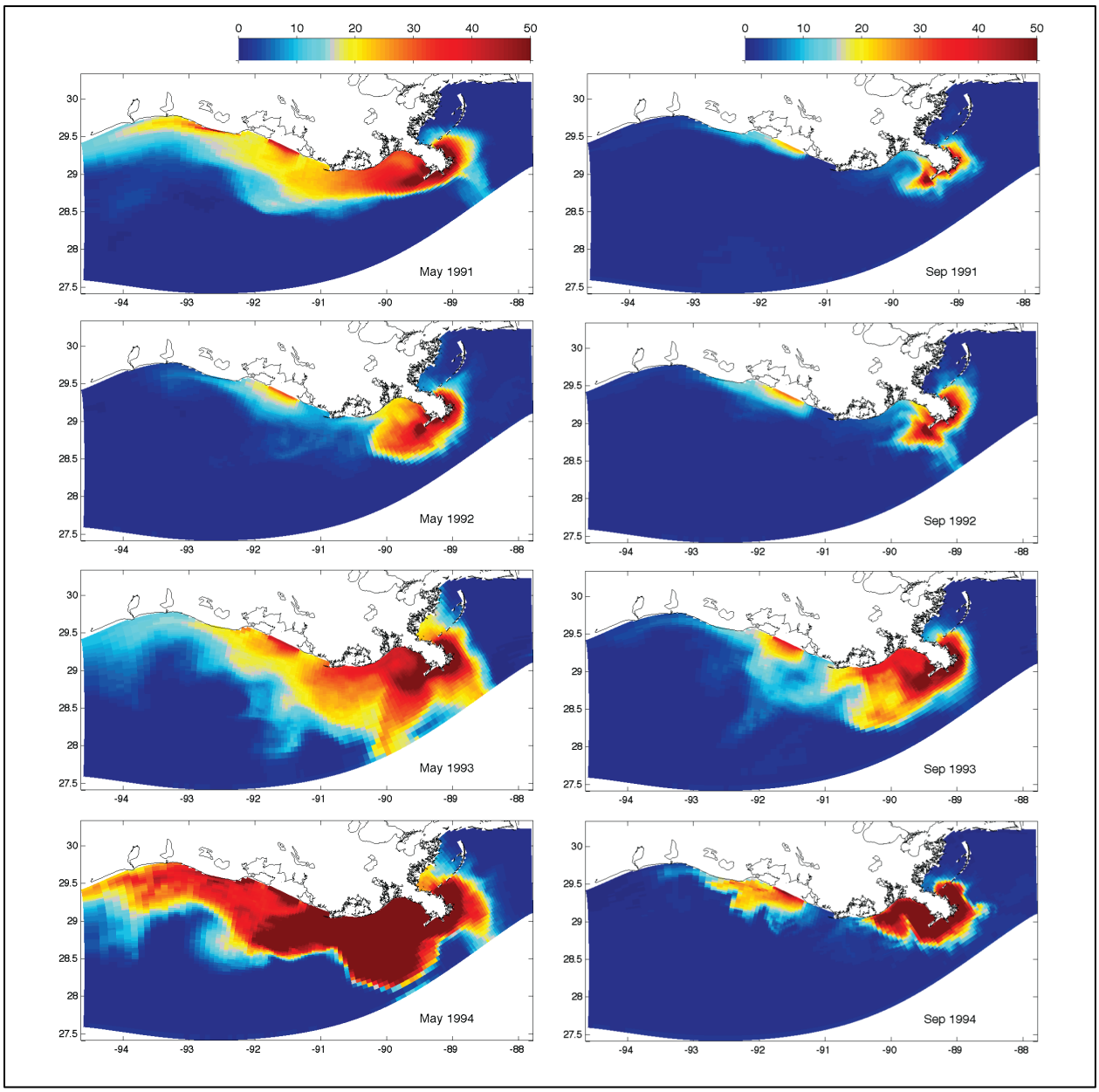

Figure 18: Simulated monthly mean DIN:PO_4 ratios at the surface for May (left column) and September (right column) for the years 1991 to 1994 (top to bottom). Yellow and red colors indicate the presence of excess DIN (suggesting P-limitation will occur as nutrients are being drawn down by phytoplankton uptake); blue colors indicate conditions conducive to N-limitation.

4.3.1 Model–Data Comparison: Sediment Accumulation

Short-lived radionuclides, including ^{137}Cs, ^{7}Be, and ^{210}Pb, have been widely-used to measure sediment accumulation rates for timescales of 150 days, 265 days and ~100 years, respectively. Since our model represented one year, we preferred to compare our estimate to available ^{137}Cs and ^{7}Be accumulation rates, but where these were unavailable, we used published ^{210}Pb accumulation rates. Radionuclides samples were not collected in 1993; we therefore used values from the literature for different years. The model estimated sediment accumulation rate near the Mississippi Delta was compared with ^{137}Cs accumulation rate derived by Allison et al. (2007). Offshore of the Atchafalaya Bay, only ^{210}Pb were available from Draut et al. (2005). Accumulation rates derived from ^{210}Pb may differ, however, from those based on ^{137}Cs / ^{7}Be by an order of magnitude. For instance, accumulation rates derived from ^{234}Th and ^{7}Be near the Mississippi subaqueous delta (0.8-3.9 cm/month) significantly exceeded those based on ^{210}Pb (1.3–2.0 cm/year) from the exactly same study sites (Corbett et al., 2004).

Model estimates (blue italic numbers and contour lines in Figure 19A) indicated that at the end of the model year the highest sediment accumulation (>5 cm/yr) was adjacent to the mouth of Southwest Pass of Mississippi delta, and decreased rapidly to 1 cm/yr about 20-40 km offshore. The modeled accumulation rates matched the observations obtained using ^{137}Cs radionuclide analysis of box cores collected in July 2003 (Allison et al., 2007). In addition, the modeled isopach captured the bird-foot shape of the Southwest Pass of Mississippi Delta (Figure 19A). Slight differences between modeled and observed accumulation rates seem reasonable given the fact that the year 1993 was a flood year while 2003 experienced normal discharge.

South of Atchafalaya Bay, modeled sediment accumulation rates peaked near the Bay mouth (>2 cm/yr), but decreased rapidly to 0.1 cm/yr around the 5m isobath (Figure 19B). Westward sediment flux was estimated along the inner-most shelf toward the Chenier Plain (Figure 19B). South of Atchafalaya Bay, ^{210}Pb accumulation rates (Draut et al., 2005; Allison et al., 2005) indicated that the inner shelf immediately adjacent to the Atchafalaya Bay mouth effectively sequestered fine-grained sediment (3-4 cm/yr), and that much of the Atchafalaya sediment was confined to the inner shelf landward of the 10 m isobath by the westward residual flow (Figure 19C). Modeled accumulation patterns were similar to ^{210}Pb, but more concentrated near the Bay mouth. The difference might be due to (a) the year 1993 was a flood year which caused higher/faster accumulation than that in normal years; (b) the model represented only a one-year time scale while ^{210}Pb characterized 100 years, and rare but severe hurricanes likely impact longer-term redistribution; (c) the simplification of Atchafalaya Bay might cause higher sediment accumulation directly offshore of the Bay mouth.

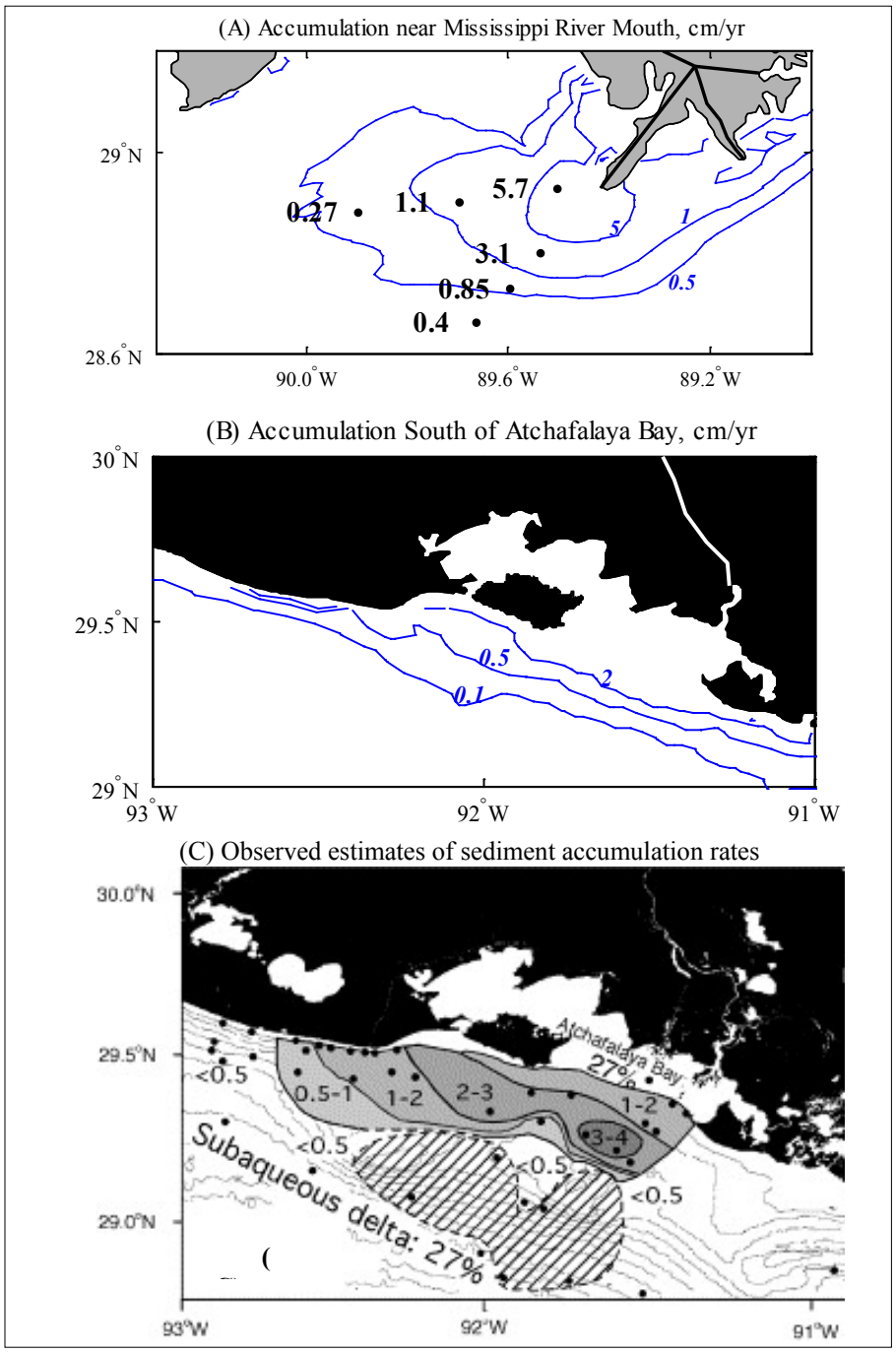

Figure 19: (A) Comparison between modeled sediment accumulation (contours of 0.5, 1, and 5 cm/yr in italics) with the rates derived from ^{137}Cs geochronology (in bold) at six sites by Allison et al. (2007). (B) Modeled 1-yr time scale sediment accumulation south of Atchafalaya Bay (contours of 0.1, 0.5, and 2 cm/yr). (C) Sediment accumulation rate (cm/yr) based on ^{210}Pb geochronology (100-yr time scale) and acoustic transects by Draut et al. (2005). The hatched area indicates shoals where relict sediment is exposed and Atchafalaya sediment accumulation is heterogeneous and poorly defined.

4.3.2 Overall Sediment and Wave Estimates for 1993

The 1993 sediment - wave model estimated that currents flowed westward at 0.1-0.2 m/s, being relatively strong on the shelf and weakening offshore (Figure 20A). Time-averaged wave height barely reached 1 m on the shelf and increased offshore (Figure 20C) in agreement with observations by Curray (1960). These waves generated near-bed orbital velocities that rarely exceeded 0.15 m/s, and decreased rapidly with water depth (Figure 20B). On average, bed stresses were only energetic enough to suspend muddy sediment in water shallower than 10 m, such as on the shoals south of Atchafalaya Bay. Time-averaged and depth-integrated suspended sediment in the water column was estimated to be as high as 1 kg/m^2 close to the mouths of Mississippi River and Atchafalaya Bay. Sediments from the Mississippi River spread around the delta and reached water depths of 300 m in the south. In contrast most of the Atchafalaya River sediment was confined to the inner-most part of the shelf (Figure 20D).

The model's estimate of cumulative deposition for 1993 resembled the pattern of suspended sediment (Figure 21A). In light of the relatively high settling velocities assumed for Mississippi sediment, about 90% of it accumulated within 20 km of the radius of the Delta, and most of the remaining 10% stayed within 50 km. Shokes (1976) and Rotter (1985) also concluded that the region of highest Mississippi accumulation was confined to a 20 km radius of distributary mouths (see Figure 21B). Less than 1% of Mississippi sediment was estimated to be transported to the middle shelf west of 90˚W. Most Atchafalaya sediment deposited landward of the 10-m isobath, settling quickly to the sea bed in the shallow water there. Coastal currents carried some Atchafalaya sediment westward to be deposited along the Chenier Plain (Figure 21A). The sandy shoals offshore of Atchafalaya Bay, however, did not accumulate much sediment during this one-year model run, consistent with Draut et al. (2005) observations of low modern accumulation there. This may be due to (a) perennial westward currents along the inner shelf that carry sediment away from the shoals (Figure 21A), and (b) stronger near bed wave orbital velocity on the sandy shoals causing more sediment resuspension (Figure 21B). In addition, DiMarco et al. (2010) showed that sandy shoals offshore of the Atchafalaya Bay enhance local ventilation and mixing in the water column.

4.3.3 Sediment and Wave Estimates: Storm of March 1993

From 12 to 17 March 1993, a large cyclonic storm passed the Gulf of Mexico. Named the "Storm of the Century" or "93 Super Storm," it was unique for its intensive snow fall, massive size, and wide-reaching effects along the eastern seaboard of the United States. While it was not exceptionally intense on the Louisiana-Texas shelf, it produced the biggest winds and waves of the year. The wind speed recorded at the Southwest Pass of the Mississippi Delta reached 26 m/s, and wave height calculated for the LATEX tetrapod location peaked at 3.7 m (Figure 4B). Wind direction was mainly to the south during the storm. This period coincided with the onset of flood water discharge from the Mississippi and Atchafalaya Rivers, but the antecedent water discharge was relatively low (Figure 4C).

For 12 to17 March 1993, the model estimated surface currents to be mainly toward the southwest, with fresh water (<30 ppt) confined to the inner and middle shelf (Figure 22A). Strong surface currents, as fast as 0.3 m/s, moved water offshore, while bottom waters flowed

shoreward under upwelling circulation (Figure 22C). Wave orbital velocity exceeded 0.1 m/s in water shallower than 10 m (Figure 22B). Under the influence of strong winds, turbulence from energetic currents mixed the water column. Sea surface sediment concentration was highest (~0.3 kg/m^3) next to fluvial sources and remained elevated (0.1 kg/m^3) over almost the entire shelf (Figure 22A). During these six days, the largest sediment fluxes were around the Mississippi Delta and Atchafalaya Bay mouth (Figure 22D). Mississippi sediment was transported offshore of the Mississippi Delta, indicating extensive storm remobilization of previously-deposited sediment on the delta front. During the storm, the maximum erosion was estimated to be about 2 centimeters around the Mississippi Delta. Atchafalaya sediment was transported mainly to the south and west.

Dominated by waves, bed shear stress peaked along the inner Louisiana-Texas shelf landward of the 20 m isobaths during the storm (Figure 23). Shear stresses due to currents were at least one order of magnitude smaller than those generated by waves, and most resuspension occurred in areas of high wave shear stresses (Figure 23B, C). Wave-generated shear stress, however, was reduced in the shallow water northeast of Mississippi Delta due to shielding by Chandelier Island. Current-generated shear stress was highest in shallow water, sometimes reaching the critical level (0.11 Pa) to suspend sediment (Figure 23C).

4.3.4 Sediment and Waves during Fairweather Conditions of May 1993

For comparison to the storm period, we considered hydrodynamics and sediment processes during relatively calm conditions in May 1993 that coincided with LATEX observations (Wright et al., 1997). At this time, winds were very weak in the northern Gulf of Mexico, barely reaching 10 m/s and the Mississippi and Atchafalaya River floodwaters were receding, but similar to levels seen during the March storm (Figure 4A, C). Sediment discharge was lower in May than in March (Figure 4D). Based on data from the tetrapod, the model did reasonably well at estimating wave orbital velocities that reached 13 cm/s at the tetrapod location (Figure 24).

Between May 11 and 22, surface currents were estimated to be weak and mainly offshore, impacted by seaward movement of river discharge (Figure 25 A). Because of high antecedent water discharge, surface water was fresher than normal. The area with salinity less than 30 ppt expanded compared to storm conditions, helping to stratify the water column (Figure 25). Sediment concentration was estimated to be very low in most areas: only areas shallower than 10 m and near the Mississippi Delta and Atchafalaya Bay had concentrations that reached 0.01 kg/m^3, about one order of magnitude smaller than the storm average (0.1 kg/m^3). Some sediment was estimated to be carried horizontally by fresh water plumes but the distances traveled did not generally exceed 50 km (Figure 25A). Wave-current-combined shear velocity only reached the critical level of 0.11 Pa in water shallower than 10m (Figure 26). In the inner shelf, waves still dominated shear stresses, but in the middle shelf between 20- and 50-m isobaths, waves and currents contributed equally to bed stresses in some areas (Figure 26).

4.3.5 Physical and Sediment Control on Hypoxia

Modeled physical and sediment conditions between mid-June and mid-July were compared with the distribution of hypoxic water in mid-July, 1993 as determined by Rabalais et al. (2002)

and shown in Figure 27C. Estimated stratification, defined as the density difference between surface and bottom water from the model, was relatively high on the entire Louisiana-Texas shelf (Figure 27A), Interestingly, most hypoxic water was located in the bottom boundary layer of the stratified water column (Figure 27A, C). Hypoxic water, however, did not develop in areas where the model indicated that depth-integrated suspended sediment exceeded 0.01 kg/m^2 (Figure 27B, C). Based on the comparisons, stratification seemed to facilitate the development of hypoxic water whereas turbid water tended to inhibit photosynthesis and thus hypoxia in the northern Gulf of Mexico.

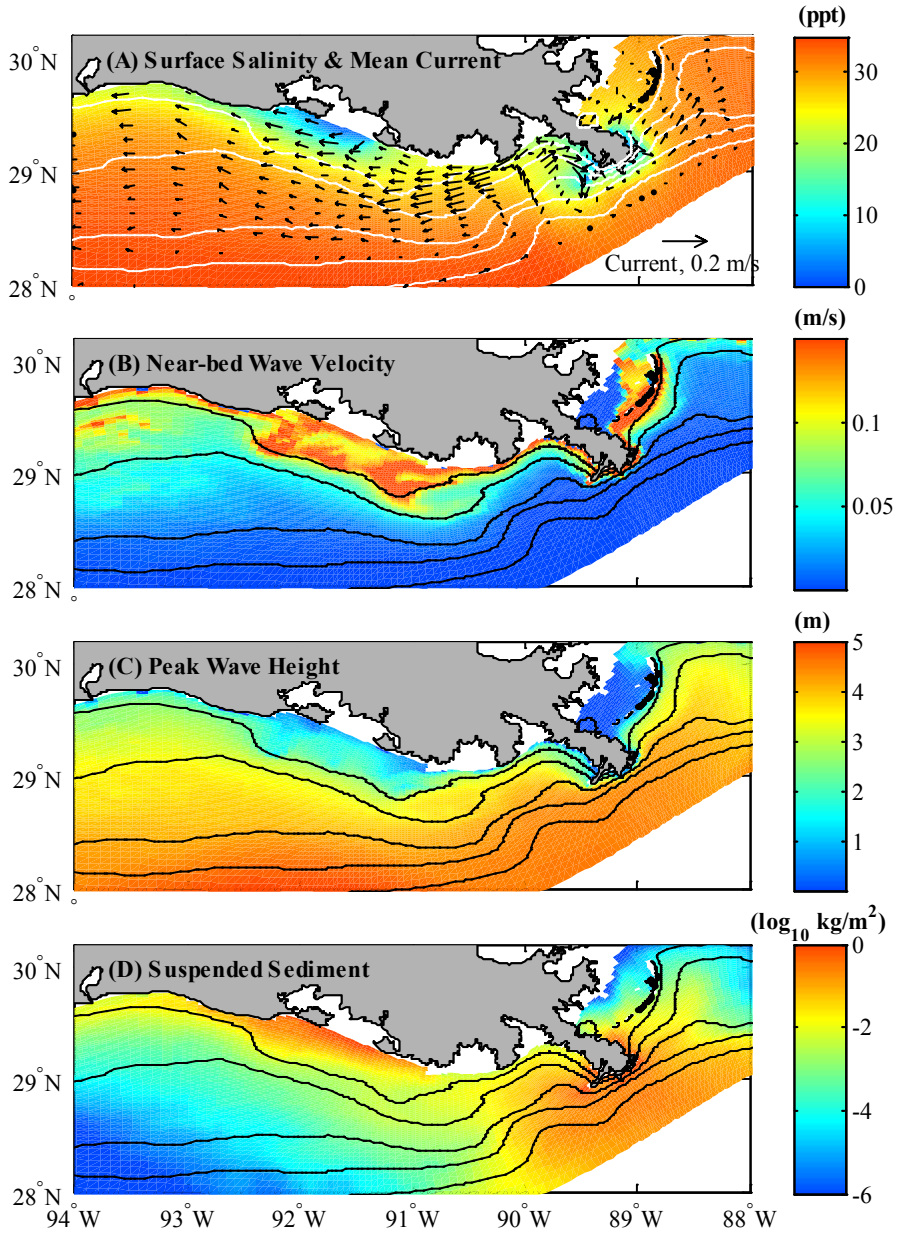

Figure 20: (A) Time-averaged surface salinity (ppt, color) and mean current (m/s) calculated for 1993. (B and C) Time-averaged near-bed wave orbital velocity (m/s) and significant wave height (m) estimated by SWAN. (D). Time-averaged and depth-integrated fluvial suspended sediment (kg/m2 in log scale) in the water column calculated for 1993. Isobaths drawn at 10, 20, 50, 100, 300 m water depths.

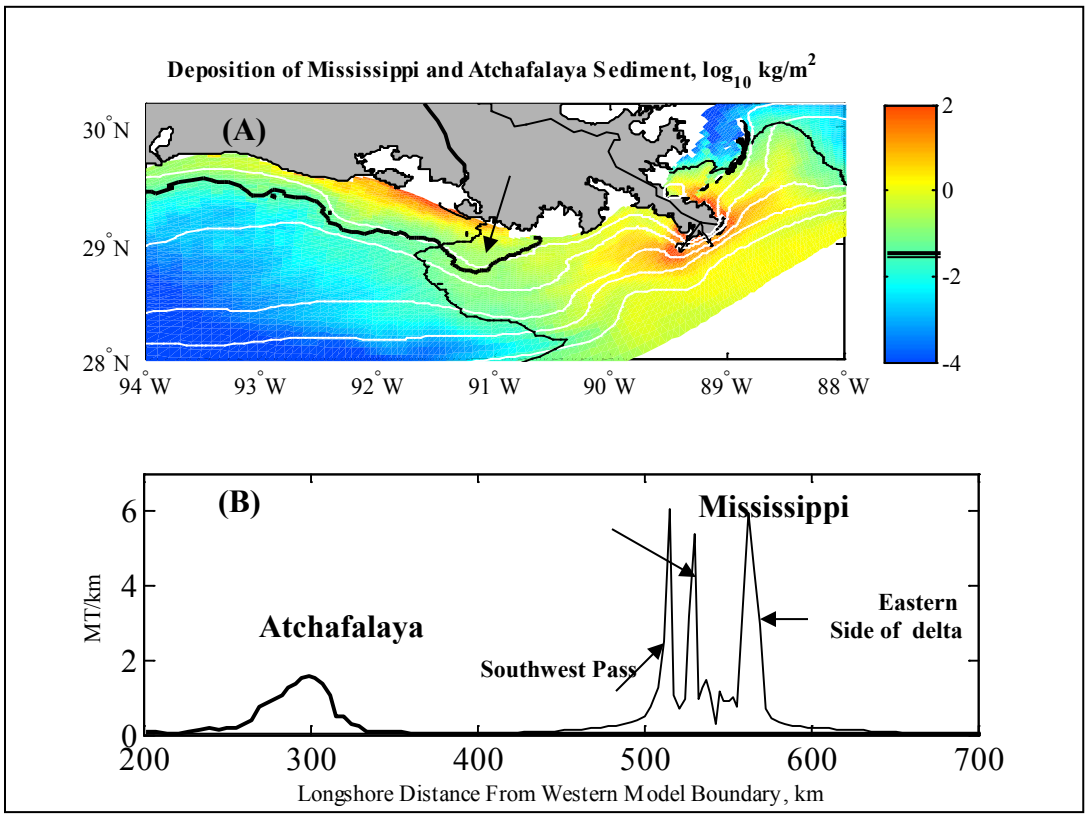

Figure 21: (A). Estimated deposition of both Mississippi and Atchafalaya sediment, overlaid by dispersal extents (at a level of 10-1.5 kg/m2, in regular and bold black lines respectively). Isobaths drawn at 10, 20, 50, 100, 300 m. (B) Longshore sediment deposition (MT/km, million tons per km) of Mississippi and Atchafalaya sediment on a linear scale.

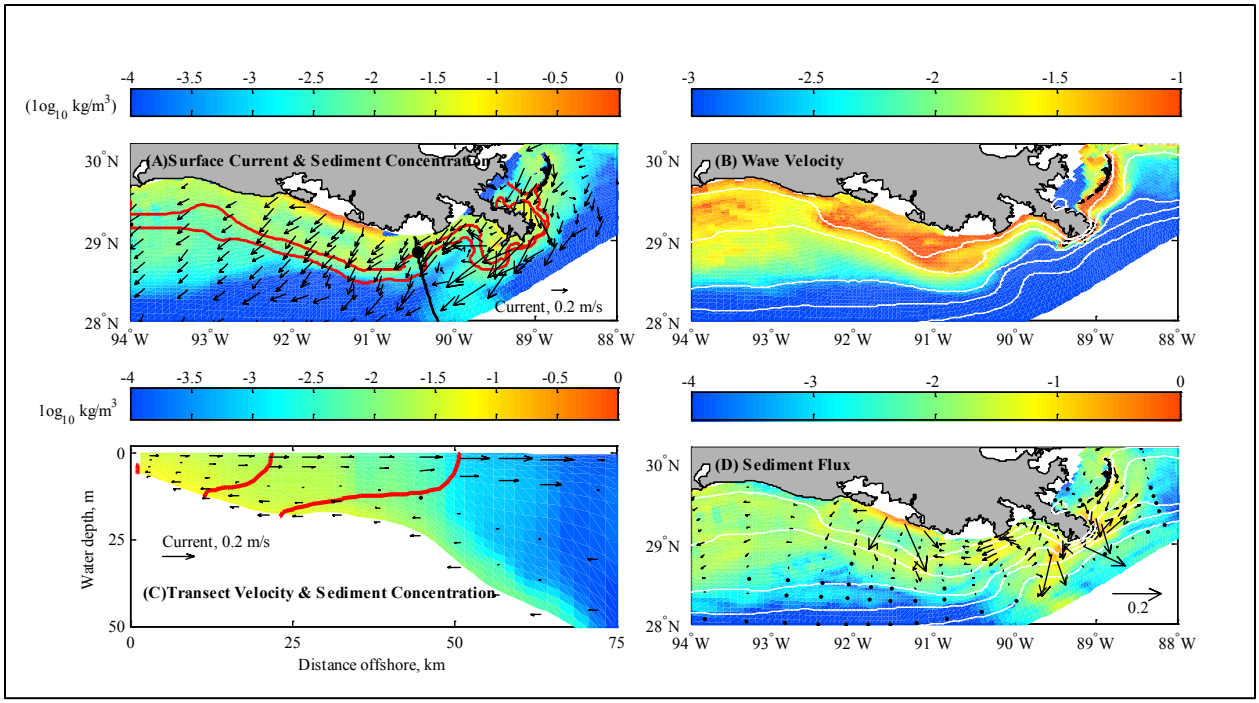

Figure 22: Calculations averaged for 12 – 17 March 1993. (A) Surface current (arrows, cm/s), sea surface sediment concentration (color, kg/m^3 on a logarithmic scale) with surface salinity contour lines at 30 and 32 ppt. (B) Mean near-bed wave orbital velocity in m/s on a logarithmic scale. (C) Current velocity (arrows) and sediment concentration (color, kg/m^3 on a logarithmic scale) for a cross-shelf transect that goes through the LATEX tetrapod (transect shown as a black line and tetrapod location shown as a black dot in panel A Salinity contoured at 30 and 32 ppt. (D) Sediment flux in kg/m/s. White isobaths in (B) and (D) are 10, 20, 50, 100, 300 m.

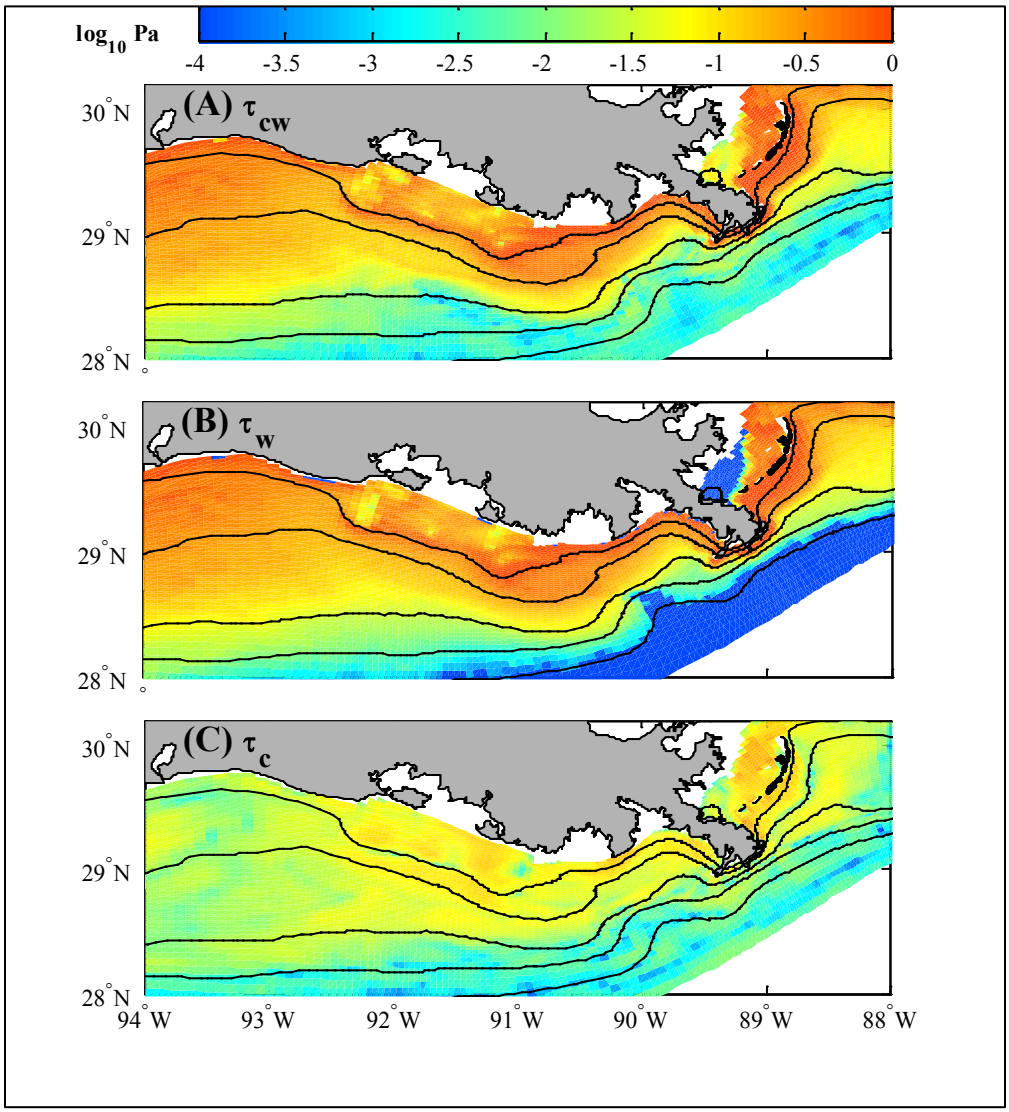

Figure 23: Bed shear stresses (Pa on a logarithmic scale) calculated for 12 – 17 March 1993. (A) Combined wave-current stress (τ_{cw}), (B) Wave component (τ_w), and (C) Current component (τ_c). Isobaths drawn 10, 20, 50, 100, 300 m.

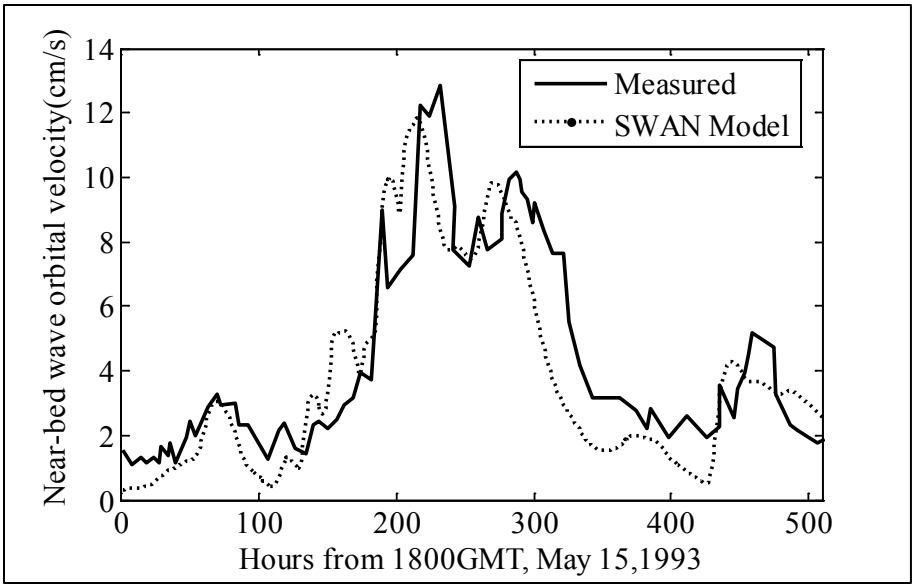

Figure 24: Comparison between measured (Wright et al., 1997) and modeled near-bed wave orbital velocity at the LATEX Tetrapod location (see Figure 1) for May 1993.

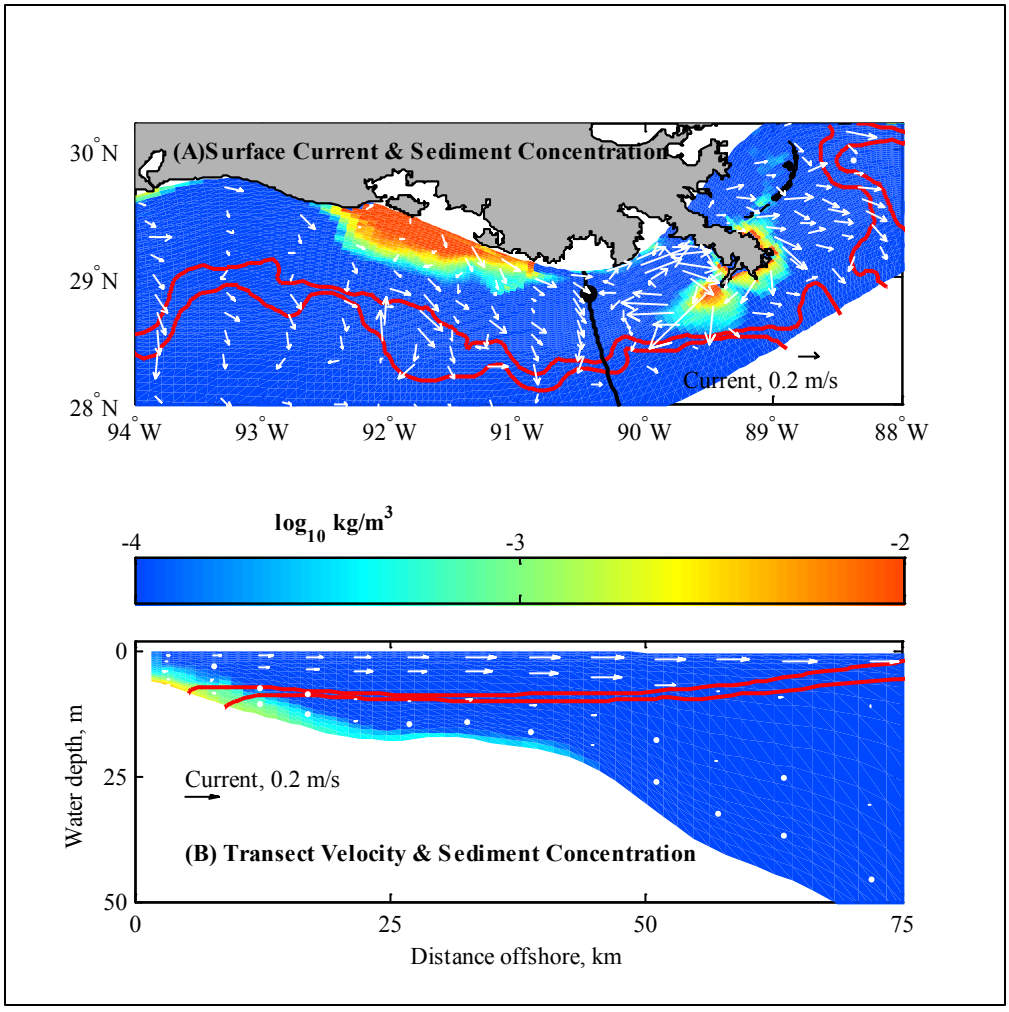

Figure 25: Averages calculated during the fair-weather period of 11 – 21 May, 1993. (A) Surface current (arrows, cm/s), sediment concentration (color, kg/m^3 on a logarithmic scale), and surface salinity contoured at 30 and 32 ppt. (B) Current velocity (arrows) and sediment concentration (color, kg/m^3 on a logarithmic scale) for a cross-shelf transect through the LATEX tetrapod (transect shown as a black line and tetrapod location shown as a black dot in panel A). Salinity contoured at 30 and 32 ppt.

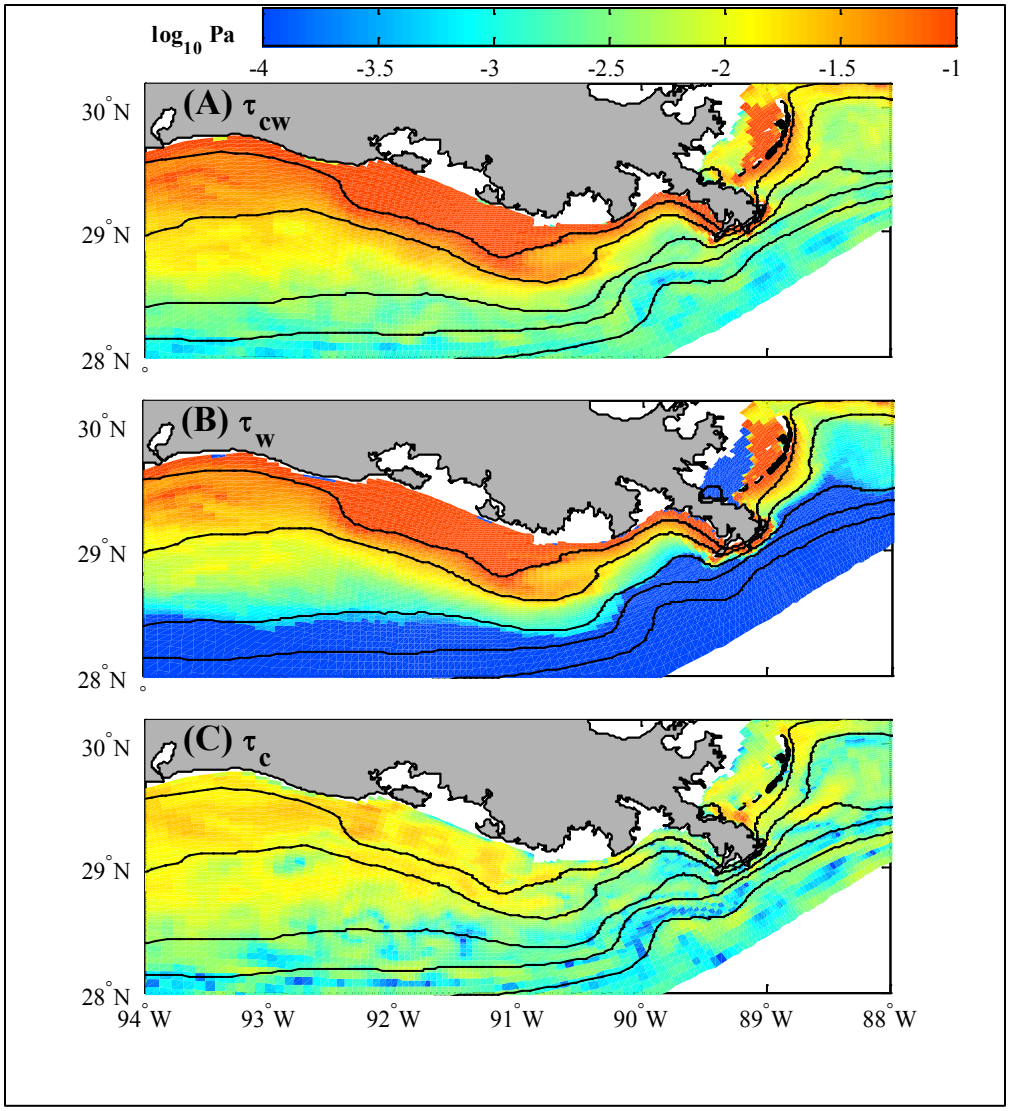

Figure 26: Bed shear stresses (Pa on a logarithmic scale) calculated for 11–21 May 1993. (A) Combined wave-current stress (τcw), (B) Wave component (τw), and (C) Current component (τc). Isobaths drawn 10, 20, 50, 100, 300 m.

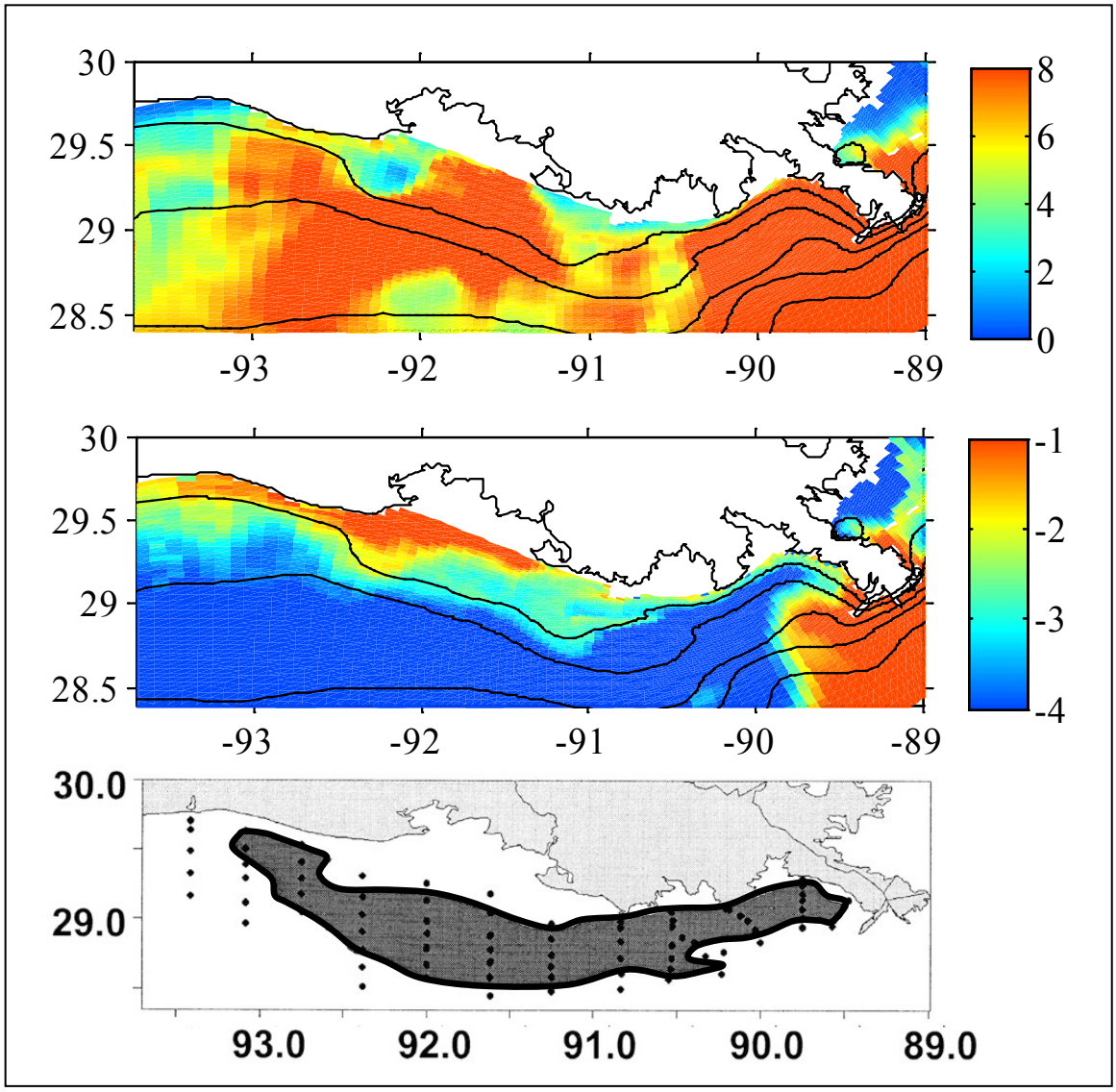

Figure 27: (A) Stratification calculated by subtracting surface from bottom water density in June 15-July 15, 1993. (B) Time-averaged and depth-integrated total suspended sediment (kg/m^2 in log scale) in water column calculated for the period of 15 June through 15 July 1993. (C) Hypoxic water (oxygen concentration less than 2 mg/L) observed around mid-July 1993 (from Rabalais et al. 2001). The boundary of hypoxic water is overlaid on stratification and sediment for comparison.

5. CONCLUSIONS AND RECOMENDATIONS

In this study we integrated a numerical hydrodynamical model of the Louisiana-Texas shelf with biogeochemical and sediment/wave components. The physical model was run for the years 1992-2008, the physical/biological model for the years 1990-1998, and the physical/sediment transport model for 1994, 2004, and 2005. These years were chosen based on available data for forcing and model skill assessment. The model showed good skill at reproducing standard physical property distributions of temperature, salinity, and current velocity of the shelf at multiple time and spatial scales when compared to observational data from the region. Eddy variability at the model boundary contributes noise at scale lengths of 20-50 km. The model can reproduce the seasonality, duration, severity, and time of onset of low oxygen concentration variability of the Louisiana-Texas shelf when compared to annual July shelfwide surveys of near bottom dissolved oxygen concentration. The sediment component of the numerical model showed that resuspension and transport of sediment loading is primarily driven by surface gravity wave activity.

Hydrodynamic model errors can generally be classified into two categories: large spatial- and temporal-scale errors (>50 km and >3 weeks) associated with offshore circulation not included in the present numerical model configuration, and small spatial- and temporal-scale errors (<50 km and <2 weeks) associated with mesoscale features on the shelf. Mesoscale features have been documented for the Louisiana-Texas shelf by DiMarco et al. (2010). Although, a portion of the observed mesoscale variability was linked to three shallow banks near the mouth of the Atchafalaya, this study suggests that such mesoscale features are ubiquitous. Comparisons between the simulated currents and salinity structure at the six mooring locations show an enhanced error variance at the eastern transect relative to the western transect. The eastern transect is west of the Mississippi River Delta, and east of the three topographic shoals, suggesting that the surface trapped Mississippi River plume is responsible for much of the energetic mesoscale variability there.

Large-scale errors in the numerical simulation may be corrected by including boundary conditions with a more accurate representation of the off-shelf circulation. However, it is not clear if the small scale errors may be corrected using data assimilation, as these features are poorly sampled either spatially or temporally. It is certainly possible that improvements in predicting small-scale features may be achieved using higher resolution, better bathymetry, or surface forcing. However, given our understanding of other mesoscale fields, it seems likely that a significant portion of the variance is chaotic, and therefore unpredictable.

To the extent which small-scale features are unpredictable, they must be considered unresolved by the model. The variance of small-scale features may be reduced in the simulation by either simplified or reduced physics, as done by Bogden et al. (1996), or by taking the mean of an ensemble of simulations. However, the error variance of these small-scale features must be added to the observational error variance. Because the observational error variance is a significant fraction of the total variance for tracer and flow fields over the Louisiana-Texas continental shelf, accurate predictions will require a greater number of measurements in these systems as compared to systems that do not contain such energetic small-scale flow fields.

The water column biogeochemical model describes the spatial and temporal patterns of nitrate and phytoplankton in agreement with observations and predicts rates of primary production and grazing that agree with experimentally determined rates. In the model differences in phytoplankton biomass and primary production across the ecological gradient from the delta, to the intermediate and far- field region are not primarily driven by differences in phytoplankton growth rates, but by differences in phytoplankton losses. While phytoplankton growth rates are similar, there are pronounced spatial differences in the rate of phytoplankton accumulation and phytoplankton losses, and there is a net transport of phytoplankton from the delta to the intermediate region and into the far-field region.

Our model shows that the existence of a statistically significant correlation between primary production and nitrogen load in the delta region near the Mississippi River delta does not reflect a direct stimulation of phytoplankton growth by nutrients as expected given the lack of nutrient-limitation in this region. When investigating this relationship it is necessary to first remove the seasonal cycle or, since this is less practical with sparse observational data sets, take into account the autocorrelation between primary production and nitrogen load by increasing the degrees of freedom and adjusting the p-levels appropriately. We find a statistically significant relationship between anomalies of primary production and nitrogen load for the months of June through September. We also find a statistically significant relationship between the anomalies of phytoplankton biomass and nitrogen load for the same months, but not for the anomalies of phytoplankton growth rates and nitrogen load. Since primary production is the product of growth rate and phytoplankton biomass the relationship between primary production and nitrogen load simply reflects the relationship between phytoplankton biomass and nitrogen load, which results from differences in phytoplankton accumulation likely due to differences in loss terms. We hypothesize that higher rates of biomass accumulation in high discharge years result from stronger retention of river water near the delta.

Using the sediment transport model, coupled to the SWAN wave model, we estimated the dispersal of Mississippi and Atchafalaya sediment on the Louisiana-Texas shelf. Our model year 1993 included a large storm in March, high discharge in spring-summer, and a typical fair-weather period in summer. Based on model estimates, we concluded the following. For the year 1993, the model reproduced both hydrodynamic conditions and sediment dispersal on the Louisiana-Texas shelf. Sediment deposition was highly localized: the pattern of Mississippi deposition was “bird-foot” shaped and rounded whereas that of the Atchafalaya accumulation was narrow and elongated. Due to high settling velocities assumed for Mississippi flocs and shallow bathymetry offshore the Atchafalaya Bay, most sediment only traveled a short distance (20 to 40 km) before initial deposition. Mississippi sediment was more widely dispersed due to deep water depth (thus longer settling time), steep slope and highly variable mean-current direction. The westward “elongated” dispersal of Atchafalaya sediment was mainly due to shallowness of water depth, stronger wave suspension and perennially-westward depth-averaged currents south of the Atchafalaya Bay. During fair-weather conditions, the Mississippi River plumes spread onto the stratified shelf water column. Wave-current-combined shear stress episodically reached the critical level sufficient to resuspend sediment at depths shallower than 10m. During the storm of March 1993, sediment flux peaked near the Mississippi subaqueous delta and Atchafalaya Bay mouth, and most resuspension occurred in areas where wave shear stresses dominated total bed stresses. Longshore sediment-transport fluxes were generally greater

than cross-shore fluxes at both Mississippi Delta and Atchafalaya Bay areas. The flux changes in the Atchafalaya were episodic and "stepwise-like" (flat lines after sudden changes) whereas these around the Mississippi were relatively gradual.

5.1 RECOMMENDATIONS FOR FUTURE WORK

The integrated physical-biogeochemical-sediment model developed in this study has been shown to provide reasonable simulations of seasonal hypoxia of the Louisiana-Texas shelf. This model is appropriate for use in other hazards known to occur in the northern Gulf of Mexico including oil spill prediction and fate. In light of the Macondo *Deepwater Horizon* disaster of 2010, a coupled hydrodynamic model circulation model which includes biological activity and vertical transformations of spilled oil can be useful for determining fate and impacts on living resources. Future model development could include nested vertical oil plume dynamics and transformation, surface weathering, and biological degradation.

Nesting the shelf model into a basin scale mesoscale model of the Gulf of Mexico will allow offshore features such as the Loop Current and its associated eddies to influence shelf and river plume dynamics, particularly in the eastern region of the Louisiana-Texas shelf. We note that currently several independent, separately funded modeling activities by the Principal Investigators of this study will work toward developing methods to nest a shelf model in the larger scale model.

One of the important findings of this study was the presence of an energetic mesoscale eddy field in the vicinity of the Mississippi/Atchafalaya River plume front. It is not yet clear if the prediction of this eddy field could be improved through modern data assimilation techniques. Future work could include a study of the temporal and spatial scales required for observations to define this field, and improve predictions of the shelf. This might also include an effort to identify critical points along the shelf where observations are effective in defining the flow state.

We still lack critical information on many important aspects of the mesoscale eddy field. For example, we do not understand the mechanisms which cause these eddies to form. DiMarco et al. (2010) suggest that topographic effects are important in creating mesoscale features near three shoals south of Atchafalaya Bay, but we do not know if this process is true for the remainder of the shelf. We do not yet understand the seasonality of these eddies. Numerical model results suggest that these eddies are more prevalent in the summer, however, this has not been quantified. Finally, we do not yet understand how the mesoscale eddy field relates to biogeochemical or sediment transport processes. For example, we do not know to what extent this mesoscale field enhances cross-shore transport of carbon, nitrogen, phosphorus, and other biogeochemical constituents. Future work should focus on describing the mesoscale eddy field, and investigating its effects on shelf processes.

The physical modeling domain has been recently been extended, with other funding, to include the entire Louisiana and Texas coasts. However, this model has not yet been tested with the biogeochemical or sediment transport modules. The advantages of this new domain are that essentially the entire along-shore extent of the Mississippi/Atchafalaya plume is resolved. The

model also has higher resolution, and is better able to resolve bathymetric features and the initial simulations show a well-developed mesoscale eddy field. We would like to use this extended and revised model as the basis for future work in the region.

REFERENCES

Allison, M.A., T.S. Bianchi, B.A. McKee and T.P. Sampere. **2007**. Carbon burial on river-dominated continental shelves: Impact of historical changes in sediment loading adjacent to the Mississippi River. *Geophys. Res. Lett.* **34**(L01606), doi:10.1029/2006GL028362.

Allison, M.A., G.C. Kineke, E.S. Gordon and M.A. Goñi. **2000**. Development and reworking of a seasonal flood deposit on the inner continental shelf off the Atchafalaya River. *Continental Shelf Research* **20**(16), 2267-2294.

Allison, M.A., A. Sheremet, M.A. Gõni and G.W. Stone. **2005**. Storm layer deposition on the Mississippi-Atchafalaya subaqueous delta generated by Hurricane Lili in 2002. *Continental Shelf Research* **25**:2213-2232.

Aulenbach, B.T., H.T. Buxton, W.A. Battaglin, and R.H. Coupe. **2007**, Streamflow and nutrient fluxes of the Mississippi-Atchafalaya River Basin and subbasins for the period of record through 2005: U.S. Geological Survey Open-File Report 2007-1080.

Bever, A.J., C.K. Harris, C.R. Sherwood and R.P. Signell. **2009**. Deposition and flux of sediment from the Po River, Italy: an idealized and wintertime numerical modeling study. *Marine Geology*, **260**(1-4): 69 – 80.

Bogden,P.S., P. Malanotte-Rizzoli and R.P. Signell. **1996**. Open-ocean boundary conditions from interior data: Local and remote forcing of Massachussetts Bay. *J. Geophy. Res.* **101**, 6487-6500.

Booij, N., R.C. Ris, and L.H. Holthuijsen. **1999**. A third generation wave model for coastal regions. 1. Model description and validation. *J. Geophys. Res.* **104**, 7649-7666.

Brezonik, P.L., V.J. Bierman, R. Alexander, J. Anderson, J. Barko, M. Dortch, L. Hatch, G.L. Hitchcock, D. Keeney, D. Mulla, V. Smith, C. Walker, T. Whitledge and W.J. Wiseman. **1999**. Effects of reducing nutrient loads to surface waters within the Mississippi River Basin and the Gulf of Mexico: Topic 4 Report for the Integrated Assessment on Hypoxia in the Gulf of Mexico. NOAA Coastal Ocean Program Decision Analysis Series No. 18. NOAA Coastal Ocean Program, Silver Spring, MD. 158 pp.

Cho, K., R.O. Reid and W.D. Nowlin. **1998**. Objectively mapped stream function fields on the Texas-Louisiana shelf based on 32 months of moored current meter data. *J. Geophys. Res.*, **103**(C5):10,377–10,390.

Cochrane, J. D. and F.J. Kelly. **1986**. Low-frequency circulation on the Texas-Louisiana Continental Shelf. *J. Geophys. Res.*, **91**(C9):10,645–10,659.

Corbett, D.R., B. McKee and D. Duncan. **2004**. An evaluation of mobile mud dynamics in the Mississippi River deltaic region. *Marine Geology* **209**(1-4): 91-112.

Curray, J.R., **1960**. Sediments and history of the Holocene transgression Continental Shelf, Northwest Gulf of Mexico. Recent sediments Northwest Gulf of Mexico. *Amer. Assoc. Petrol. Geol. Bull.,* Tulsa, OK, 221–226 pp.

da Silva, A.M., C.C. Young-Molling, and S. Levitus. **1994a**. Atlas of surface marine data 1994 Vol. 3: Anomalies of fluxes of heat and momentum. NOAA Atlas NESDIS 8. Technical report, U.S. Gov. Printing Office, Wash., D.C.

da Silva, A.M., Young-Molling, C. C., and Levitus, S. **1994b**. Atlas of surface marine data 1994 Vol. 4: Anomalies of fresh water fluxes. NOAA Atlas NESDIS 9. Technical report, U.S. Gov. Printing Office, Wash., D.C.

Demas, C. **2007**. (United States Geological Survey, Louisiana State USGS Representative) Personal communications, email.

Devol, A. H. **2008**. Chapter 6: Denitrification including anammox, In: C. Capone, E. Carpenter, M. Mullholland, and D. Bronk editors, Nitrogen in the marine environment, Amsterdam, Elsevier, pp.263–302.

DiMarco, S.F., A.E Jochens, M.K. Howard. **1997**. LATEX Shelf Data Report: Current Meter Moorings, April 1992 to December 1994, Texas-Louisiana Shelf circulation and transport processes study, National Oceanographic Data Center, National Oceanic and Atmospheric Administration.http://ols.nndc.noaa.gov/plolstore/plsql/olstore.prodspecific?prodnum=W00026-CDR- S0001.

DiMarco, S. F. and R.O. Reid. **1998**. Characterization of the principal tidal current constituents on the
Texas-Louisiana Shelf. *J.Geophys.Res*.**103**(2),3093–3110.

DiMarco, S.F., P. Chapman, N. Walker, and R.D. Hetland. **2010**. Does local topography control hypoxia on the eastern Texas-Louisiana Shelf? *Journal of Marine Systems* **80**(1-2), 25-35.

Draut, A.E., G.C. Kineke, O.K. Huh, J.M. Grymes III, K.A. Westphal and C.C. Moeller. **2005**. Coastal mudflat accretion under energetic conditions, Louisiana chenier-plain coast, USA. *Marine Geology* **214**(1-3), 27-47.

Fennel, K., J. Wilkin, J. Levin, J. Moisan, J. O'Reilly and D. Haidvogel, D. **2006**. Nitrogen cycling in the Middle Atlantic Bight: Results from a three-dimensional model and implications for the North Atlantic nitrogen budget. *Global Biogeochemical Cycles* 20, GB3007, doi:10.1029/2005GB002456.

Flather, R. A. **1976**. A tidal model of the northwest Euopean continental shelf. *Memoires de la Societe Royale des Sciences de Liege*, **10**(6):141–164.

Galperin, B., L. H. Kantha and A. Rosati. **1988**. A quasi-equilibrium turbulent energy model for geophysical flows. *J. Atmos. Sci.*, **45**:55–62.

Garcia, H. E., and L.I. Gordon. **1992**. Oxygen solubility in seawater: Better fitting equations. *Limnology and Oceanography* **37**:1307-1312.

Gruber, N., H. Frenzel, S.C. Doney, P. Marchesiello, J.C. McWilliams, J.R. Moisan, J.J. Oram, G.K. Plattner, K.D. Stolzenbach. **2006**. Eddy-resolving simulation of plankton ecosystem dynamics in the California Current System, *Deep-Sea Research I*, **55**(9), 1483-1516.

Harris, C.K., C.R. Sherwood, R.P. Signell, A.J. Bever and J.C. Warner. **2008**. Sediment dispersal in the northwestern Adriatic Sea. *J. Geophys. Res*., **113**(C11S03): doi:10.1029/2006JC003868.

Harris, C.K. and P. L. Wiberg. **2001**. A two-dimensional, time-dependent model of suspended sediment transport and bed reworking for continental shelves. *Comput. Geosci*. **27**: 675-690.

Hetland, R.D. **2005**. Event-driven model skill assessment. *Ocean Modelling*, **11**(1- 2):214–223.

Hetland, R.D. and S.F. DiMarco. **2008**. How does the character of oxygen demand control the structure of hypoxia on the Texas-Louisiana continental shelf? *Journal of Marine Systems*, **70:**49-62, doi:10.1016/j.jmarsys.2007.03.002.

Hetland, R.D., and R.P. Signell. **2005** Modelling coastal current transport in the Gulf of Maine, *Deep-Sea Res. II*, **52**:2430-2449.

Justic D., N.N. Rabalais and R.E. Turner. **2002**. Modeling the impacts of decadal changes in riverine nutrient fluxes on coastal eutrophication near the Mississippi River delta, *Ecological Modeling* **152**: 33-46.

Marchesiello, P., J.C. McWilliams and A. Shchepetkin. **2001**. Open boundary condition for long-term integration of regional oceanic models. *Ocean Modeling* **3**:1–20.

Meade, R.H. and J.A. Moody. **2008**. The discharge of sediment through the Missouri-Mississippi River system, 1940-2007, Proceedings of VIII Encontro Nacional de Engenharia de Sedimentos, Campo Grande, Brazil.

Mellor, G. L. and T. Yamada. **1974**. A heirarchy of turbulent closure models for planetary boundary layers. *J. Atmos. Sci.*, **31**:1791–1806.

Neill, C.F. and M.A. Allison. **2005**. Subaqueous deltaic formation on the Atchafalaya Shelf, Louisiana. *Marine Geology* **214**(4): 411-430.

Nowlin, W. D., A.E. Jochens, S.F. DiMarco, R.O. Reid, and M.K. Howard. **2005**. Low-frequency circulation over the Texas-Louisiana Continental Shelf. In: Wilton and Lugo-

Fernandez, A., editors, Circulation in the Gulf of Mexico, American Geophysical Union pp. 219–240.

Oschlies, A. **2001**. Model-derived estimates of new production: New results point towards lower values, *Deep-Sea Res. II*, **48**:2173-2197.

Rabalais, N. N., R.E. Turner, W.J. Wiseman Jr. **2001**. Hypoxia in the Gulf of Mexico, *Journal of Environmental Quality* **30**:320-329.

Rabalais, N. N., R.E. Turner, Q. Dortch, D. Justic, V.J. Bierman and W.J. Wiseman Jr. **2002**. Nutrient-enhanced productivity in the northern Gulf of Mexico: past, present and future*, Hydrobiologia,* **475**:39-63.

Roberts H.H. **1998**. Delta Switching: Early responses to the Atchafalaya River Diversion, *Journal of Coastal Research*, **14**, no. 3, 882-899

Rotter, R.J. 1985. Pb^{210} and $Pu^{239,240}$ in nearshore Gulf of Mexico sediments. Unpublished M.S. Thesis, Texas A&M University, College Station, TX, 156 pp.

Rowe, G.T. M.E. Cruz-Kaegi, J. Morse, G. Boland, and E. Escobar Briones. **2002**. Sediment community metabolism associated with continental shelf hypoxia, northern Gulf of Mexcio. *Estuaries* **25**, 1097-11-6.

Scavia, D., N.N. Rabalais, R.E. Turner, D. Justic, and W.J. Wiseman, Jr. **2003**. Predicting the response of Gulf of Mexico hypoxia to variations in Mississippi River nitrogen load. *Limnology and Oceanography*, **48**(3):951–956

Shchepetkin, A. F. and J.C. McWilliams. **2005**. The regional oceanic modeling system (ROMS): a split-explicit, free-surface, topographically-following-coordinate oceanic model. *Ocean Modelling*, **9**:347–404.

Seitzinger, S. P. and A.E. Giblin. **1996**. Estimating denitrification in North Atlantic continental shelf sediments*, Biogeochemistry*, **35**: 235–260.

Shokes, R.F. 1976. Rate-dependent distributions of Pb-210 and interstitial sulfate in sediments of the Mississippi River delta. Unpublished Ph.D. Thesis, Texas A&M University, College Station, TX, 96pp.

Styles, R., and S.M. Glenn. **2000**. Modeling stratified wave and current bottom boundary layers on the continental shelf. *Journal of Geophysical Research*, **105**:24,119-24,130.

Sylvan J.B., Q. Dortch, D.M. Nelson, A.F. Maier Brown, W. Morrison and J.W. Ammerman. **2006**. Phosphorus limits phytoplankton growth on the Louisiana shelf during the period of hypoxia formation. *Environ Sci & Technol* **40**:7548-7553, doi:10.1021/es061417t.

U. S. Dept. of the Interior. Geological Survey. **2004**. A science strategy to support management decisions relating to hypoxia in the Northern Gulf of Mexico and excess nutrients in the

Mississippi River Basin. Mississippi River/Gulf of Mexico Watershed Nutrient Task Force, U.S. Geological Survey Circular 1270, 58 pp.

Wanninkhof, R. **1992**. Relationship between wind-speed and gas-exchange over the ocean. *J. Geophys. Res.-Oceans* **97**:7373-7382.

Wang, W., W.D. Nowlin and R.O. Reid. **1998**. Analyzed surface meteorological fields over the northwestern Gulf of Mexico for 1992–94: mean, seasonal, and monthly patterns. *Monthly Weather Rev.* **126** (11): 2864–2883.

Warner, J.C., C.R. Sherwood, R.P. Signell, C.K. Harris and H.G. Aragno. **2008**. Development of a three-dimensional, regional, coupled wave, current and sediment-transport model. *Computers & Geosciences* **34**:1284-1306.

Wells, J.T., S.J. Chinburg and J.M. Coleman. **1984**. The Atchafalaya River delta, Report 4: Generic analysis of delta development. US Army Corps of Engineers, Technical Report HL 82–15, Vicksburg, MS.

Wiberg, P.L. and C.K. Harris. **1994**. Ripple geometry in wave-dominated environments. *Journal of Geophysical Research* **99**: 775-789.

Williams, S.J., M.A. Arsenault, B.J. Buczkowski, J.A. Reid, J.G. Flocks, M.A. Kulp, S. Penland and C.J. Jenkins. **2006**. Surficial sediment character of the Louisiana offshore Continental Shelf region: a GIS Compilation. U.S. Geological Survey Open-File Report 2006-1195, online at http://pubs.usgs.gov/of/2006/1195/index.htm.

Williams, S.J., M.A. Arsenaul, B.J. Buczkowski, J.A. Reid, J.G. Flocks, M.A. Kulp, P.S. Penland, and C.J. Jenkins. **2007**. Surficial Sediment Character of the Louisiana Offshore Continental Shelf Region: A GIS Compilation, USGS Open-File Report 2006-1195.

Wright, L.D., C.R. Sherwood and R.W. Sternberg. **1997**. Field measurements of fairweather bottom boundary layer processes and sediment suspension on the Louisiana inner continental shelf. *Marine Geology*, **140**:329-345.

APPENDIX A

Weekly snapshots of simulated bottom water oxygen concentration in mmol O_2 m^{-3} for July, August and September from1990 to 1998. Hypoxic conditions (defined here as oxygen concentrations below 60 mmol O_2 m^{-3}) are shown in purple. In this model simulation the temperature- and oxygen-dependent parameterization for sediment oxygen demand of Hetland and DiMarco (2008) is imposed.

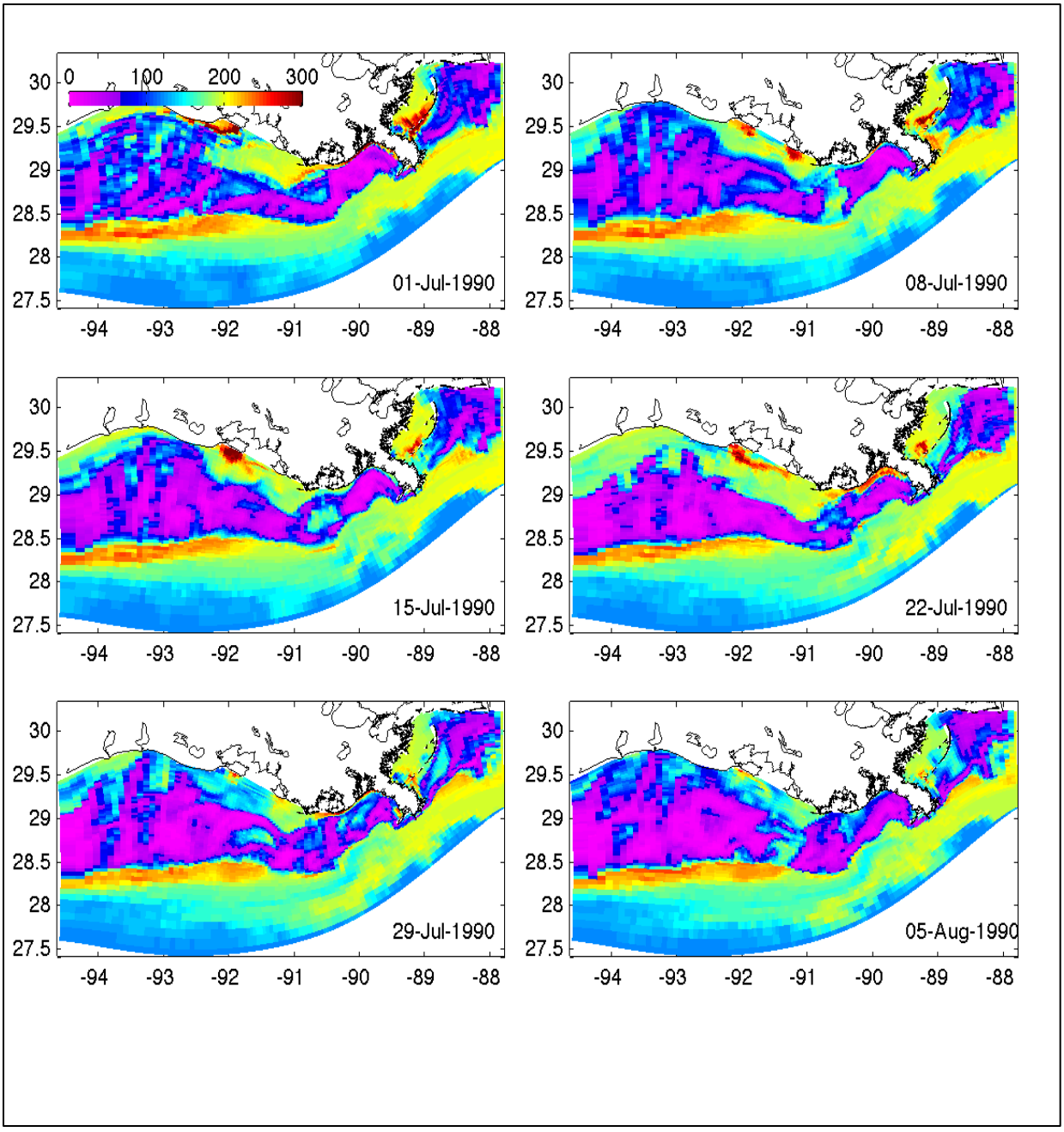

Figure A-1: Weekly snapshots of simulated bottom water oxygen concentration in mmol O_2 m^{-3} for July, August and September from1990 to 1998. Hypoxic conditions (defined here as oxygen concentrations below 60 mmol O_2 m^{-3}) are shown in purple. In this model simulation the temperature- and oxygen-dependent parameterization for sediment oxygen demand of Hetland and DiMarco (2008) is imposed.

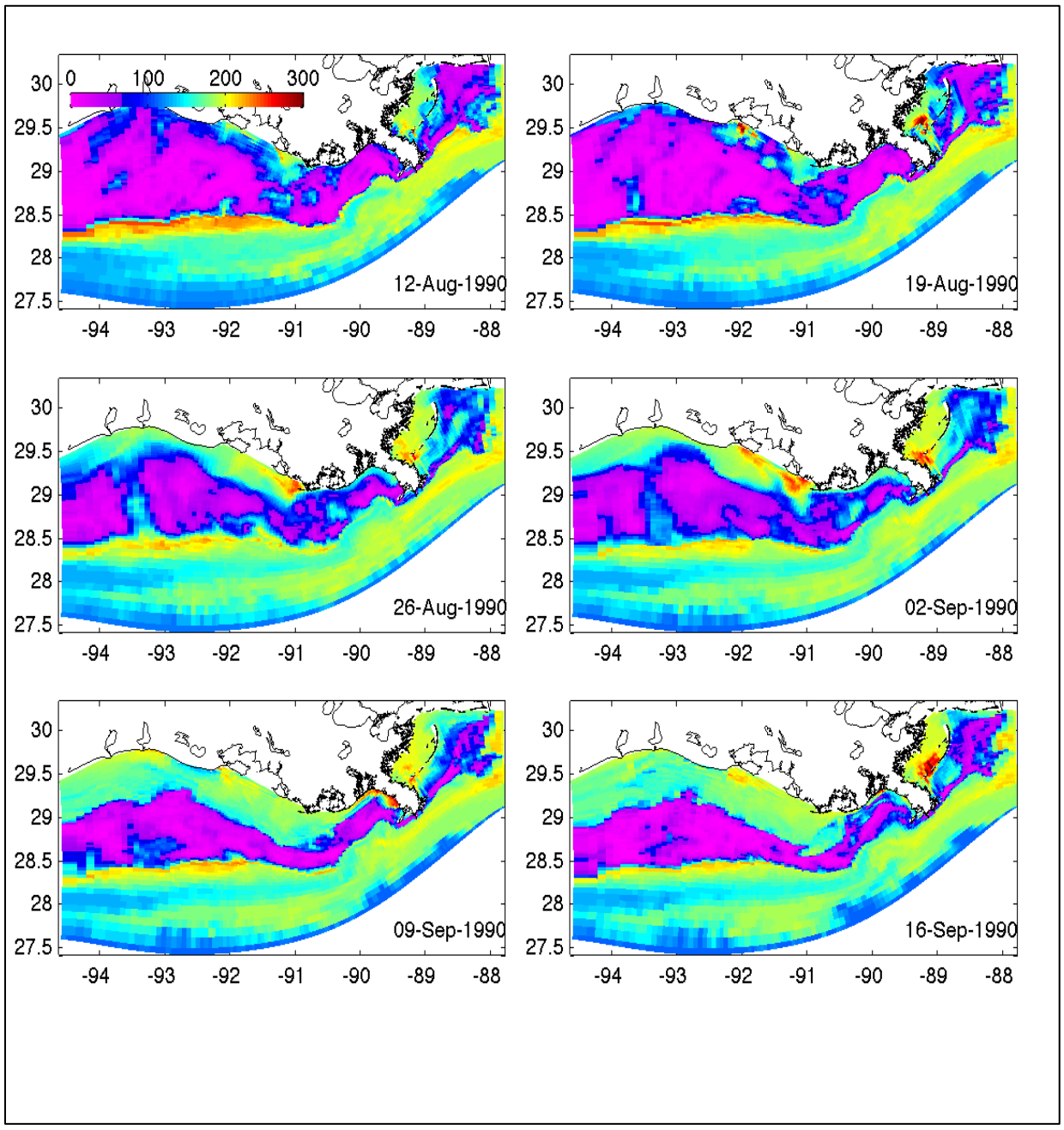

Figure A-2: Weekly snapshots of simulated bottom water oxygen concentration in mmol O_2 m^{-3} for July, August and September from1990 to 1998. Hypoxic conditions (defined here as oxygen concentrations below 60 mmol O_2 m^{-3}) are shown in purple. In this model simulation the temperature- and oxygen-dependent parameterization for sediment oxygen demand of Hetland and DiMarco (2008) is imposed.

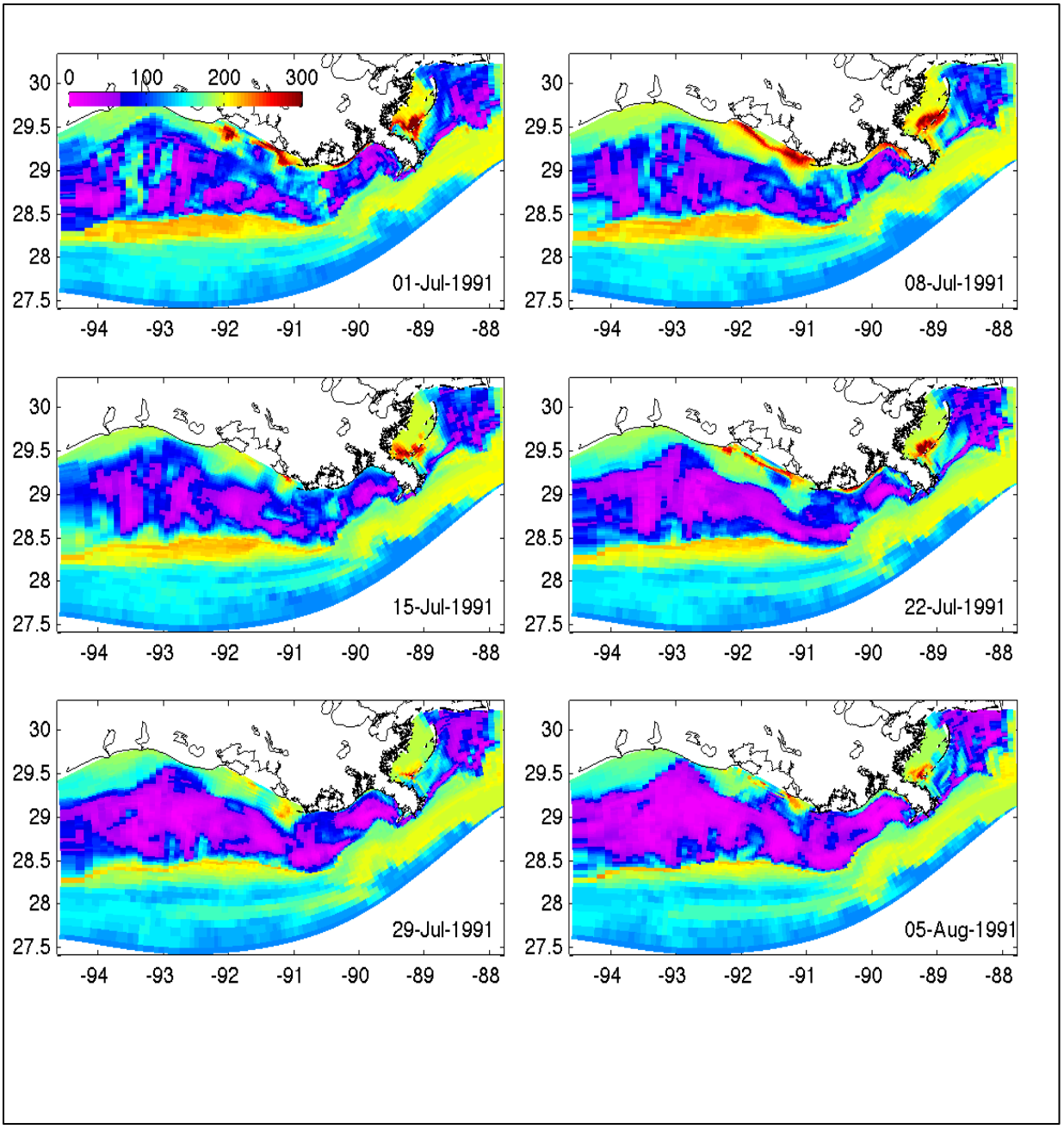

Figure A-3: Weekly snapshots of simulated bottom water oxygen concentration in mmol O_2 m^{-3} for July, August and September from1990 to 1998. Hypoxic conditions (defined here as oxygen concentrations below 60 mmol O_2 m^{-3}) are shown in purple. In this model simulation the temperature- and oxygen-dependent parameterization for sediment oxygen demand of Hetland and DiMarco (2008) is imposed.

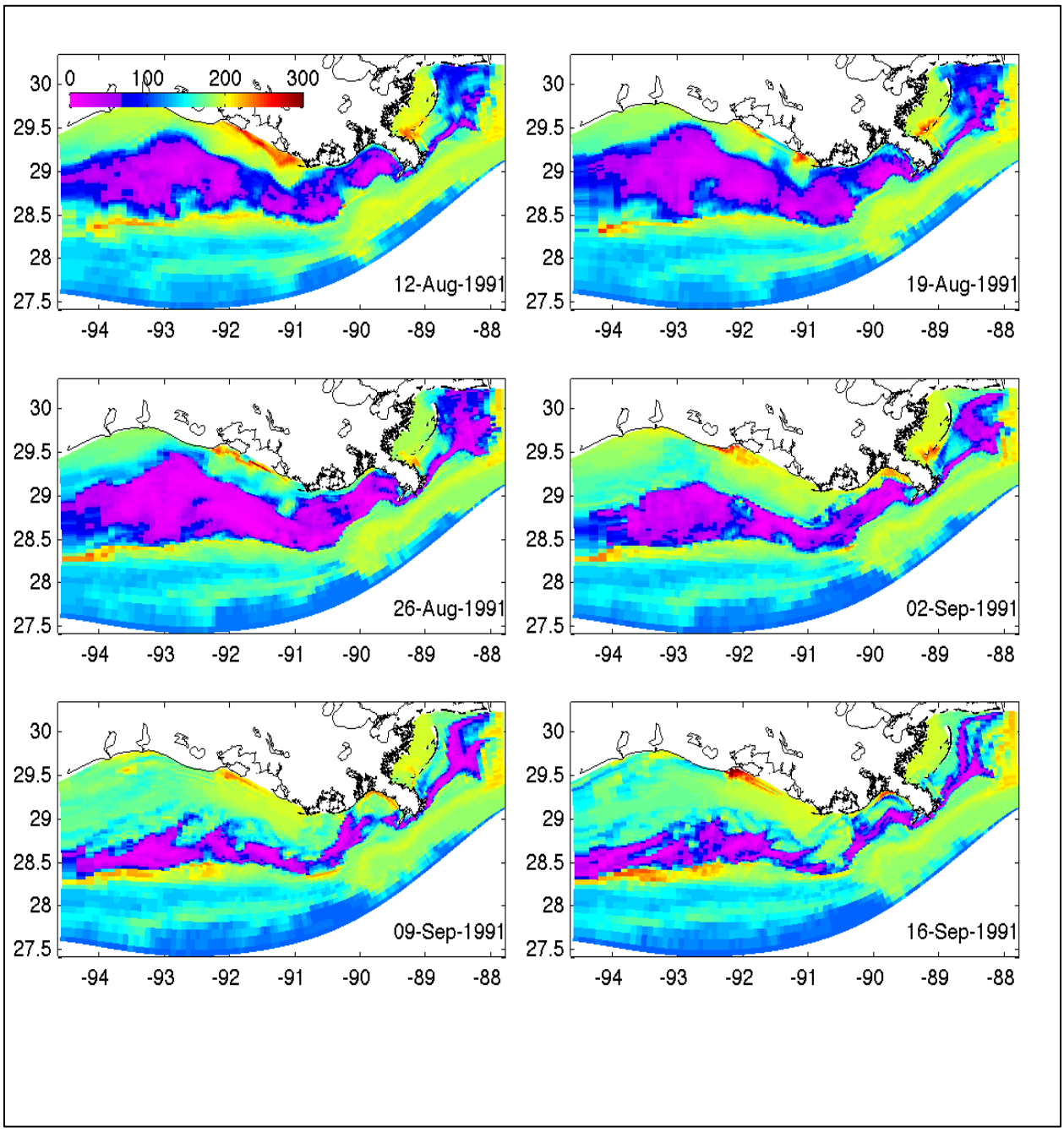

Figure A-4: Weekly snapshots of simulated bottom water oxygen concentration in mmol O_2 m^{-3} for July, August and September from1990 to 1998. Hypoxic conditions (defined here as oxygen concentrations below 60 mmol O_2 m^{-3}) are shown in purple. In this model simulation the temperature- and oxygen-dependent parameterization for sediment oxygen demand of Hetland and DiMarco (2008) is imposed.

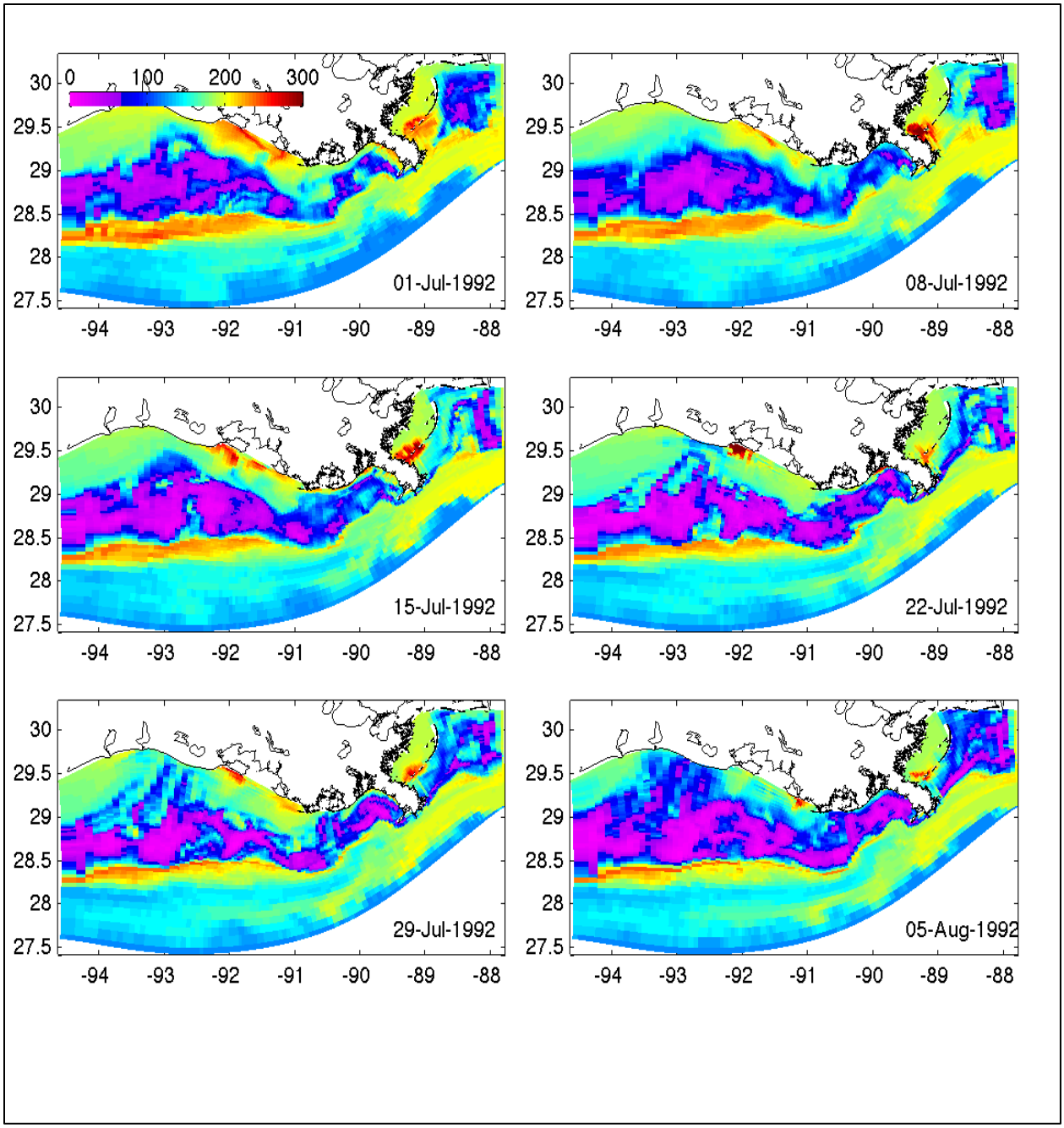

Figure A-5: Weekly snapshots of simulated bottom water oxygen concentration in mmol O_2 m^{-3} for July, August and September from1990 to 1998. Hypoxic conditions (defined here as oxygen concentrations below 60 mmol O_2 m^{-3}) are shown in purple. In this model simulation the temperature- and oxygen-dependent parameterization for sediment oxygen demand of Hetland and DiMarco (2008) is imposed.

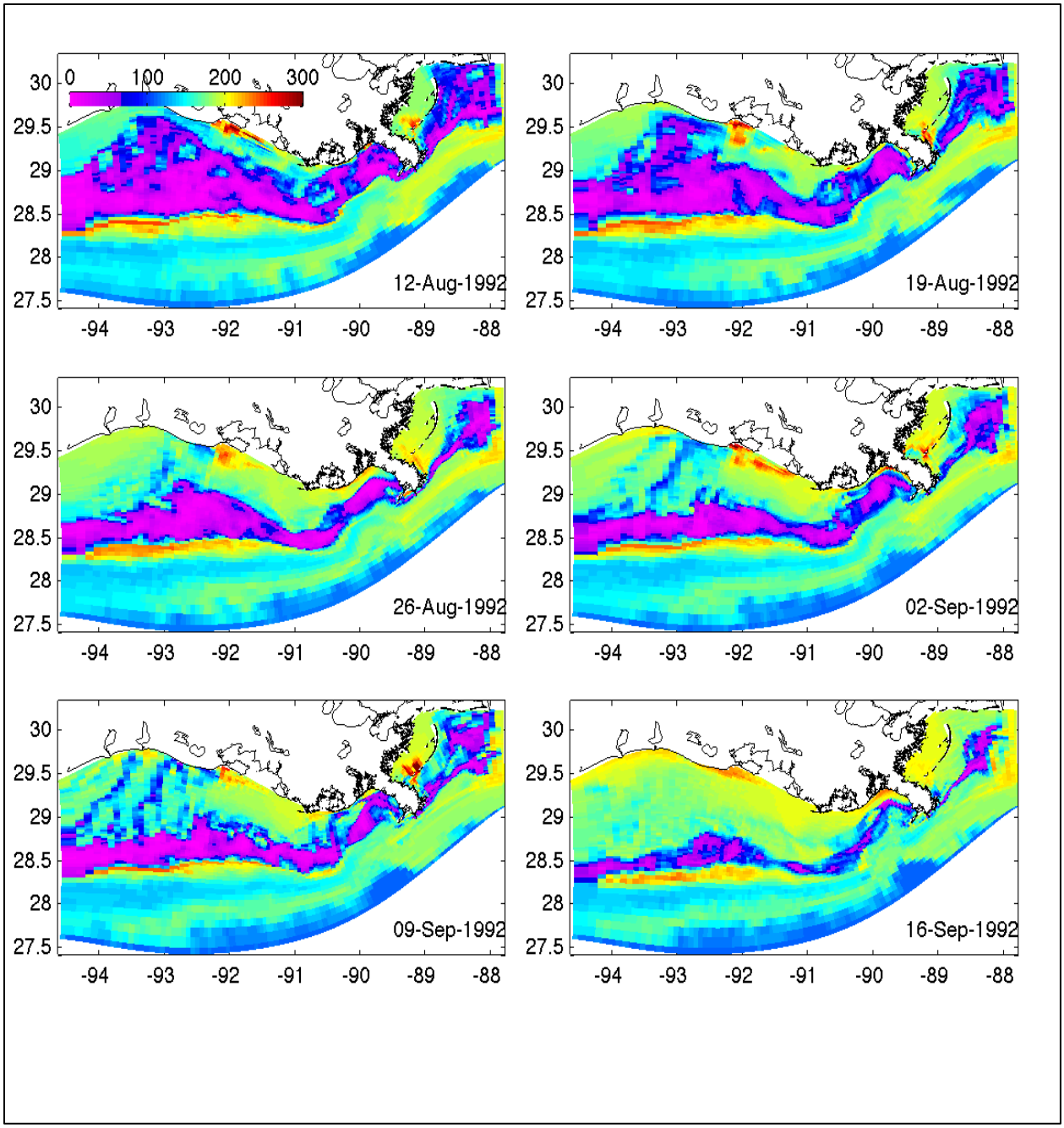

Figure A-6: Weekly snapshots of simulated bottom water oxygen concentration in mmol O_2 m^{-3} for July, August and September from1990 to 1998. Hypoxic conditions (defined here as oxygen concentrations below 60 mmol O_2 m^{-3}) are shown in purple. In this model simulation the temperature- and oxygen-dependent parameterization for sediment oxygen demand of Hetland and DiMarco (2008) is imposed.

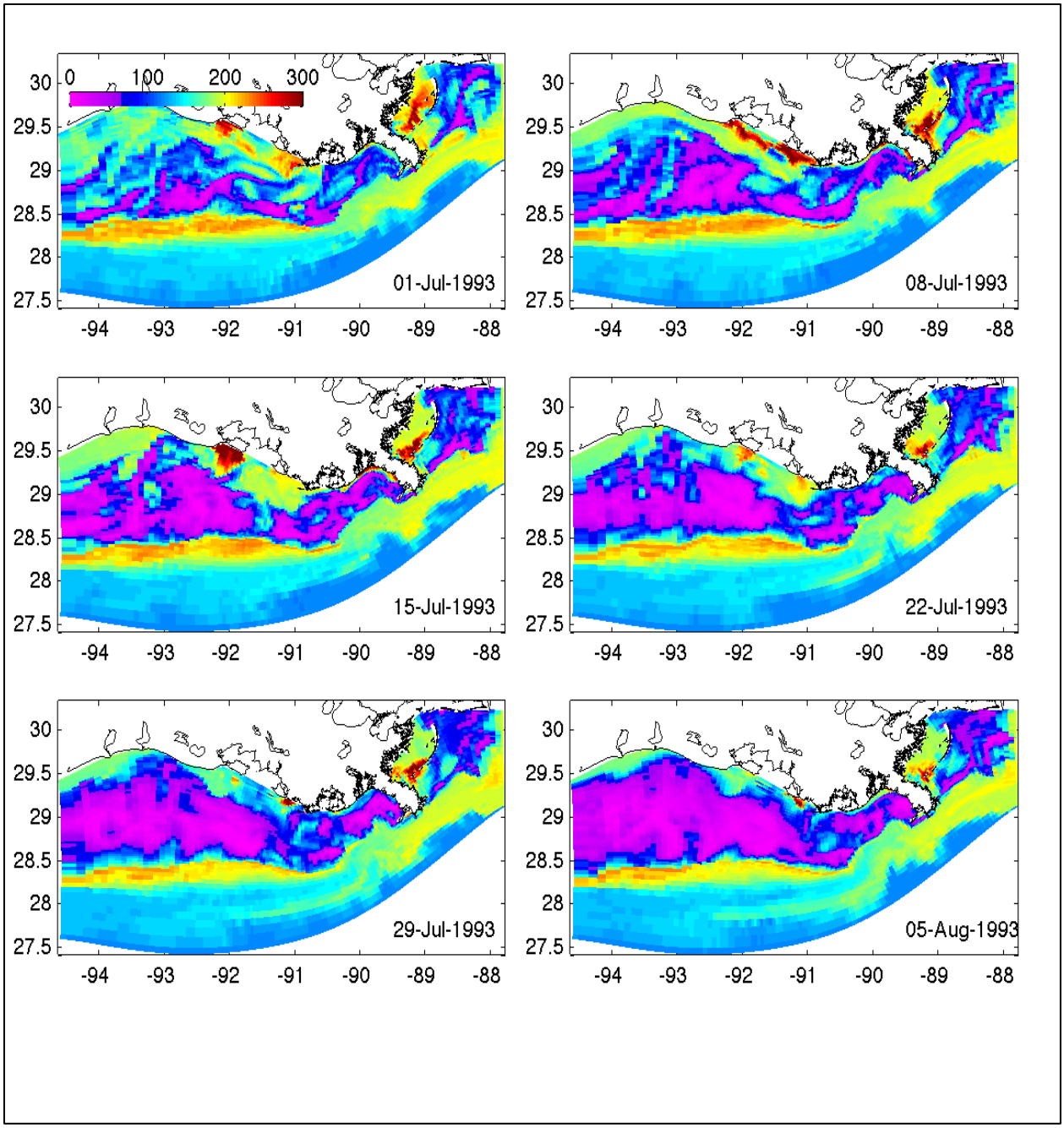

Figure A-7: Weekly snapshots of simulated bottom water oxygen concentration in mmol O_2 m^{-3} for July, August and September from1990 to 1998. Hypoxic conditions (defined here as oxygen concentrations below 60 mmol O_2 m^{-3}) are shown in purple. In this model simulation the temperature- and oxygen-dependent parameterization for sediment oxygen demand of Hetland and DiMarco (2008) is imposed.

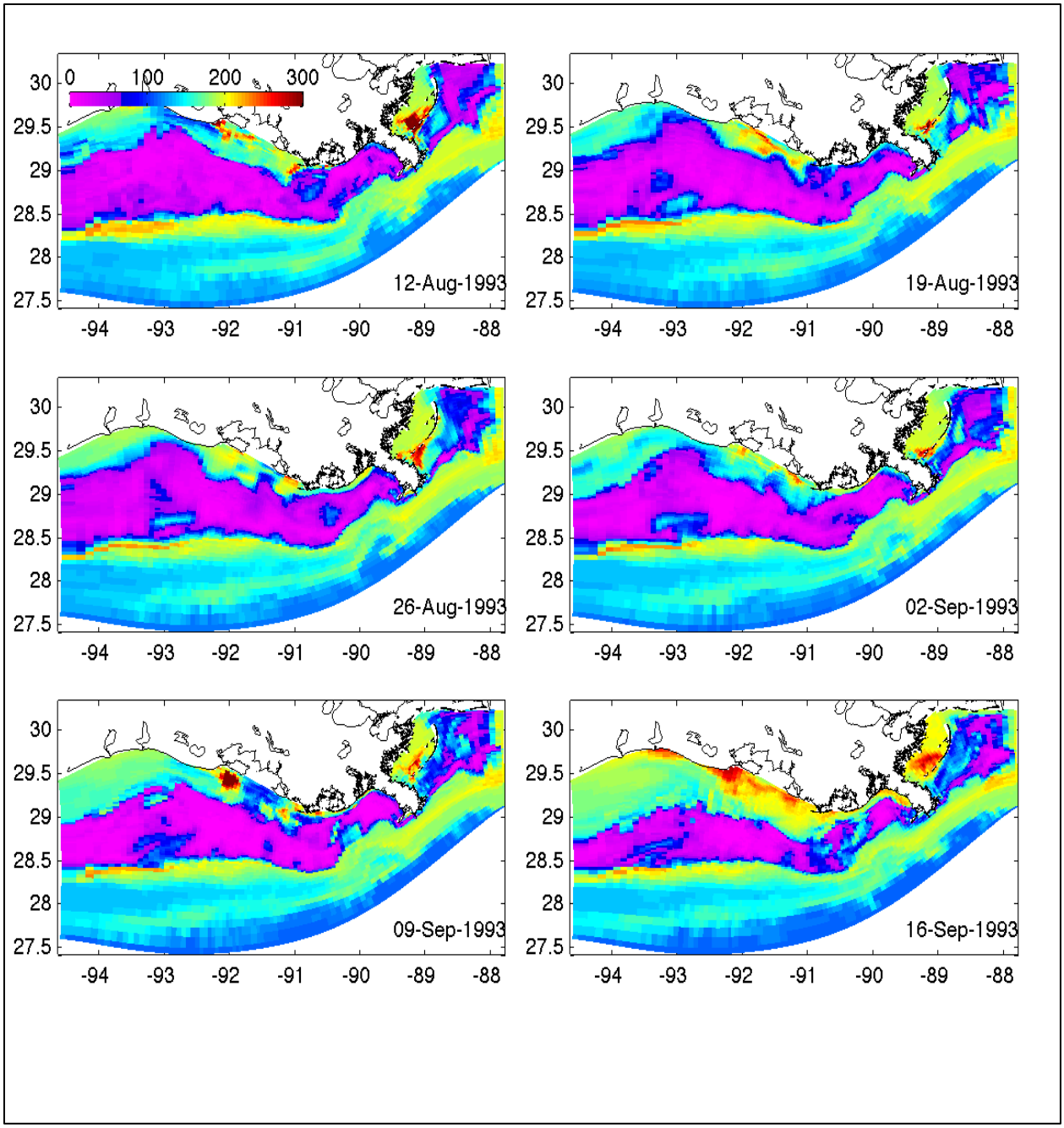

Figure A-8: Weekly snapshots of simulated bottom water oxygen concentration in mmol O_2 m^{-3} for July, August and September from1990 to 1998. Hypoxic conditions (defined here as oxygen concentrations below 60 mmol O_2 m^{-3}) are shown in purple. In this model simulation the temperature- and oxygen-dependent parameterization for sediment oxygen demand of Hetland and DiMarco (2008) is imposed.

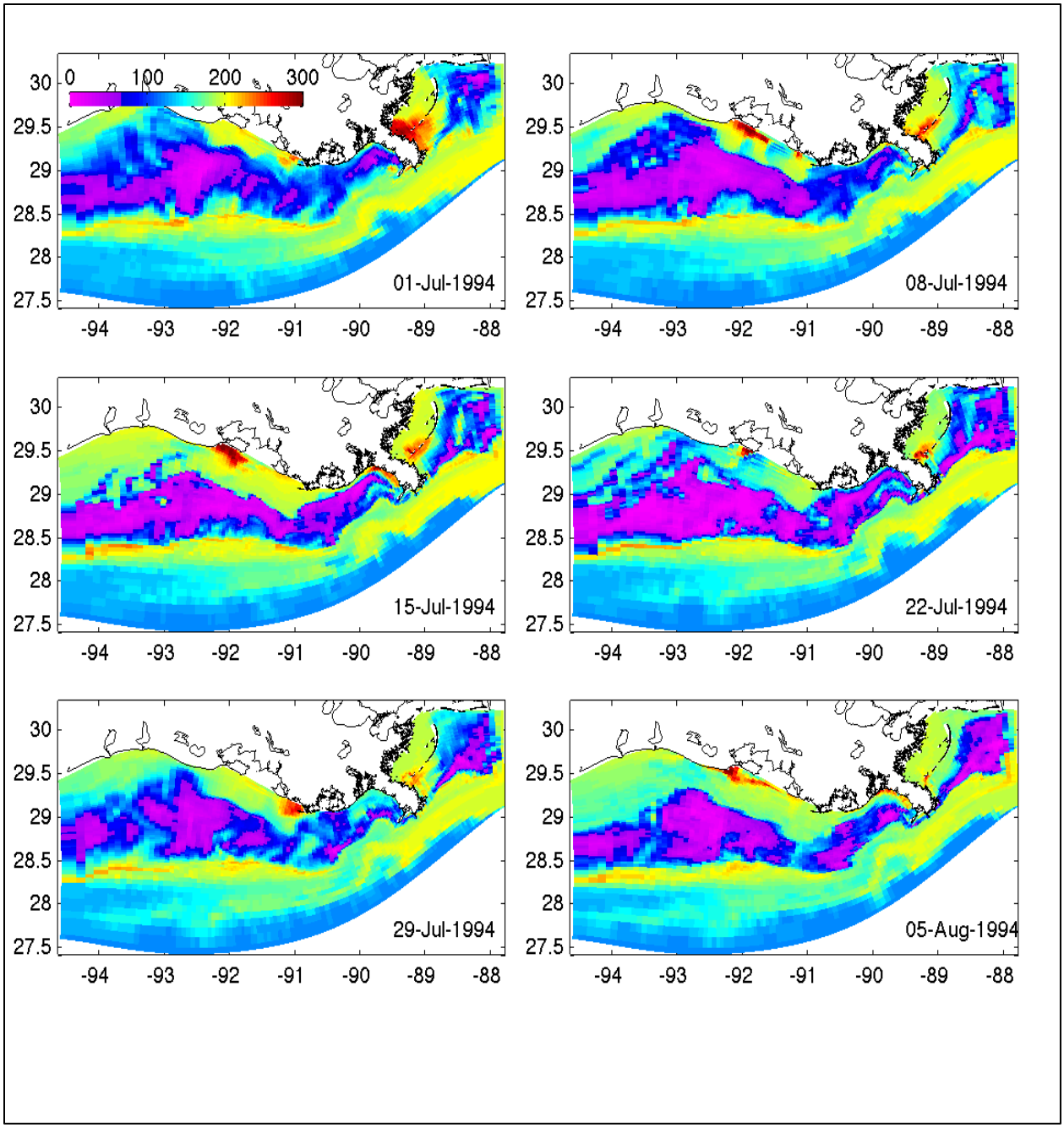

Figure A-9: Weekly snapshots of simulated bottom water oxygen concentration in mmol O_2 m^{-3} for July, August and September from1990 to 1998. Hypoxic conditions (defined here as oxygen concentrations below 60 mmol O_2 m^{-3}) are shown in purple. In this model simulation the temperature- and oxygen-dependent parameterization for sediment oxygen demand of Hetland and DiMarco (2008) is imposed.

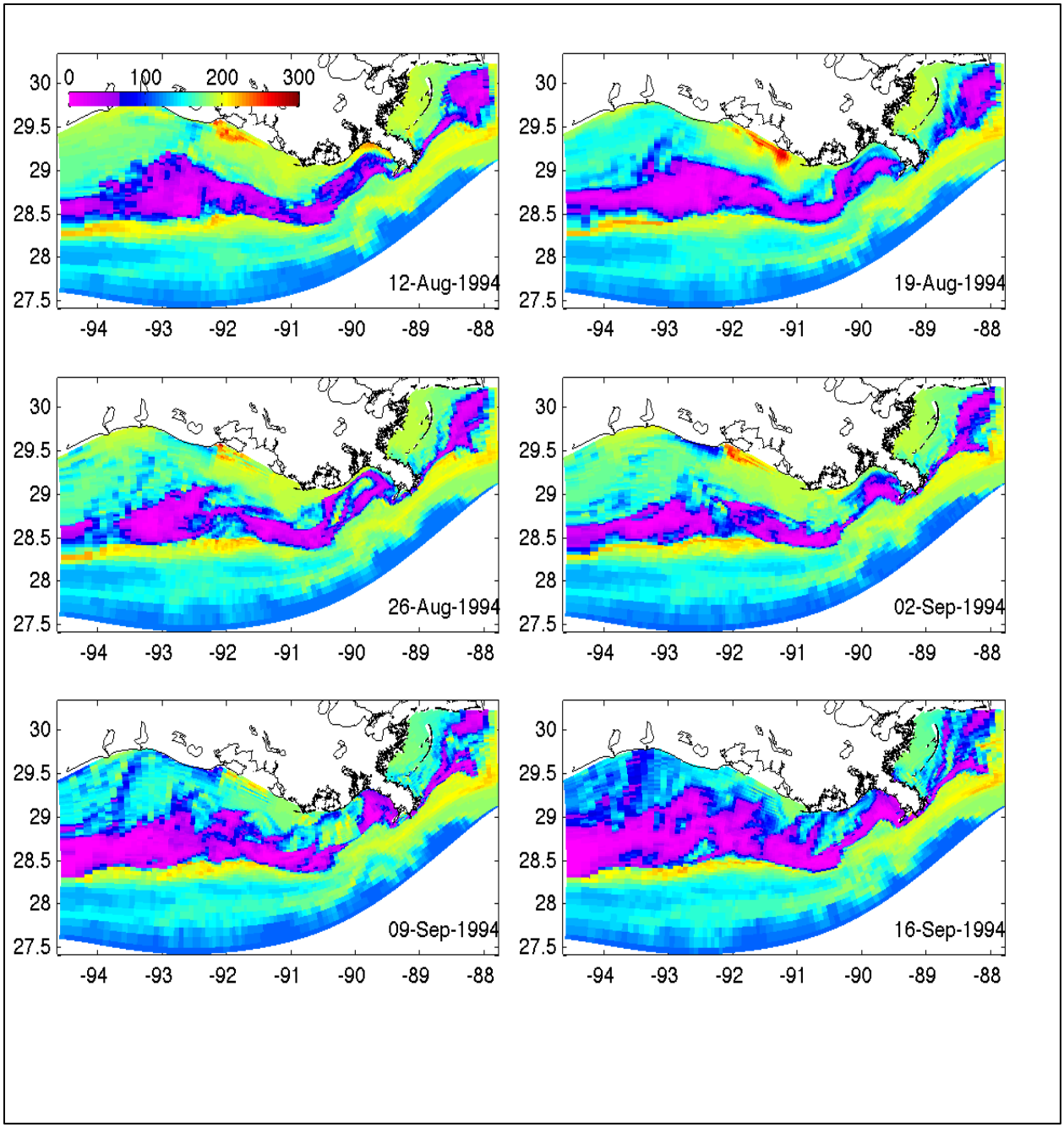

Figure A-10: Weekly snapshots of simulated bottom water oxygen concentration in mmol O_2 m^{-3} for July, August and September from1990 to 1998. Hypoxic conditions (defined here as oxygen concentrations below 60 mmol O_2 m^{-3}) are shown in purple. In this model simulation the temperature- and oxygen-dependent parameterization for sediment oxygen demand of Hetland and DiMarco (2008) is imposed.

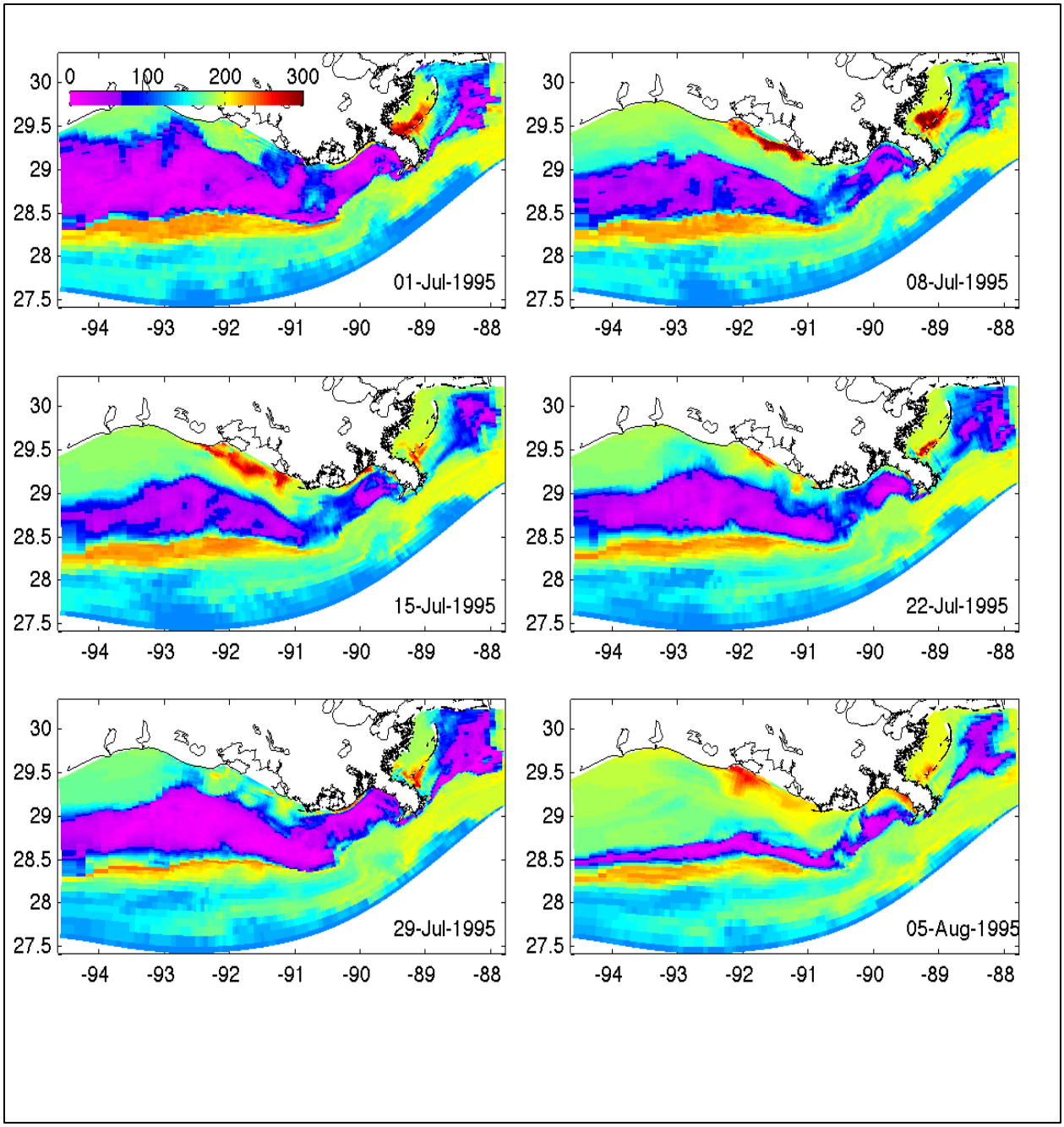

Figure A-11: Weekly snapshots of simulated bottom water oxygen concentration in mmol O_2 m^{-3} for July, August and September from1990 to 1998. Hypoxic conditions (defined here as oxygen concentrations below 60 mmol O_2 m^{-3}) are shown in purple. In this model simulation the temperature- and oxygen-dependent parameterization for sediment oxygen demand of Hetland and DiMarco (2008) is imposed.

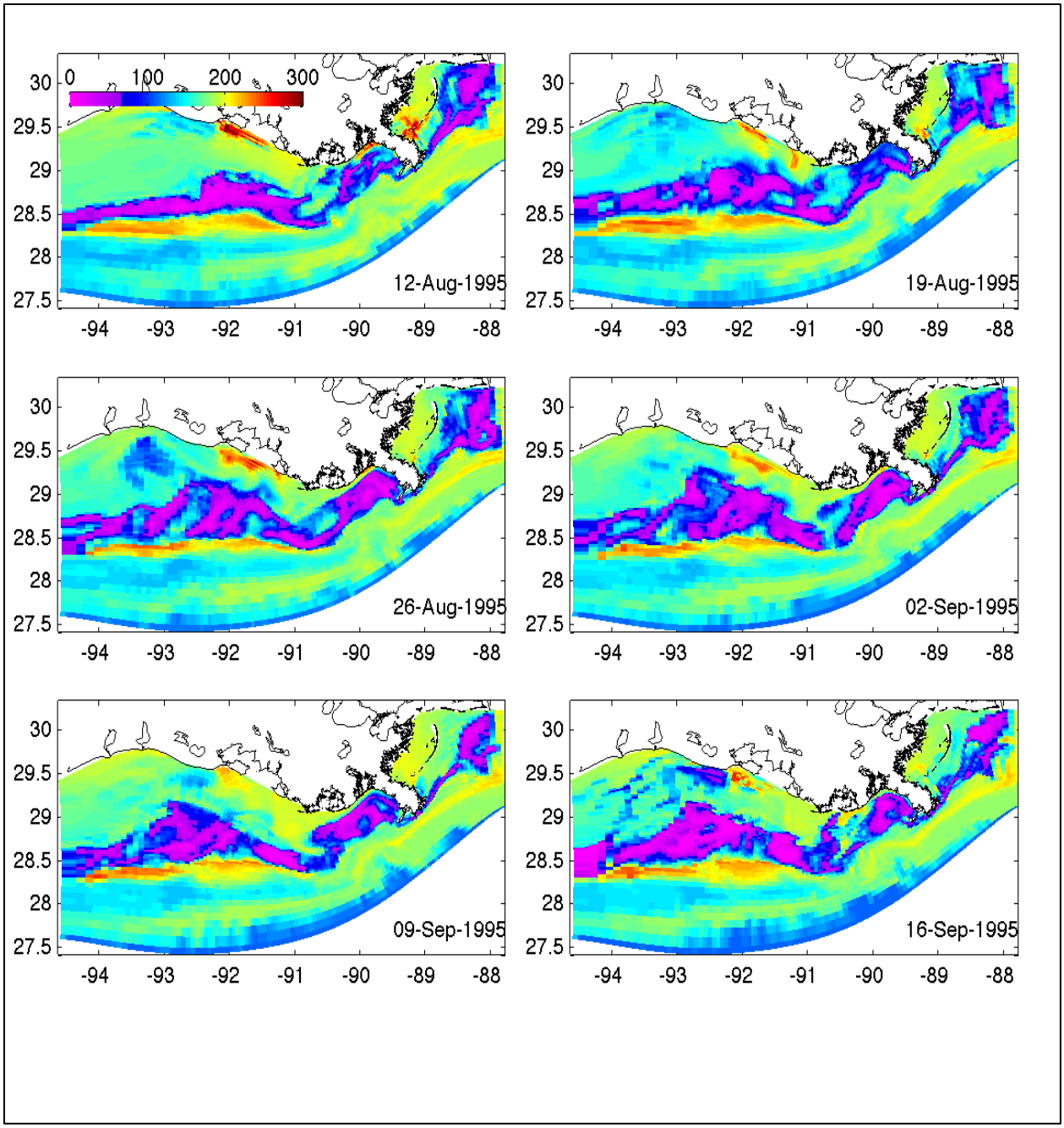

Figure A-12: Weekly snapshots of simulated bottom water oxygen concentration in mmol O_2 m^{-3} for July, August and September from1990 to 1998. Hypoxic conditions (defined here as oxygen concentrations below 60 mmol O_2 m^{-3}) are shown in purple. In this model simulation the temperature- and oxygen-dependent parameterization for sediment oxygen demand of Hetland and DiMarco (2008) is imposed.

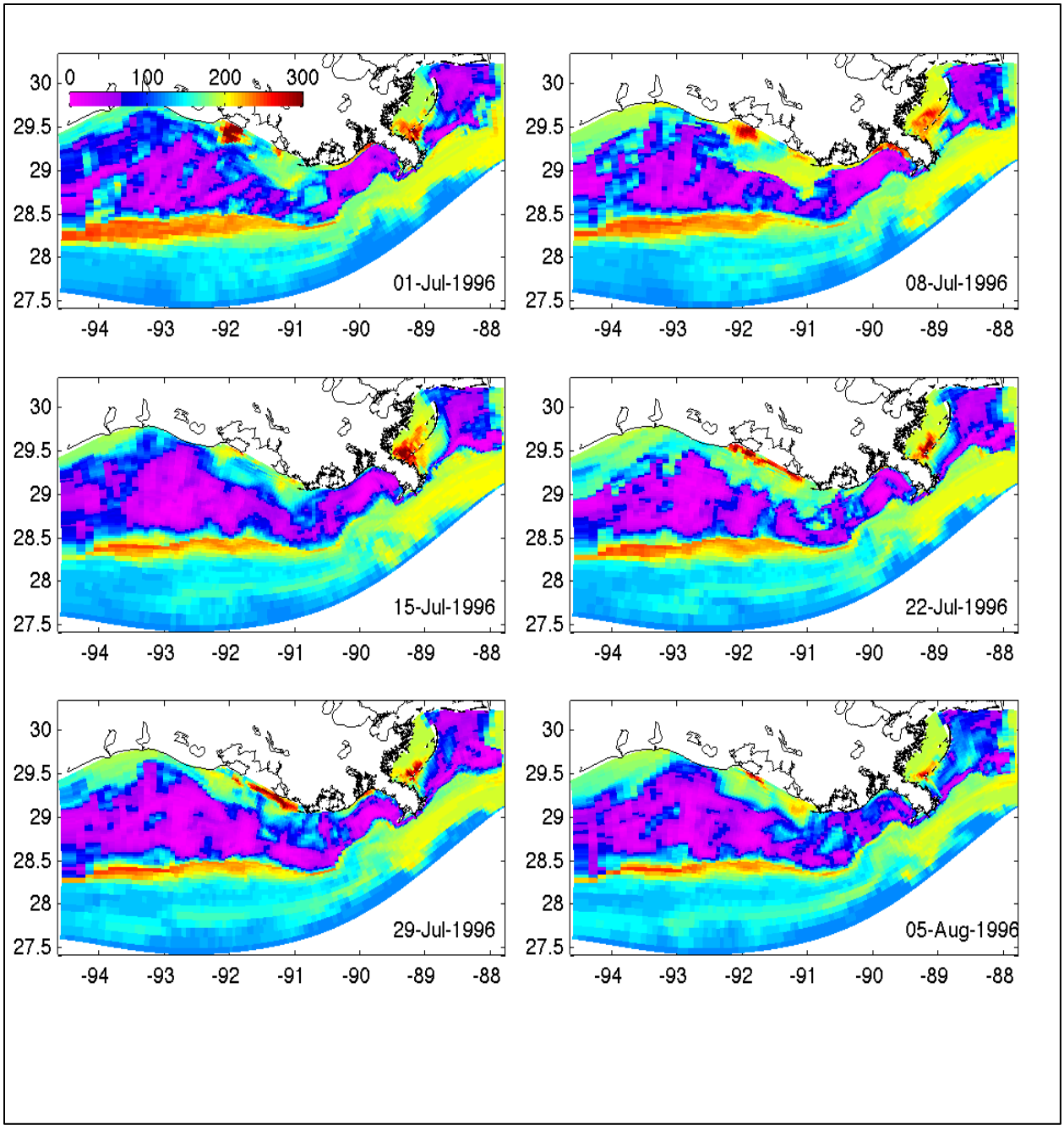

Figure A-13: Weekly snapshots of simulated bottom water oxygen concentration in mmol O_2 m^{-3} for July, August and September from1990 to 1998. Hypoxic conditions (defined here as oxygen concentrations below 60 mmol O_2 m^{-3}) are shown in purple. In this model simulation the temperature- and oxygen-dependent parameterization for sediment oxygen demand of Hetland and DiMarco (2008) is imposed.

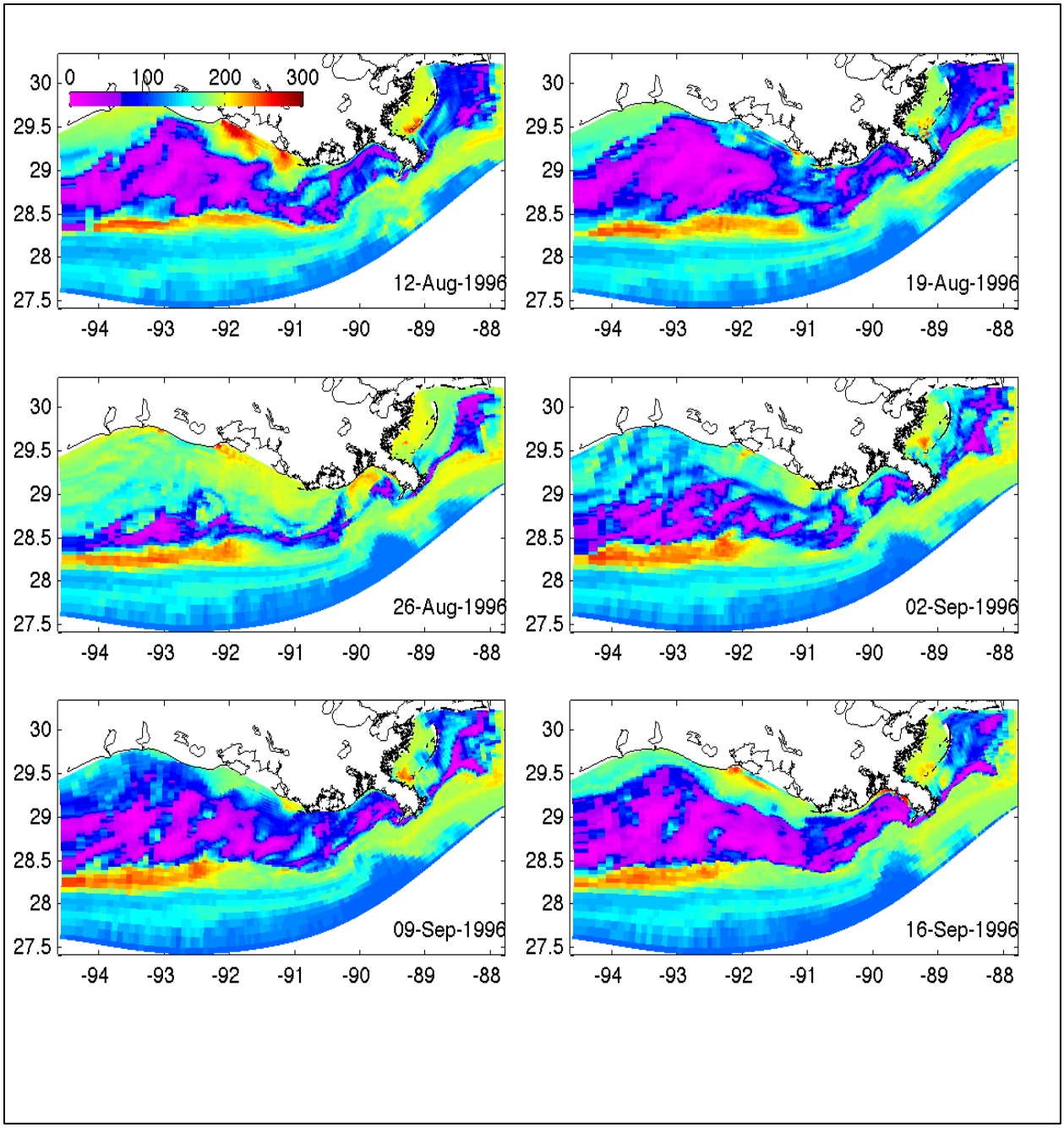

Figure A-14: Weekly snapshots of simulated bottom water oxygen concentration in mmol O_2 m^{-3} for July, August and September from1990 to 1998. Hypoxic conditions (defined here as oxygen concentrations below 60 mmol O_2 m^{-3}) are shown in purple. In this model simulation the temperature- and oxygen-dependent parameterization for sediment oxygen demand of Hetland and DiMarco (2008) is imposed.

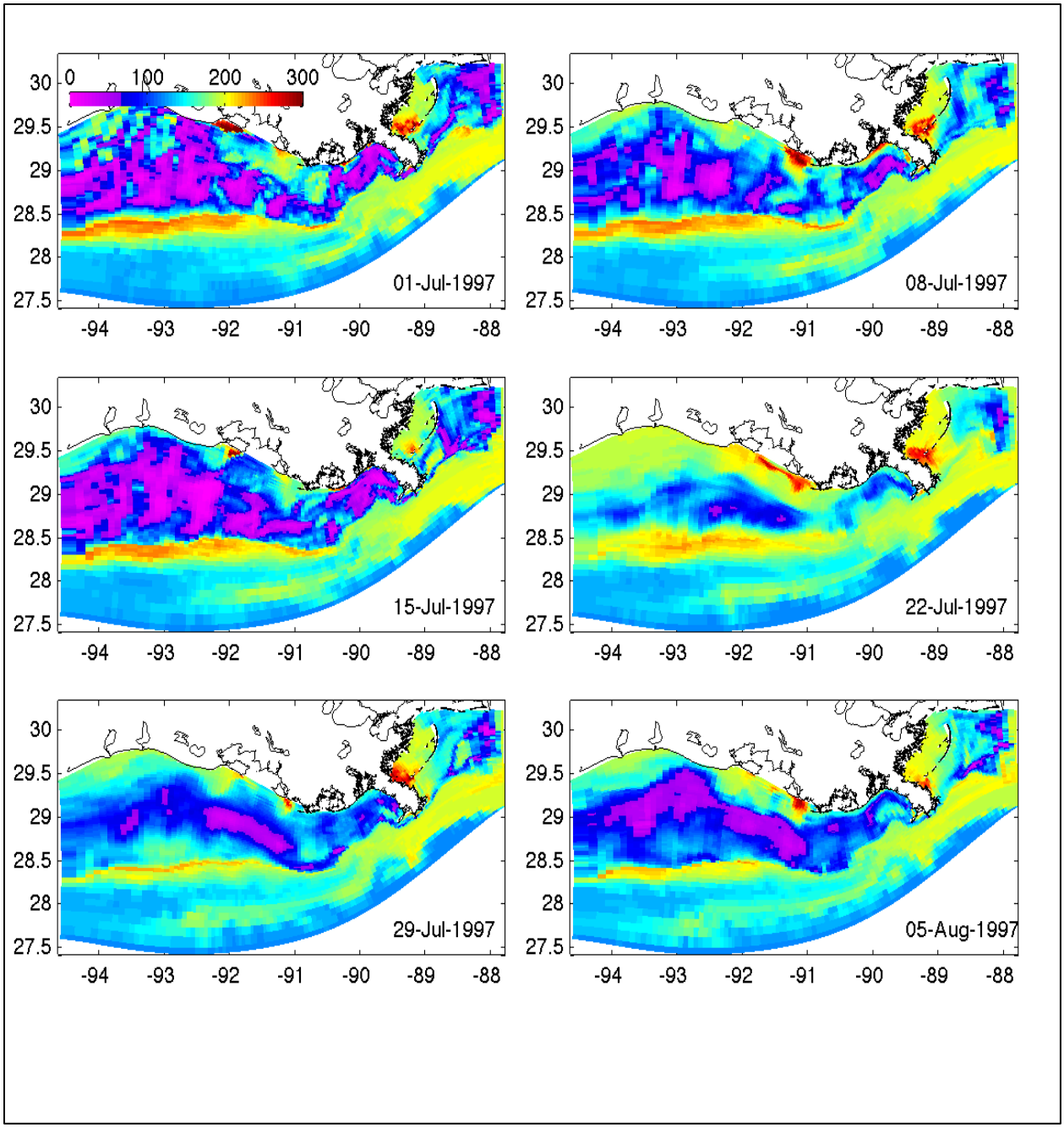

Figure A-15: Weekly snapshots of simulated bottom water oxygen concentration in mmol O_2 m^{-3} for July, August and September from1990 to 1998. Hypoxic conditions (defined here as oxygen concentrations below 60 mmol O_2 m^{-3}) are shown in purple. In this model simulation the temperature- and oxygen-dependent parameterization for sediment oxygen demand of Hetland and DiMarco (2008) is imposed.

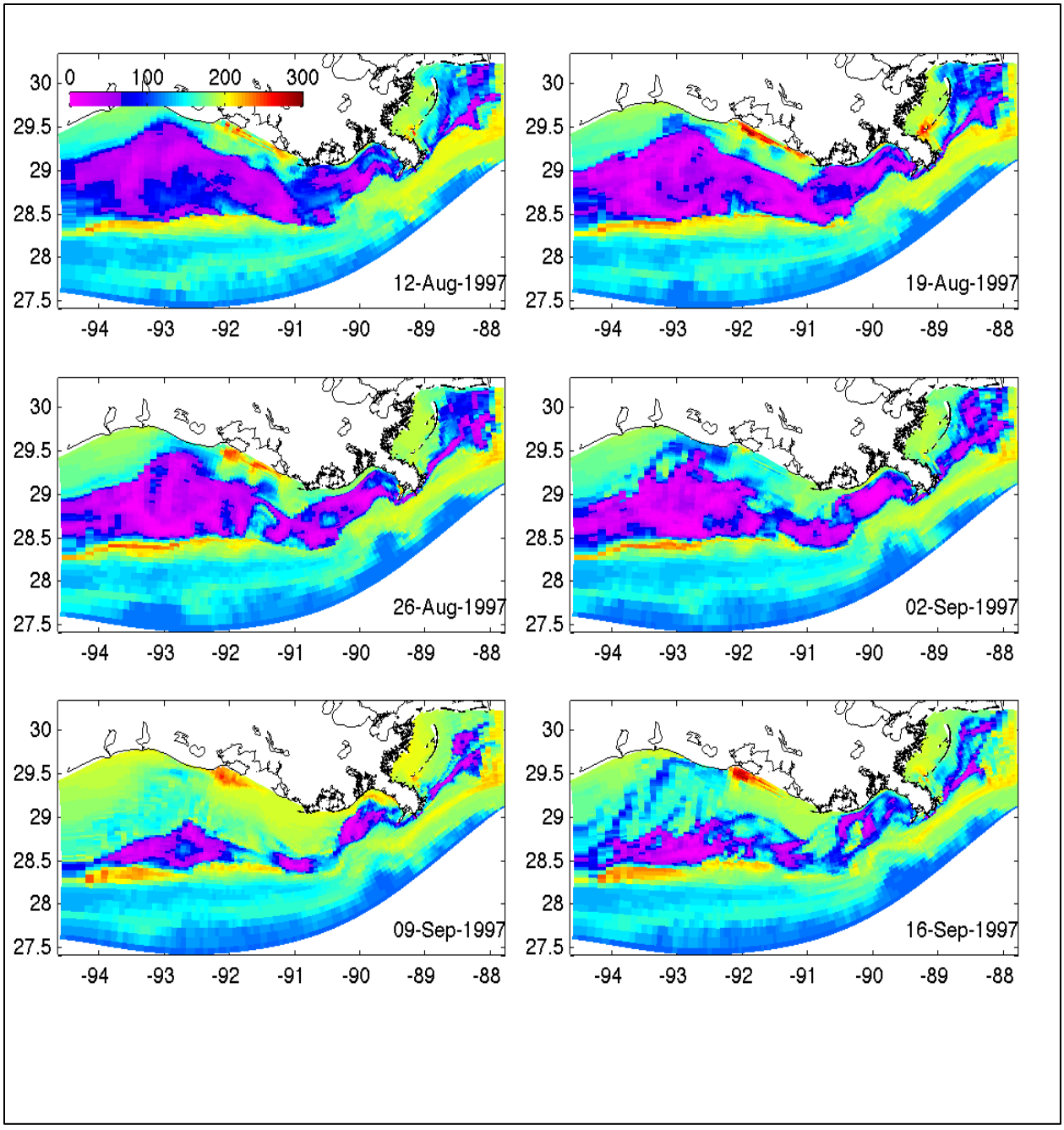

Figure A-16: Weekly snapshots of simulated bottom water oxygen concentration in mmol O_2 m^{-3} for July, August and September from1990 to 1998. Hypoxic conditions (defined here as oxygen concentrations below 60 mmol O_2 m^{-3}) are shown in purple. In this model simulation the temperature- and oxygen-dependent parameterization for sediment oxygen demand of Hetland and DiMarco (2008) is imposed.

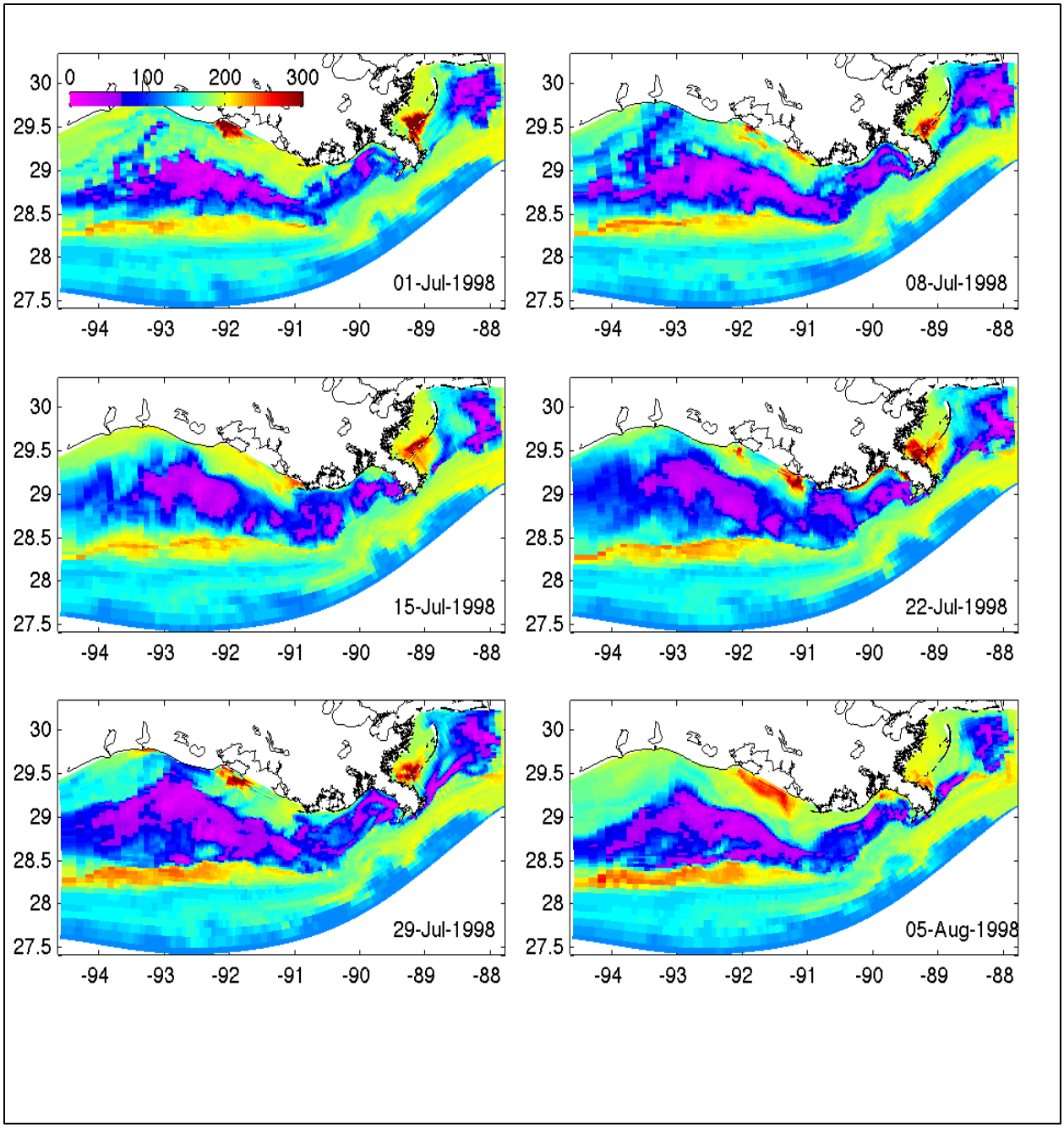

Figure A-17: Weekly snapshots of simulated bottom water oxygen concentration in mmol O_2 m^{-3} for July, August and September from1990 to 1998. Hypoxic conditions (defined here as oxygen concentrations below 60 mmol O_2 m^{-3}) are shown in purple. In this model simulation the temperature- and oxygen-dependent parameterization for sediment oxygen demand of Hetland and DiMarco (2008) is imposed.

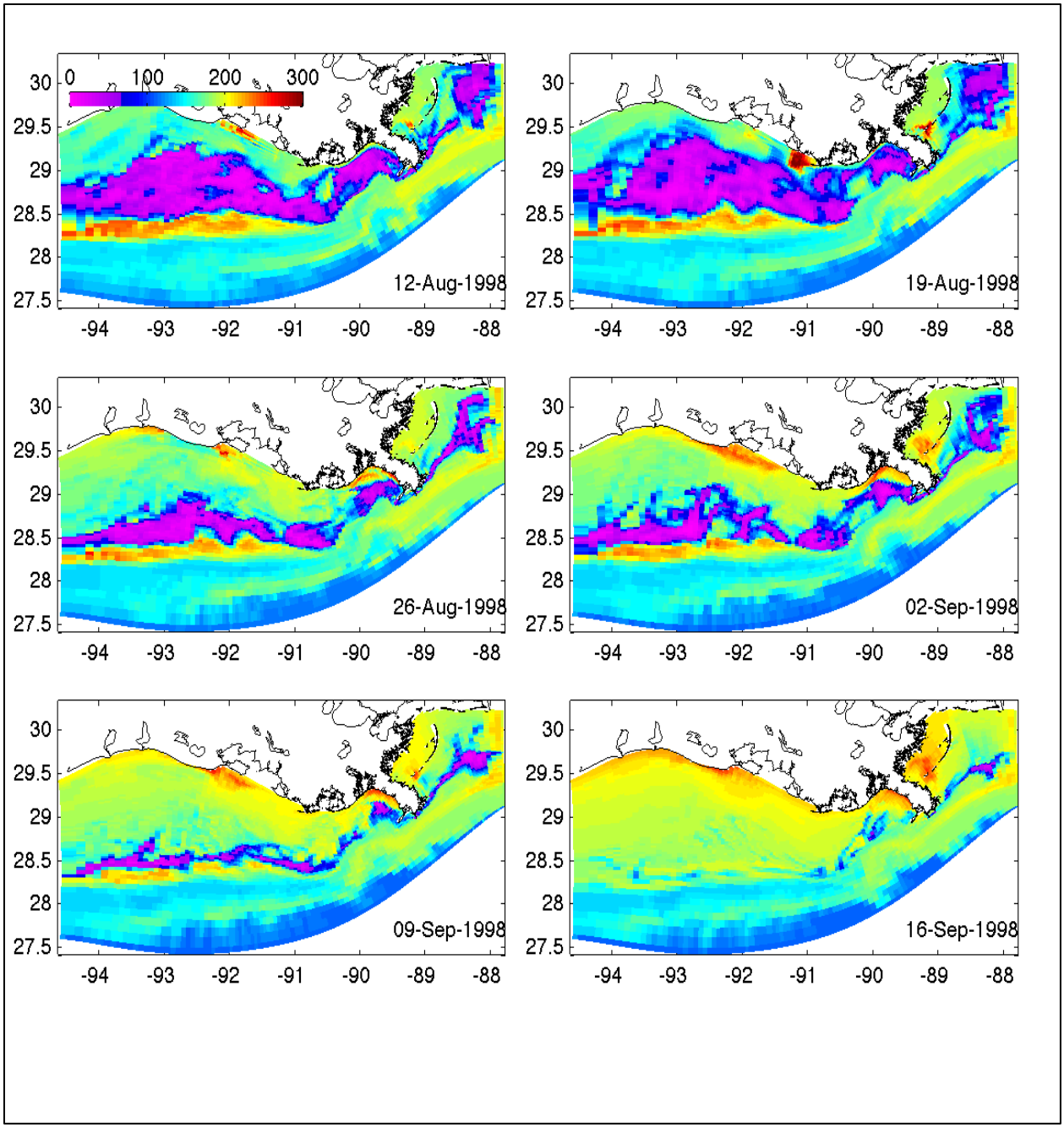

Figure A-18: Weekly snapshots of simulated bottom water oxygen concentration in mmol O_2 m^{-3} for July, August and September from1990 to 1998. Hypoxic conditions (defined here as oxygen concentrations below 60 mmol O_2 m^{-3}) are shown in purple. In this model simulation the temperature- and oxygen-dependent parameterization for sediment oxygen demand of Hetland and DiMarco (2008) is imposed.

APPENDIX B

Numerical drifters are released at a location near the Flower Gardens coral reef system each night in August at midnight. The drifters are tracked for 30 days. Corals will spawn during the first full moon in August. We chose to release drifters for the entire month so that the figures could be directly compared to each other, and so that we could gain more understanding of the dispersion caused by surface current variability that occurs in late summer.

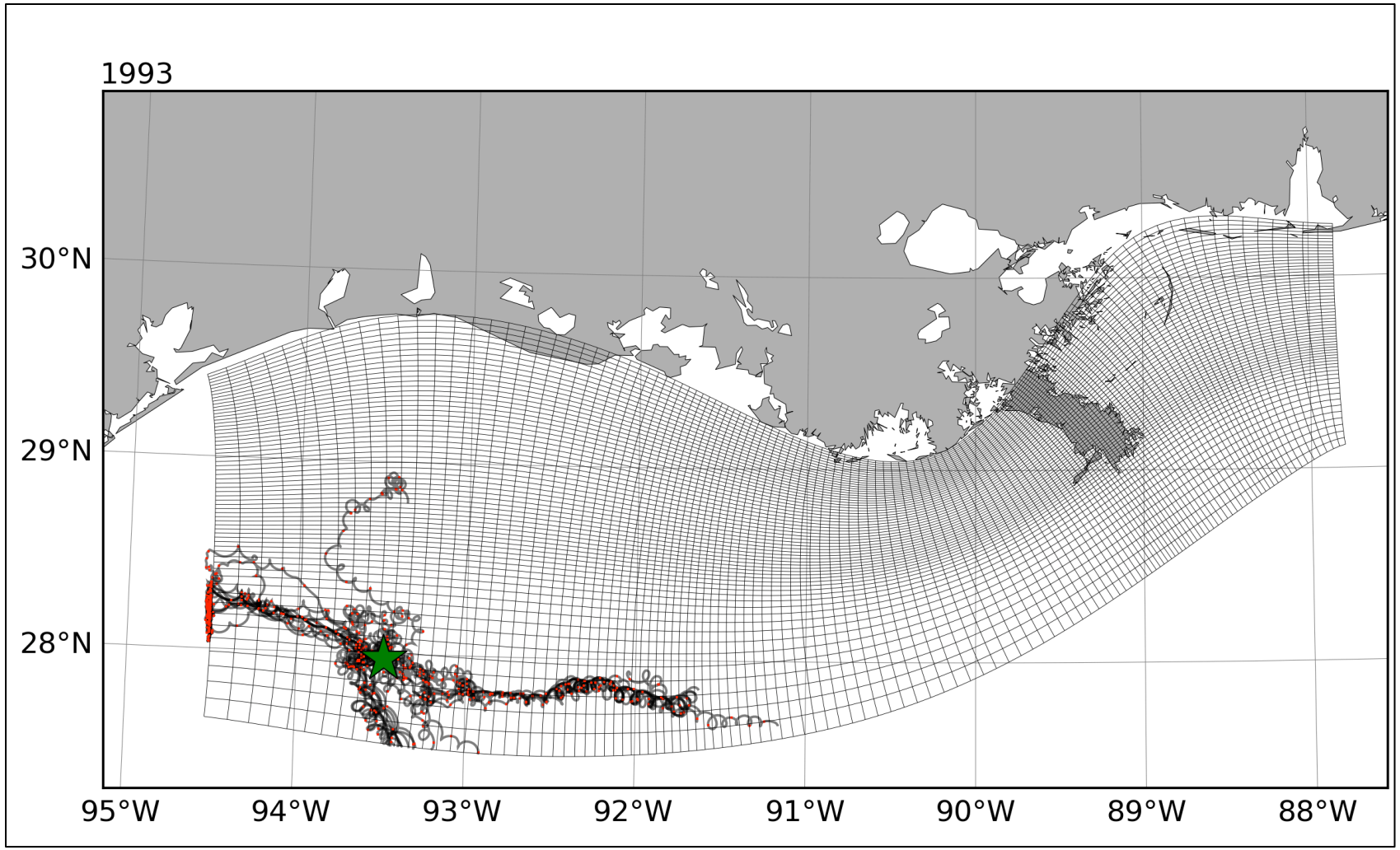

Figure B-1: Numerical drifters are released at a point near the Flower Gardens coral reef system. One drifter is released each day in August 1993, and followed for 30 days. Black lines represent the drifter tracks, with a red mark every day. The release point is marked with a green star.

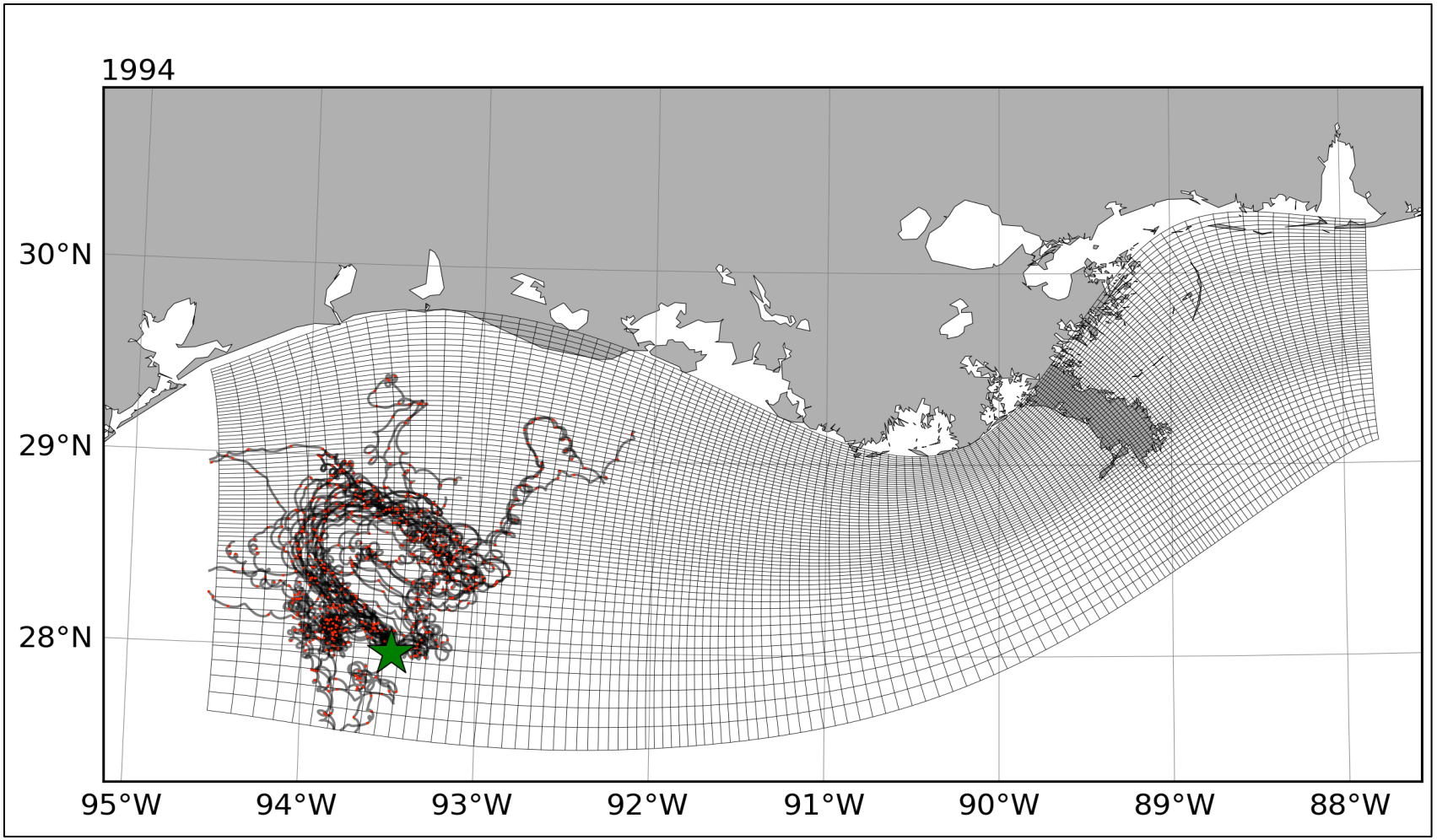

Figure B-2: Numerical drifters are released at a point near the Flower Gardens coral reef system. One drifter is released each day in August 1994, and followed for 30 days. Black lines represent the drifter tracks, with a red mark every day. The release point is marked with a green star.

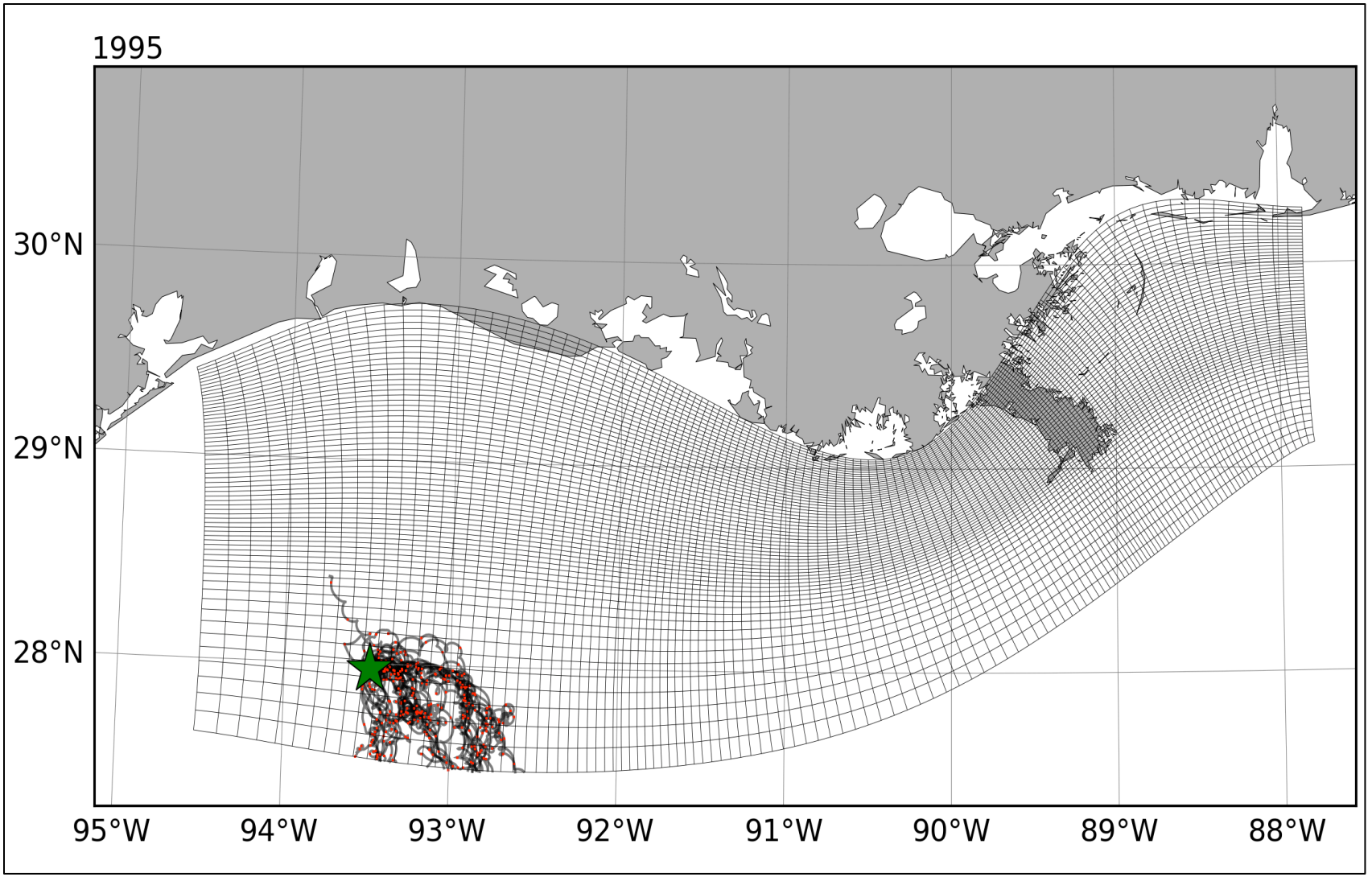

Figure B-3: Numerical drifters are released at a point near the Flower Gardens coral reef system. One drifter is released each day in August 1995, and followed for 30 days. Black lines represent the drifter tracks, with a red mark every day. The release point is marked with a green star.

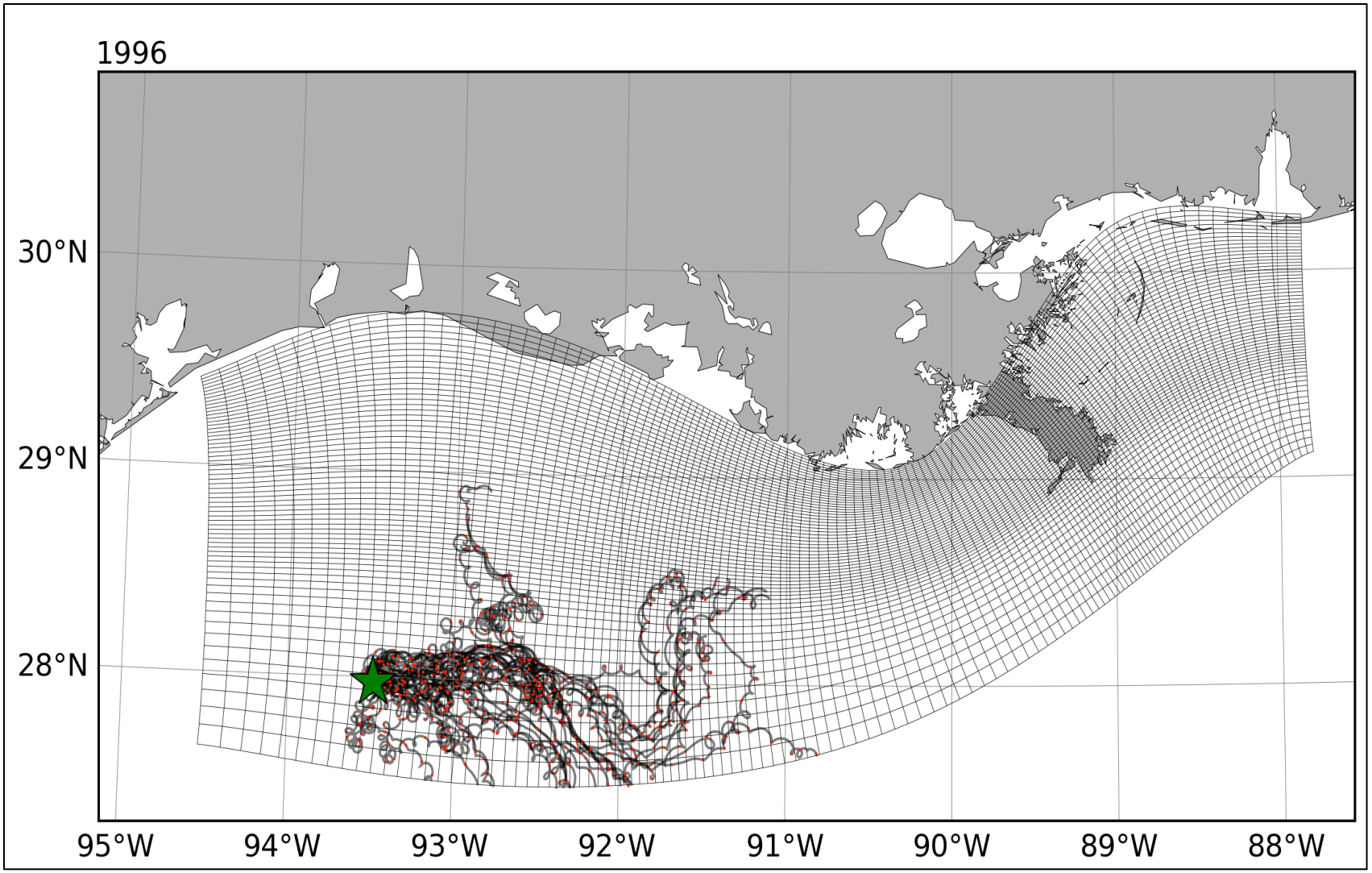

Figure B-4: Numerical drifters are released at a point near the Flower Gardens coral reef system. One drifter is released each day in August 1996, and followed for 30 days. Black lines represent the drifter tracks, with a red mark every day. The release point is marked with a green star.

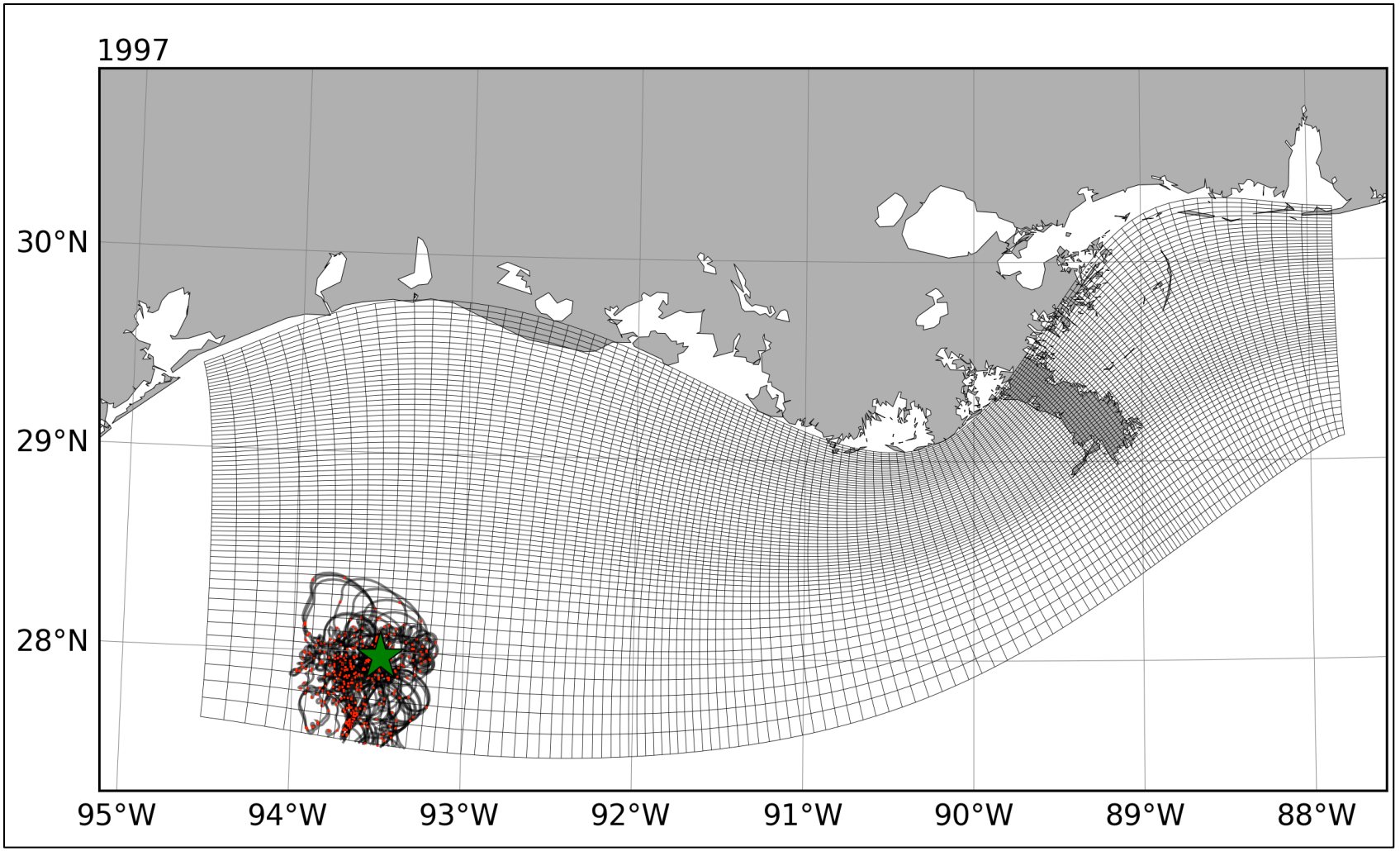

Figure B-5: Numerical drifters are released at a point near the Flower Gardens coral reef system. One drifter is released each day in August 1997, and followed for 30 days. Black lines represent the drifter tracks, with a red mark every day. The release point is marked with a green star.

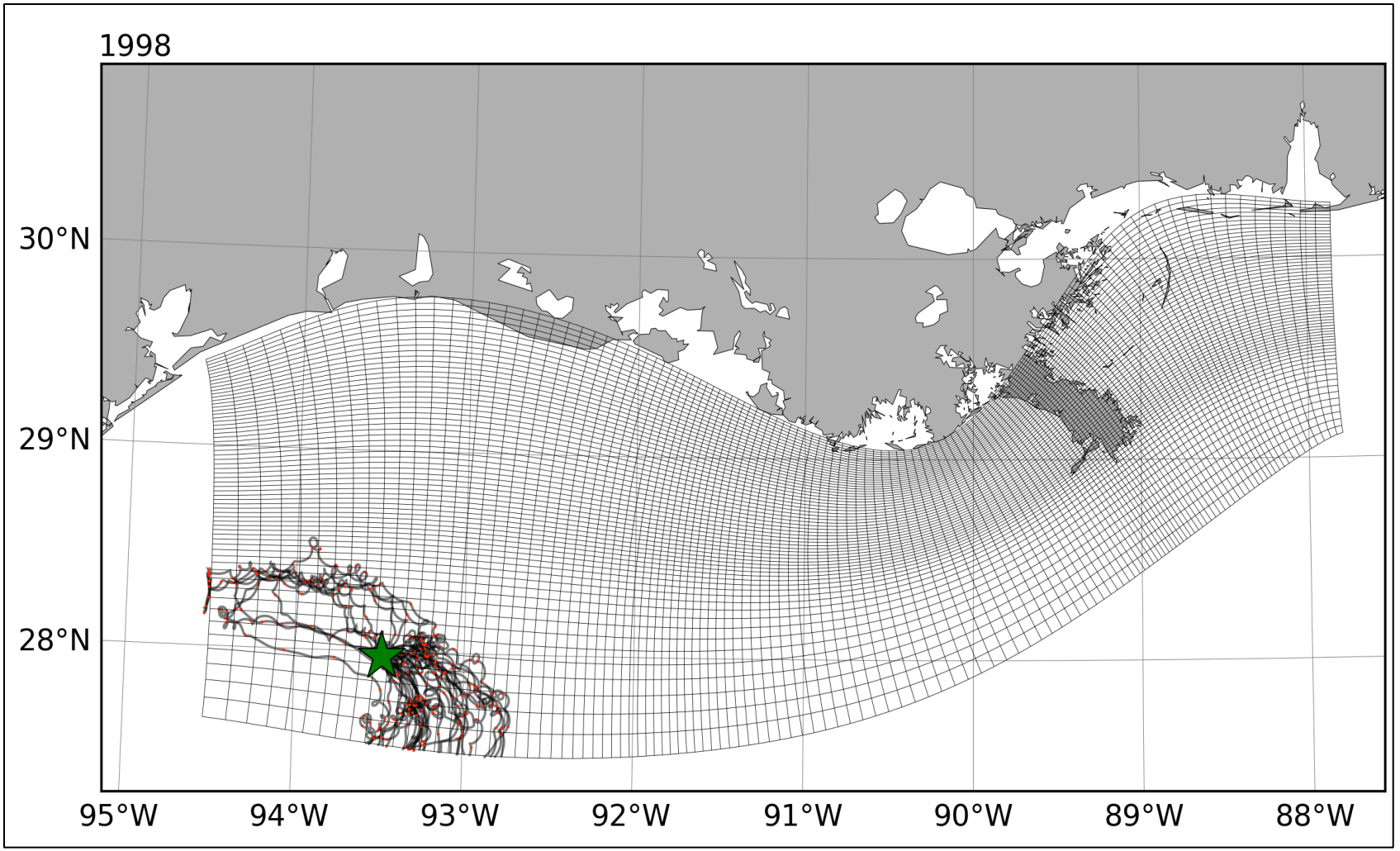

Figure B-6: Numerical drifters are released at a point near the Flower Gardens coral reef system. One drifter is released each day in August 1998, and followed for 30 days. Black lines represent the drifter tracks, with a red mark every day. The release point is marked with a green star.

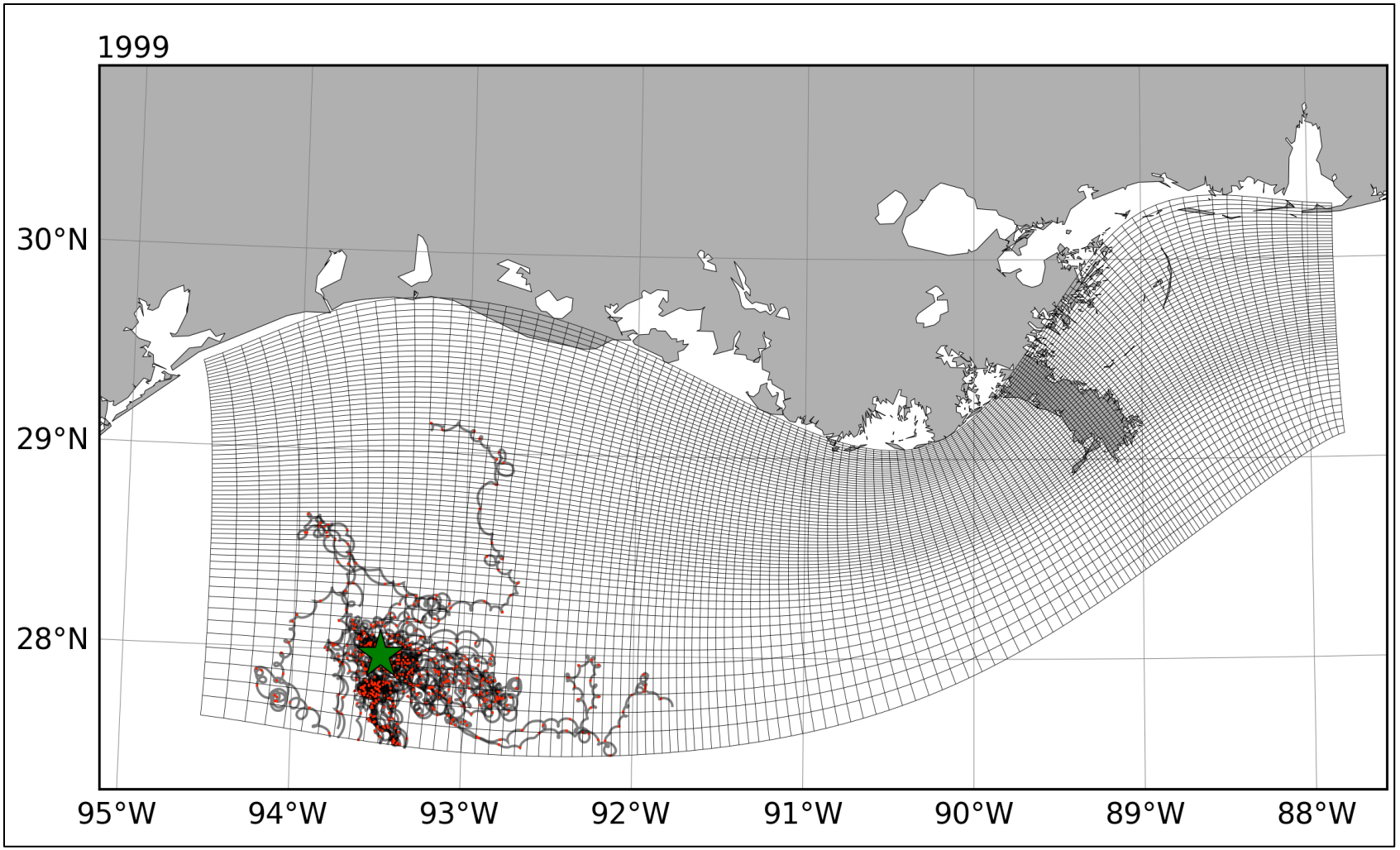

Figure B-7: Numerical drifters are released at a point near the Flower Gardens coral reef system. One drifter is released each day in August 1999 and followed for 30 days. Black lines represent the drifter tracks, with a red mark every day. The release point is marked with a green star.

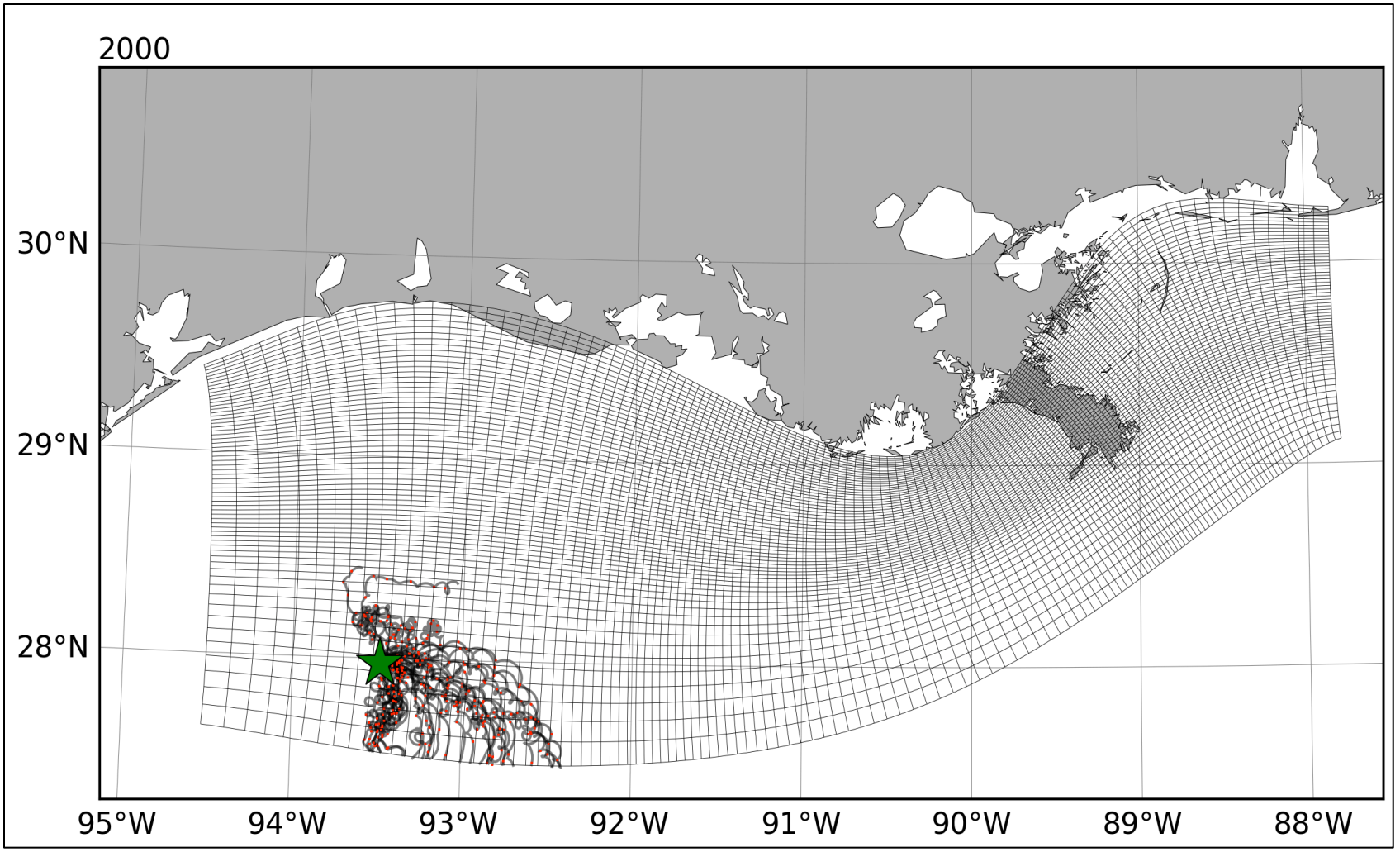

Figure B-8: Numerical drifters are released at a point near the Flower Gardens coral reef system. One drifter is released each day in August 2000, and followed for 30 days. Black lines represent the drifter tracks, with a red mark every day. The release point is marked with a green star.

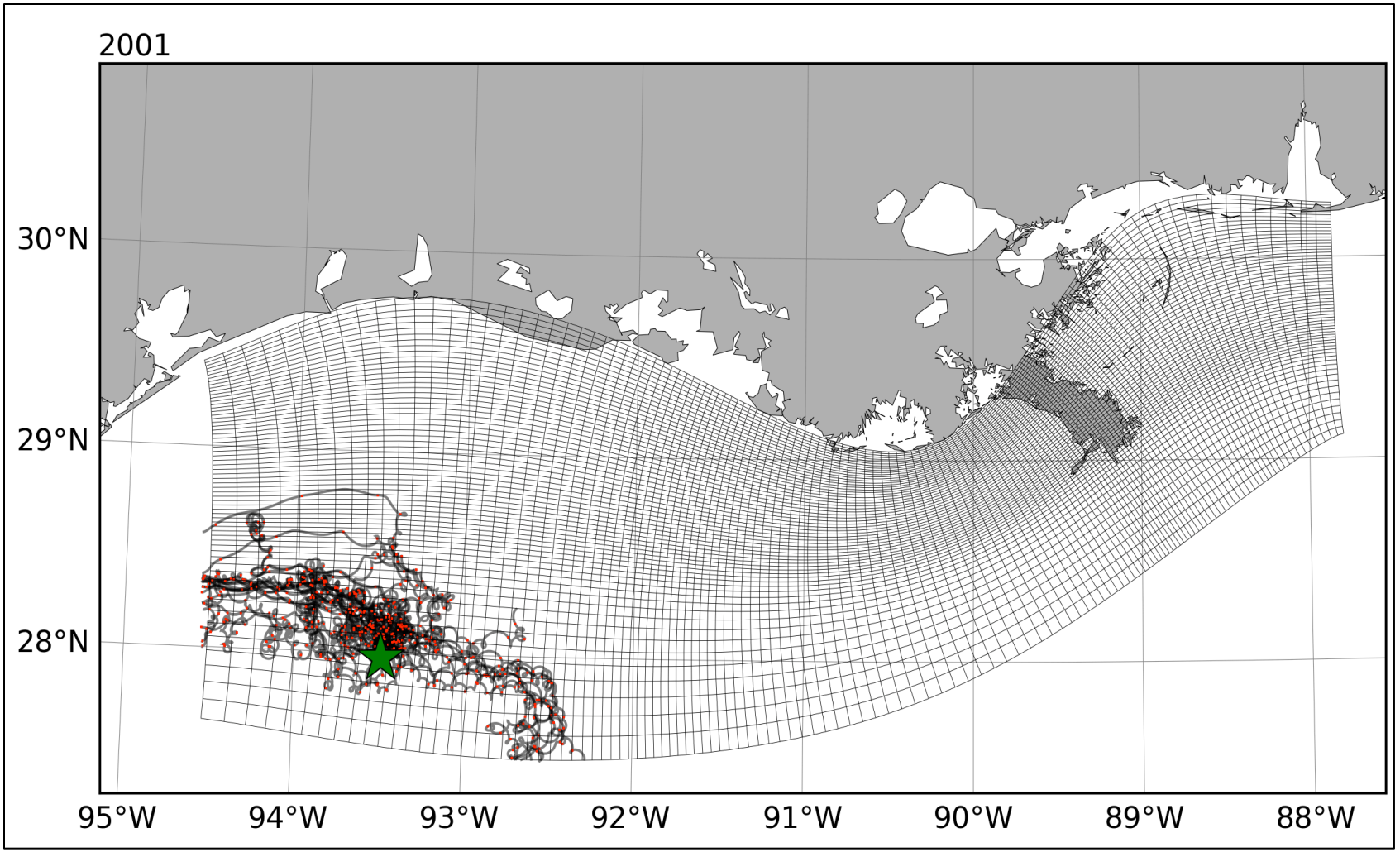

Figure B-9: Numerical drifters are released at a point near the Flower Gardens coral reef system. One drifter is released each day in August 2001, and followed for 30 days. Black lines represent the drifter tracks, with a red mark every day. The release point is marked with a green star.

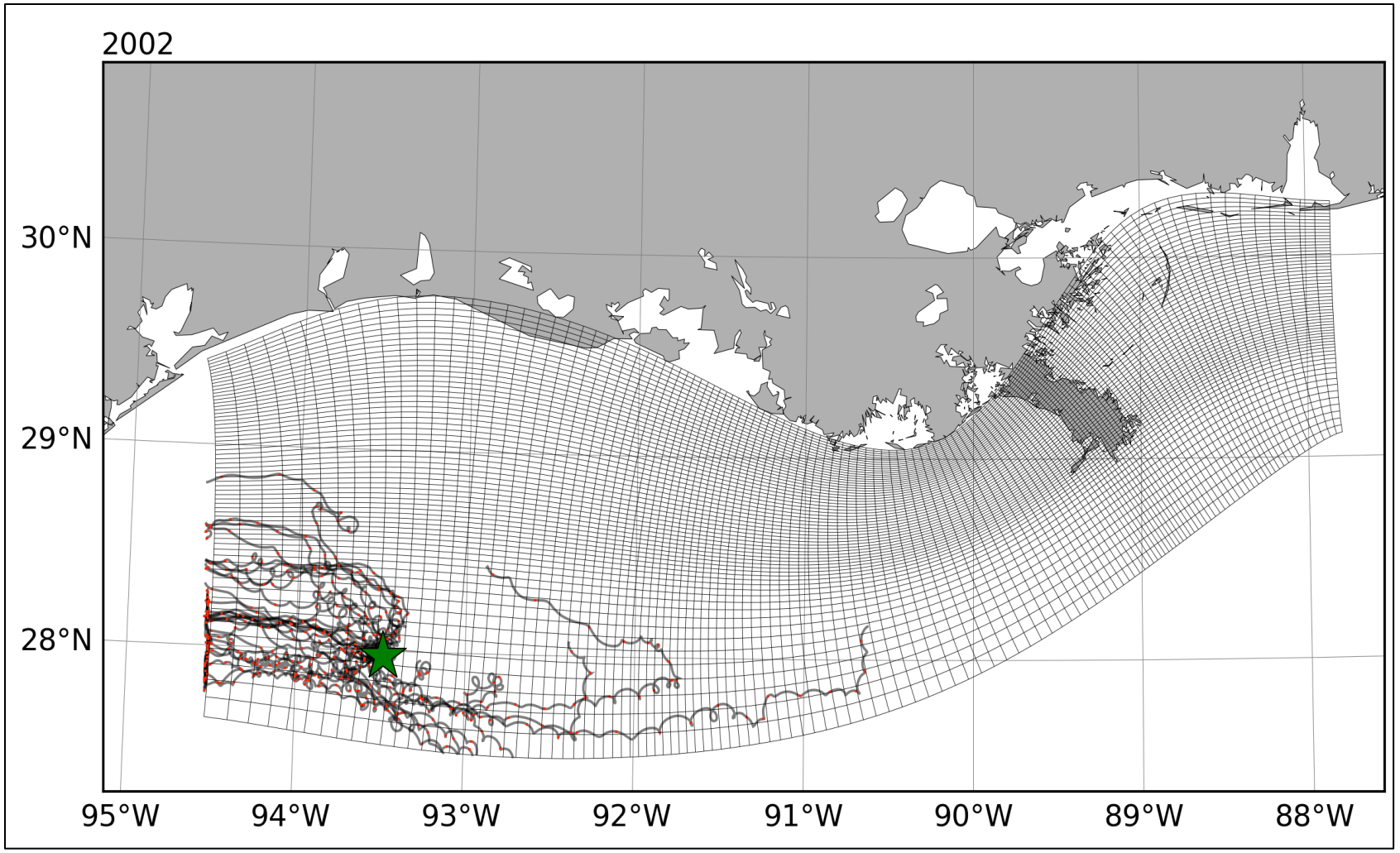

Figure B-10: Numerical drifters are released at a point near the Flower Gardens coral reef system. One drifter is released each day in August 2002, and followed for 30 days. Black lines represent the drifter tracks, with a red mark every day. The release point is marked with a green star.

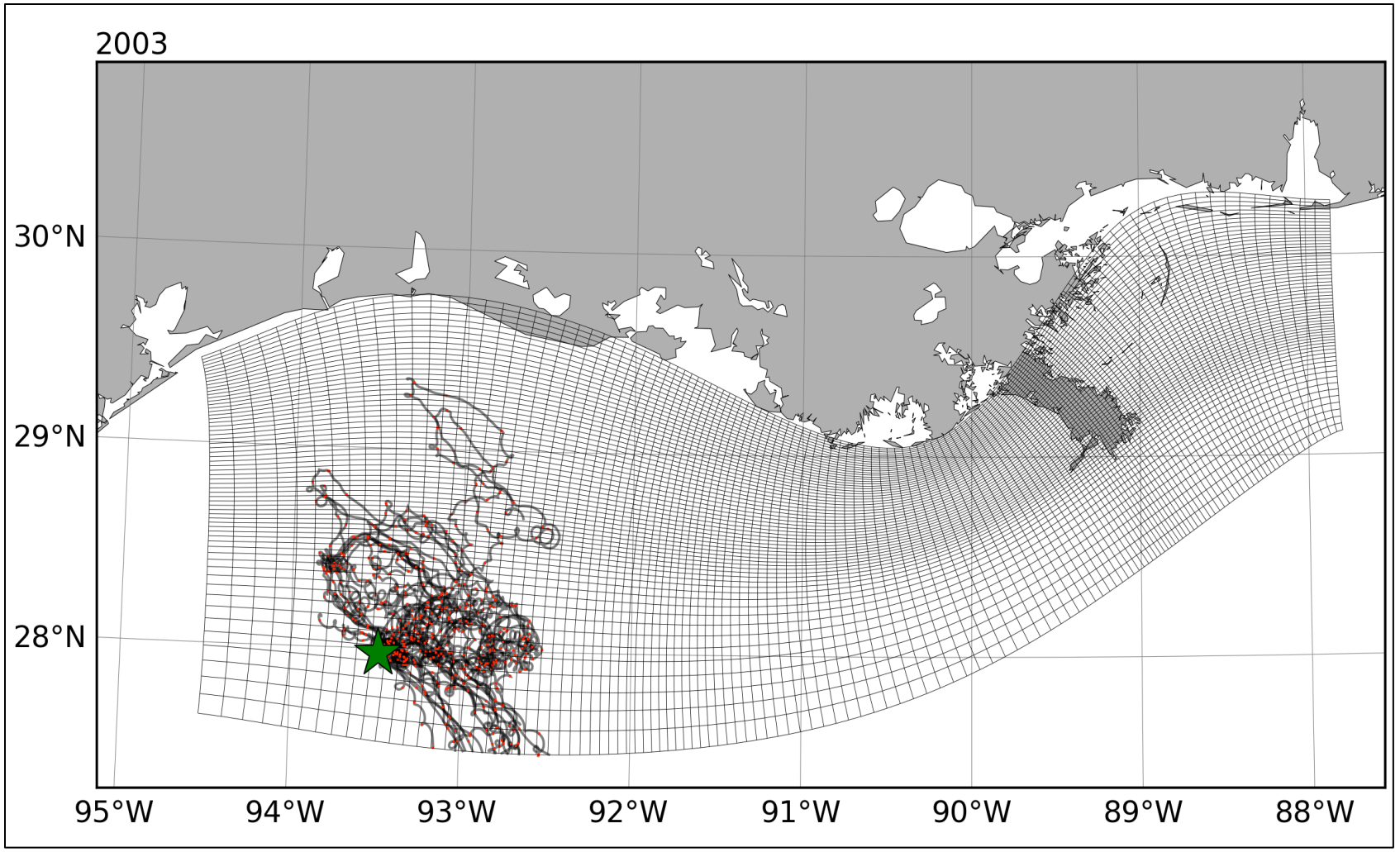

Figure B-11: Numerical drifters are released at a point near the Flower Gardens coral reef system. One drifter is released each day in August 2003, and followed for 30 days. Black lines represent the drifter tracks, with a red mark every day. The release point is marked with a green star.

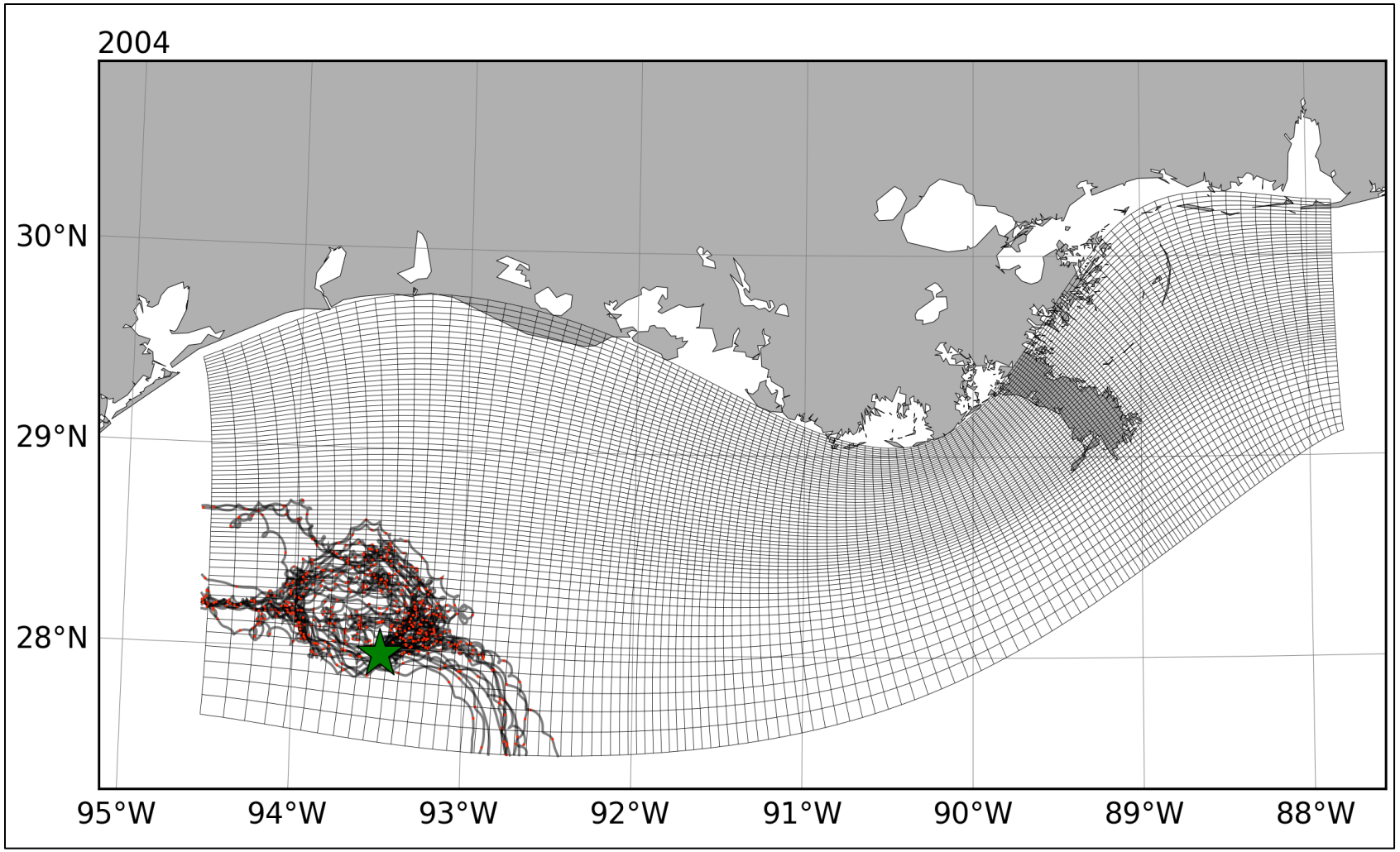

Figure B-12: Numerical drifters are released at a point near the Flower Gardens coral reef system. One drifter is released each day in August 2004, and followed for 30 days. Black lines represent the drifter tracks, with a red mark every day. The release point is marked with a green star.

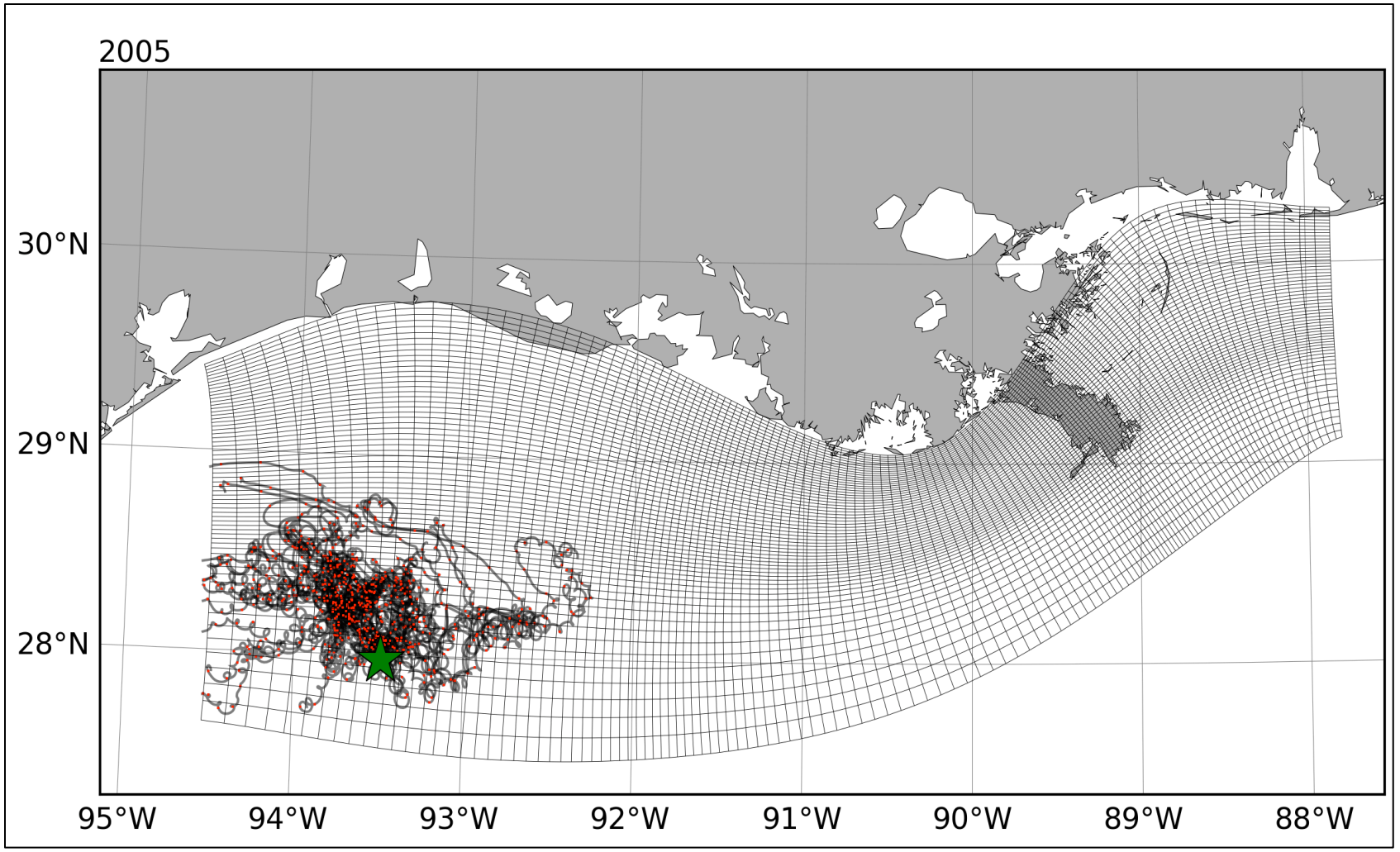

Figure B-13: Numerical drifters are released at a point near the Flower Gardens coral reef system. One drifter is released each day in August 2005, and followed for 30 days. Black lines represent the drifter tracks, with a red mark every day. The release point is marked with a green star.

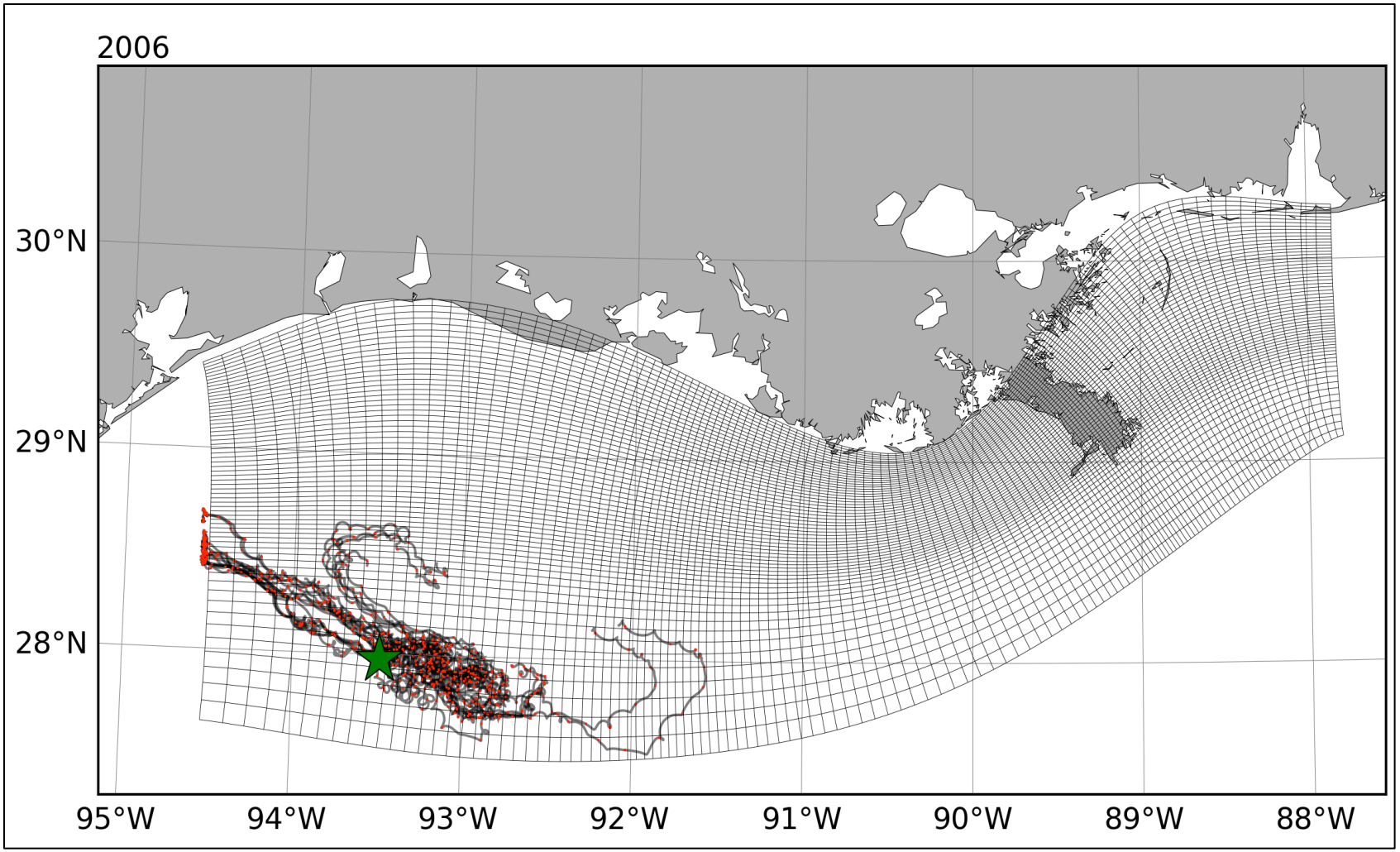

Figure B-14: Numerical drifters are released at a point near the Flower Gardens coral reef system. One drifter is released each day in August 2006, and followed for 30 days. Black lines represent the drifter tracks, with a red mark every day. The release point is marked with a green star.

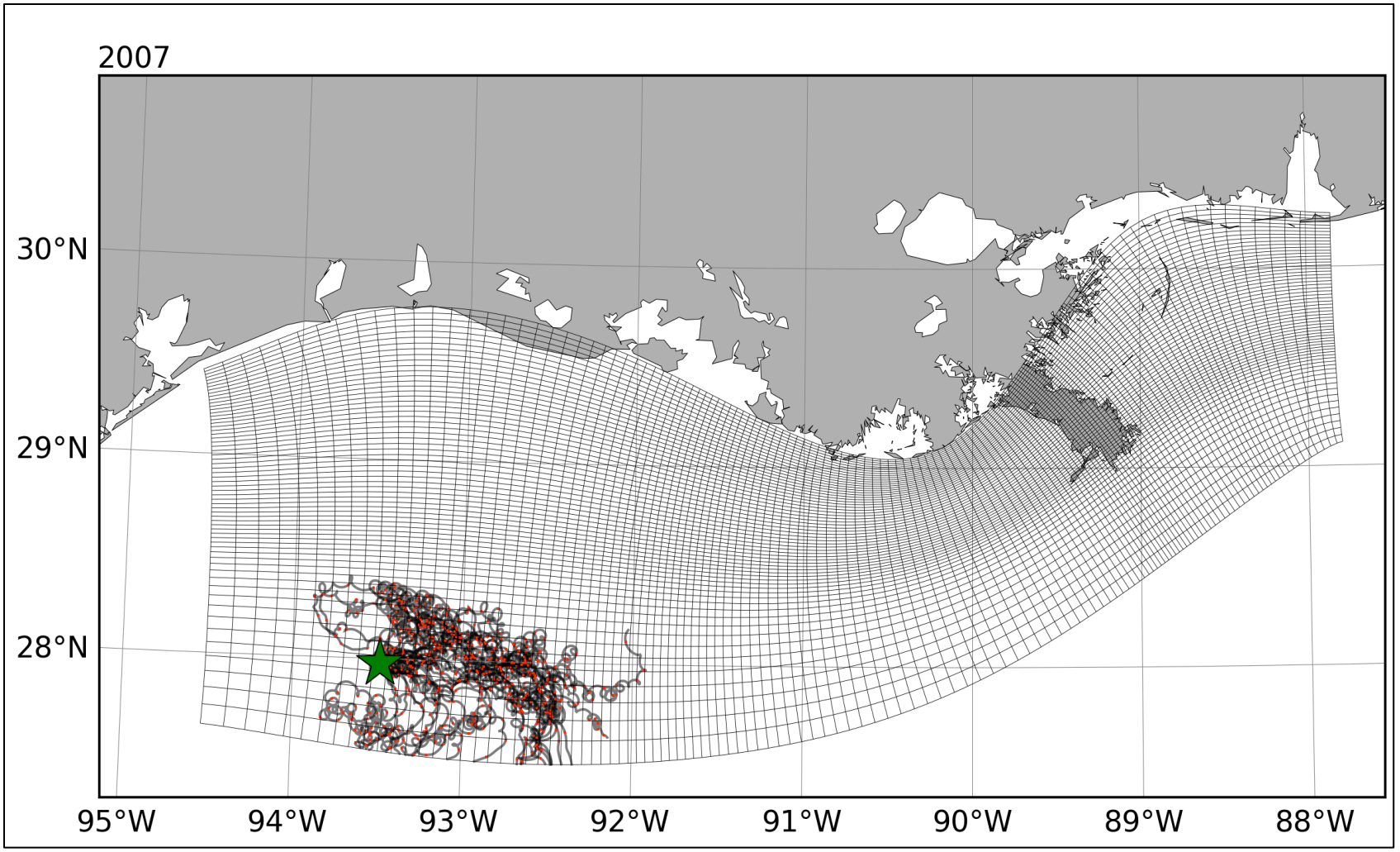

Figure B-15: Numerical drifters are released at a point near the Flower Gardens coral reef system. One drifter is released each day in August 2007, and followed for 30 days. Black lines represent the drifter tracks, with a red mark every day. The release point is marked with a green star.

APPENDIX C

Averaged monthly depth integrated suspended sediment is shown for each month in the physical/sediment transport simulation years. The surface (blue) and bottom (red) 33 psu isohaline is shown for reference, and comparison to the figures shown in Appendix D. These results demonstrate that the suspended sediment is primarily confined to within the boundaries of the Mississippi/Atchafalaya river plume system, although there is evidence for some significant suspended sediment further offshore of the Mississippi River Delta.

1993

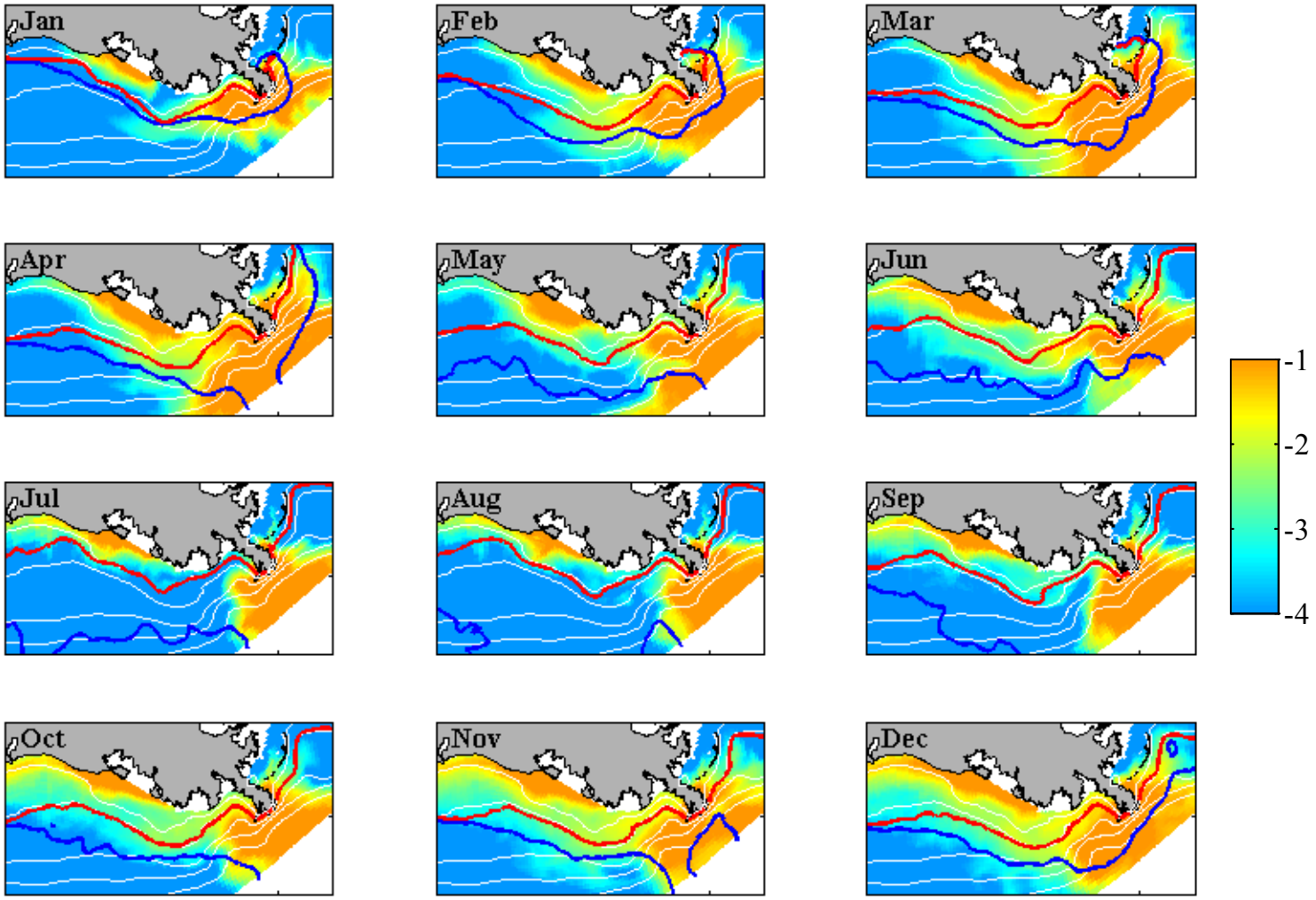

Figure C-1: Time-averaged and depth-integrated fluvial suspended sediment (kg/m^2 in log scale) in the water column calculated for each month of the year 1993. White isobaths drawn at 10, 20, 50, 100, 300 m water depths. Surface (blue) and bottom (red) isohalines are at 33 ppt.

2004

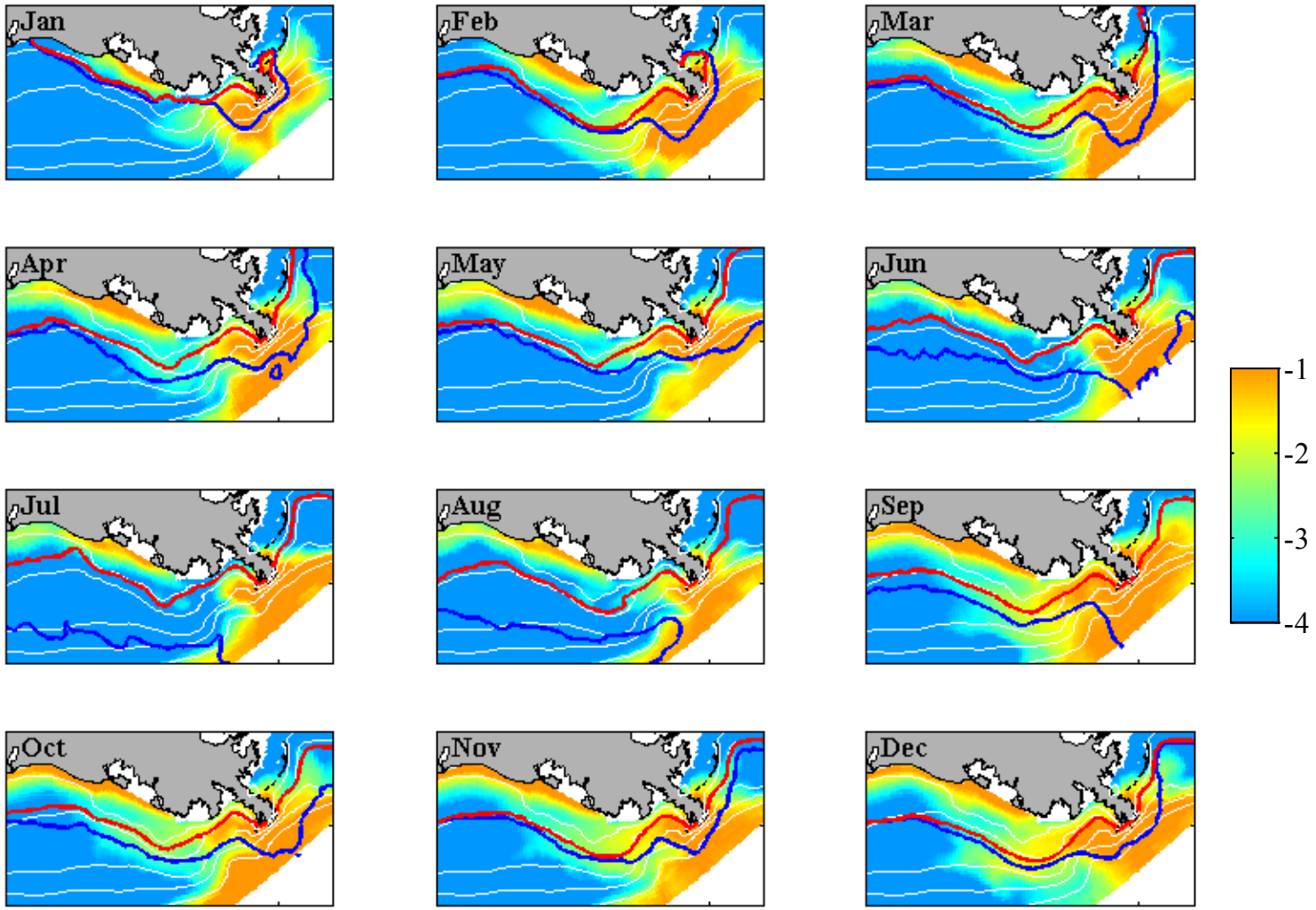

Figure C-2: Time-averaged and depth-integrated fluvial suspended sediment (kg/m^2 in log scale) in the water column calculated for each month of the year 2004. White isobaths drawn at 10, 20, 50, 100, 300 m water depths. Surface (blue) and bottom (red) isohalines are at 33 ppt.

2005

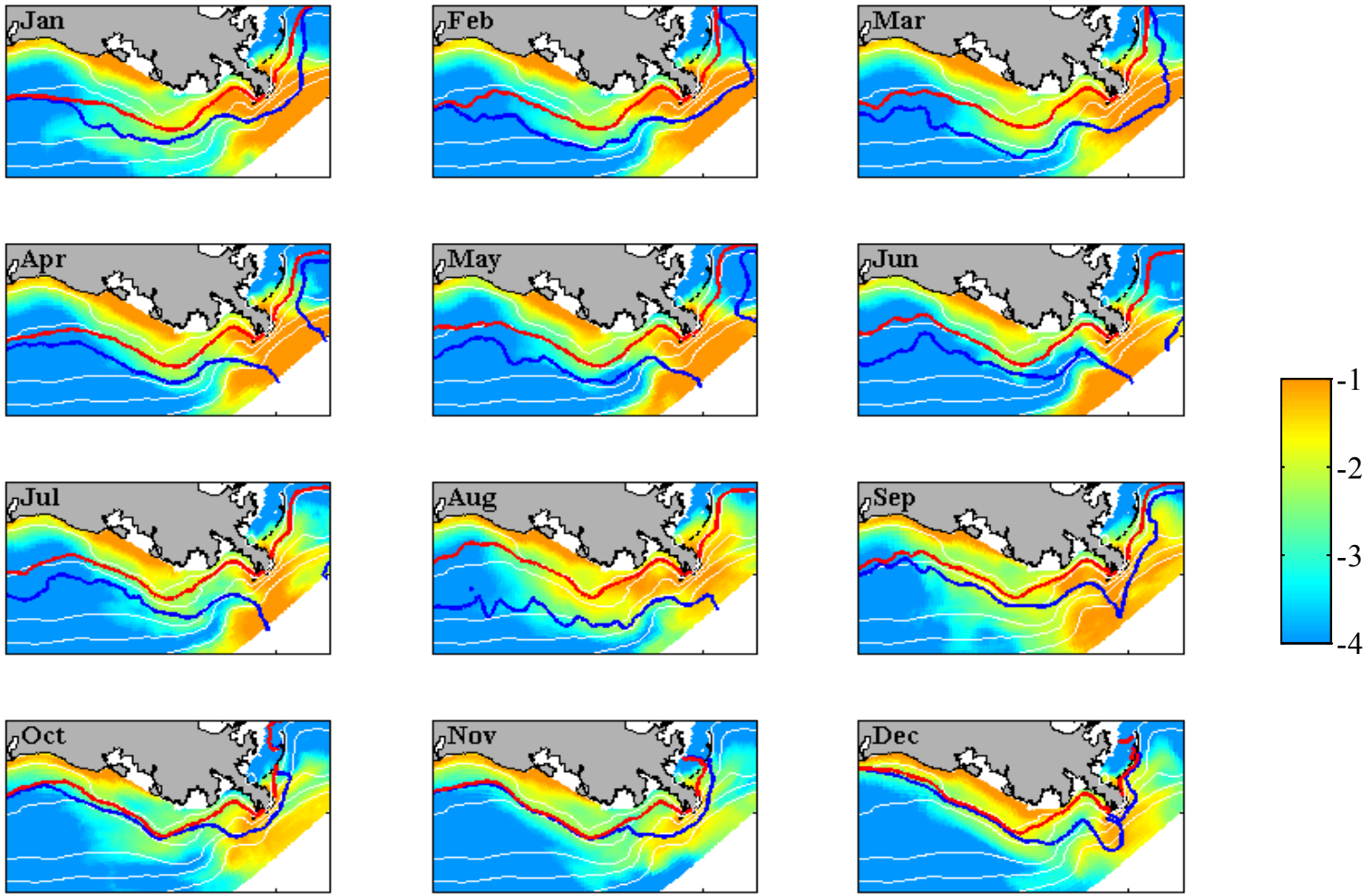

Figure C-3: Time-averaged and depth-integrated fluvial suspended sediment (kg/m^2 in log scale) in the water column calculated for each month of the year 2005. White isobaths drawn at 10, 20, 50, 100, 300 m water depths. Surface (blue) and bottom (red) isohalines are at 33 ppt.

APPENDIX D

Contours of the intersection of the 33.0 psu isohaline with the sea surface and sea floor are shown in a series of figures, for the years 1992 through 2007; the 33.0 psu isohaline is as an *ad hoc* definition of the edge of the Mississippi/Atchafalaya plume influence. Each figure is divided into 12 panels for each month, and the surface and bottom contour of the 33.0 psu isohaline are shown for every four hours (the time interval at which the model results were saved) during that month, creating a cloud of lines that mark the region visited by the 33.0 psu isohaline. Some notable features include the steadiness of the bottom contour, the persistence of eddies (roughly 50 km in size) in the surface contour, and a marked interannual variability during wet (e.g., 2003) and dry (e.g., 2000) years.

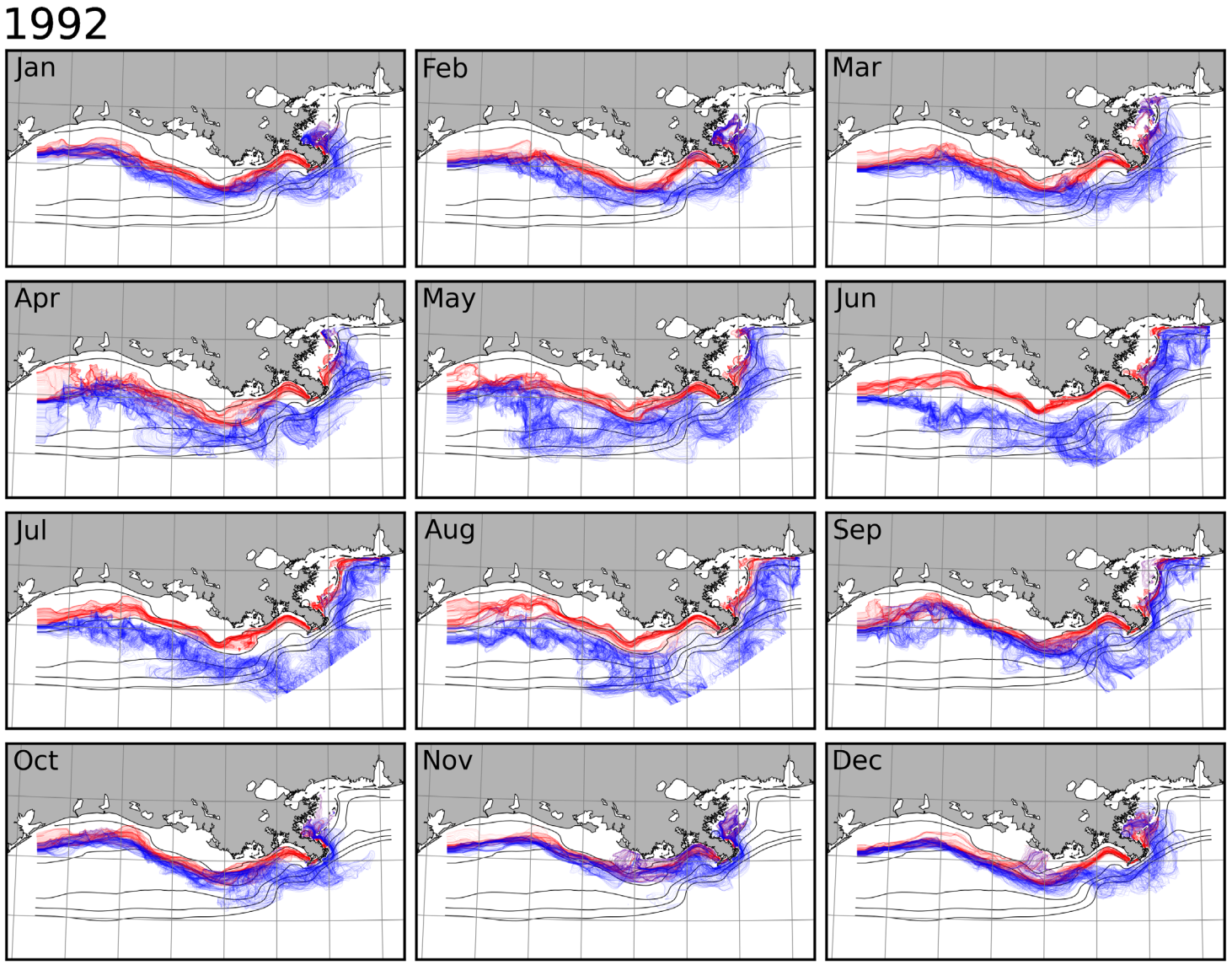

Figure D-1: Surface (blue) and bottom (red) contours of the 33 psu isohaline displayed at four hour intervals for each month in 1992.

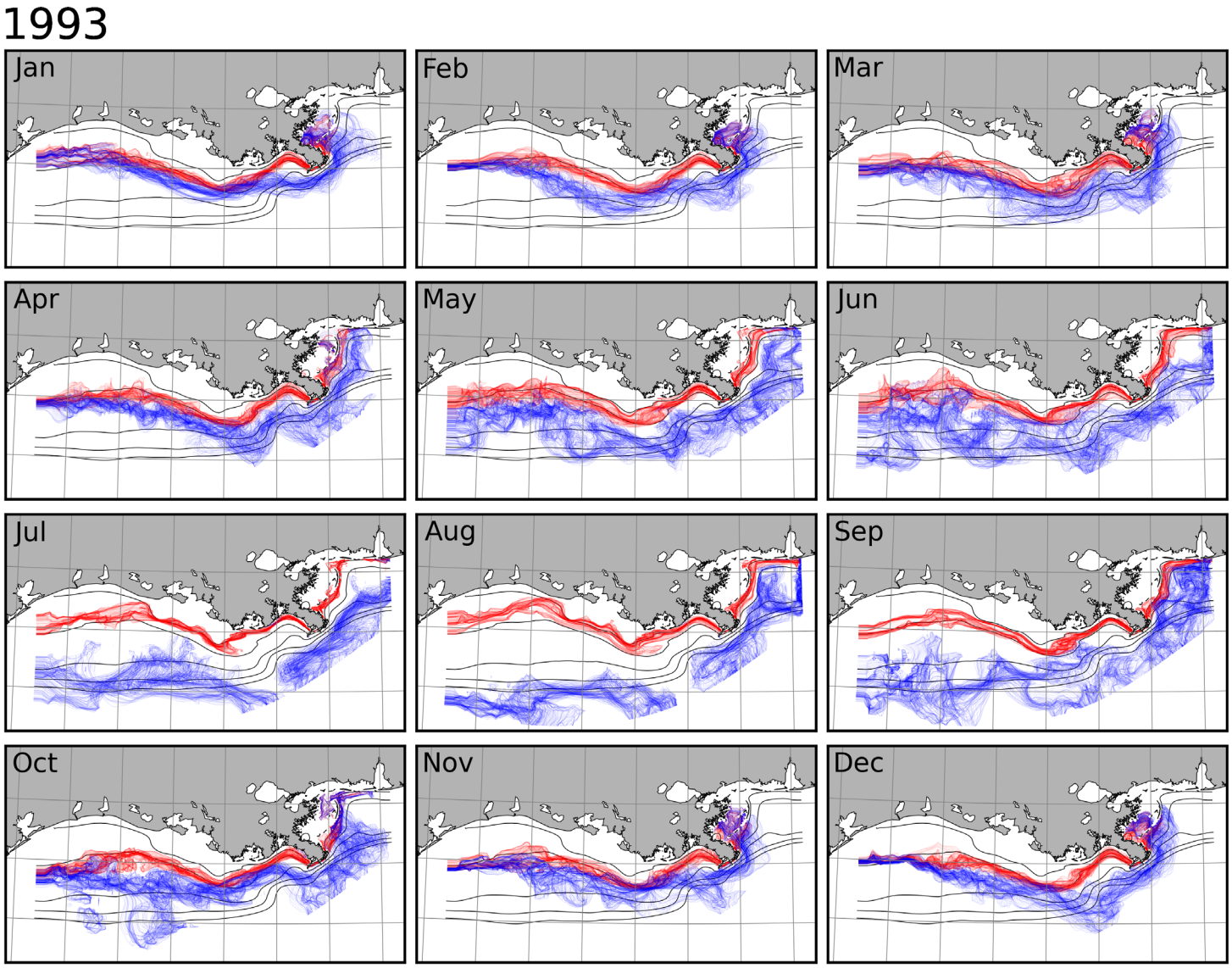

Figure D-2: Surface (blue) and bottom (red) contours of the 33 psu isohaline displayed at four hour intervals for each month in 1993.

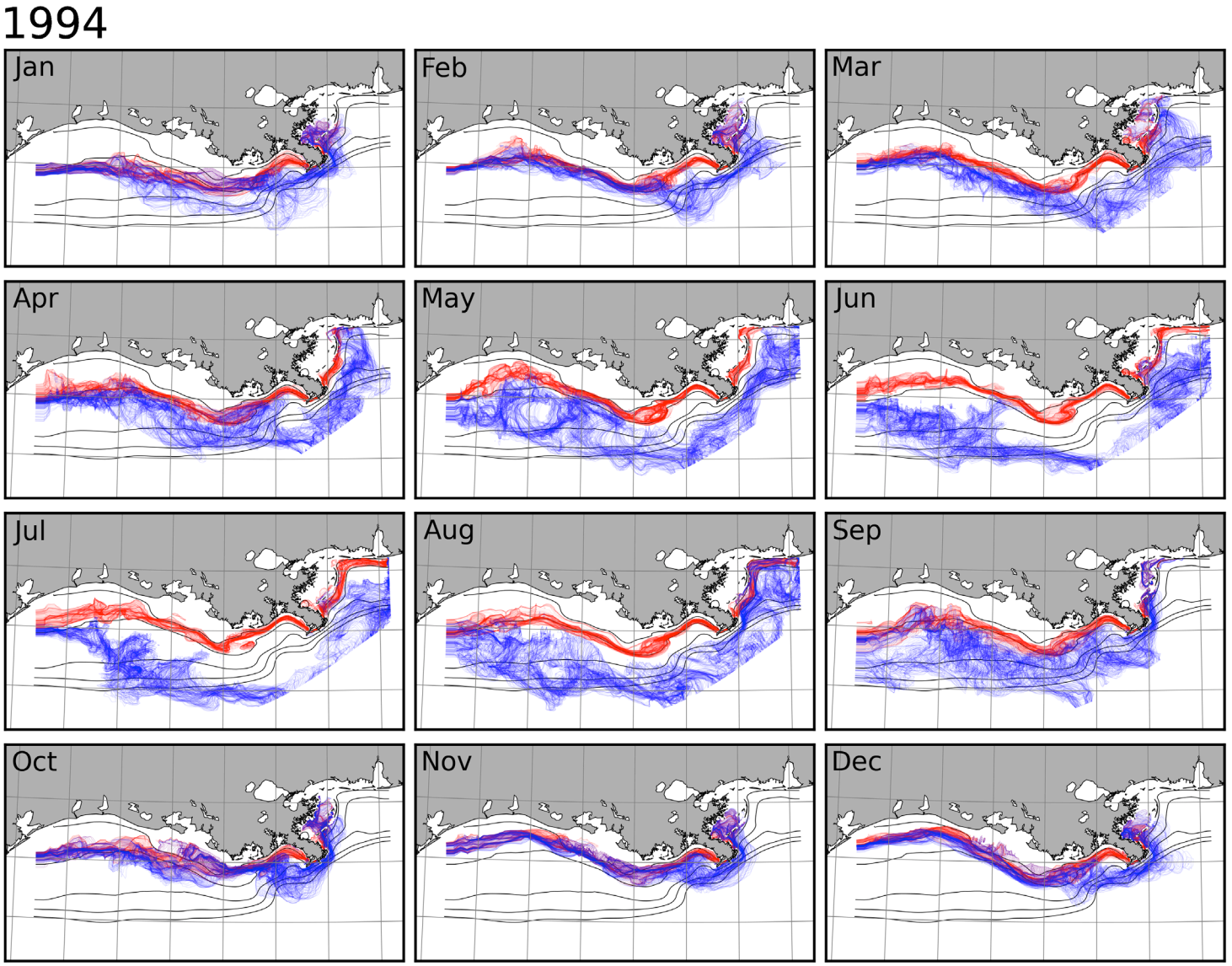

Figure D-3: Surface (blue) and bottom (red) contours of the 33 psu isohaline displayed at four hour intervals for each month in 1994.

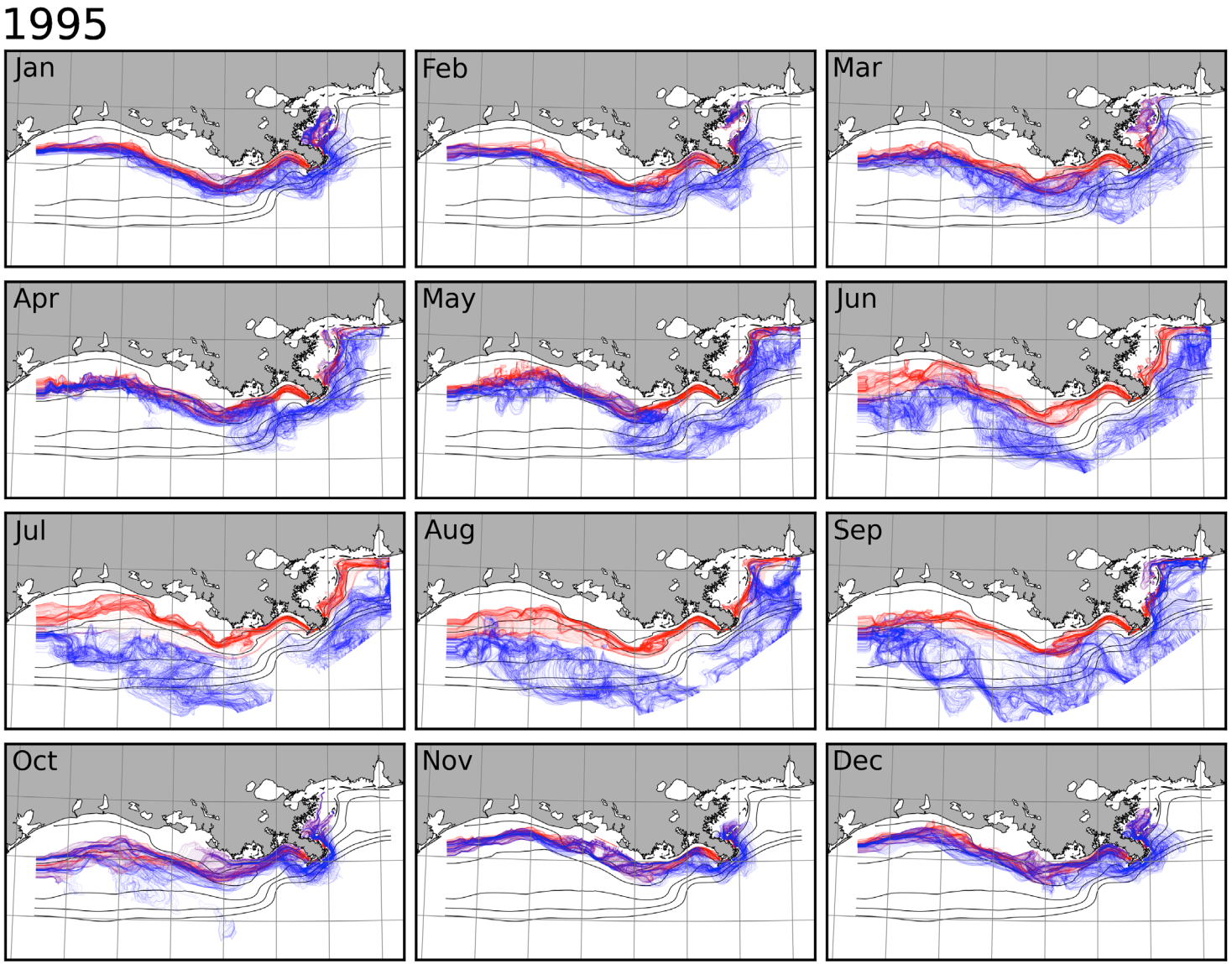

Figure D-4: Surface (blue) and bottom (red) contours of the 33 psu isohaline displayed at four hour intervals for each month in 1995.

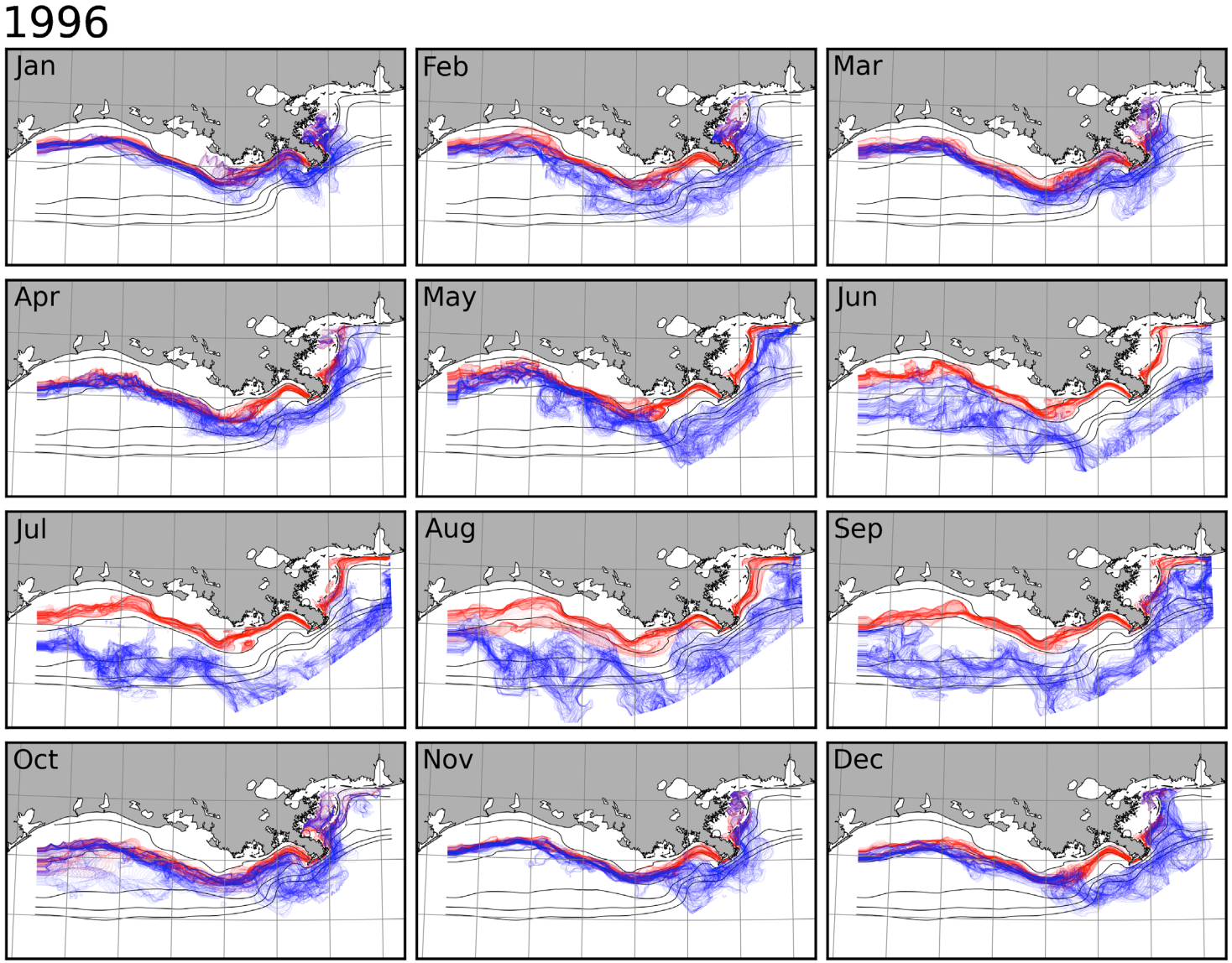

Figure D-5: Surface (blue) and bottom (red) contours of the 33 psu isohaline displayed at four hour intervals for each month in 1996.

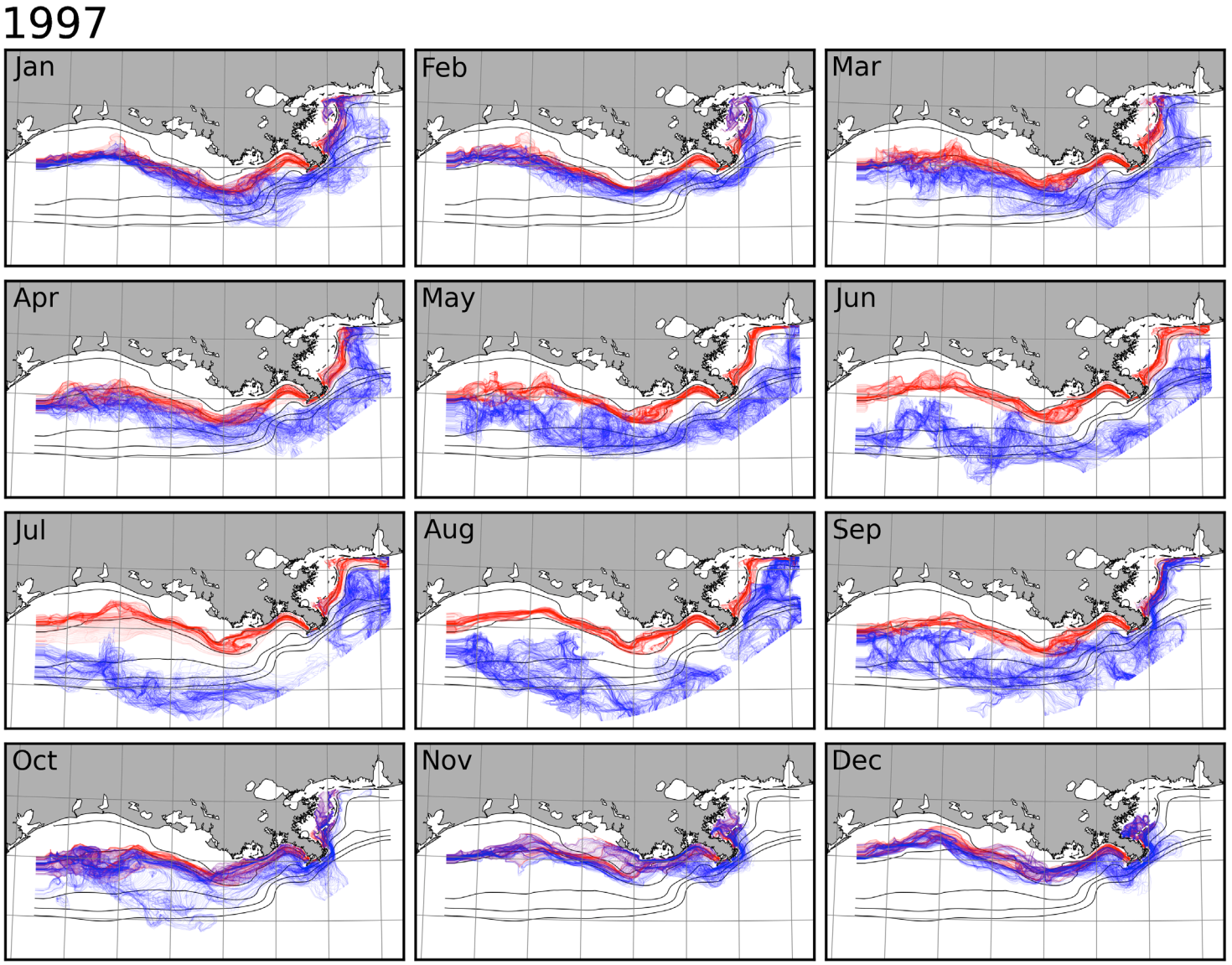

Figure D-6: Surface (blue) and bottom (red) contours of the 33 psu isohaline displayed at four hour intervals for each month in 1997.

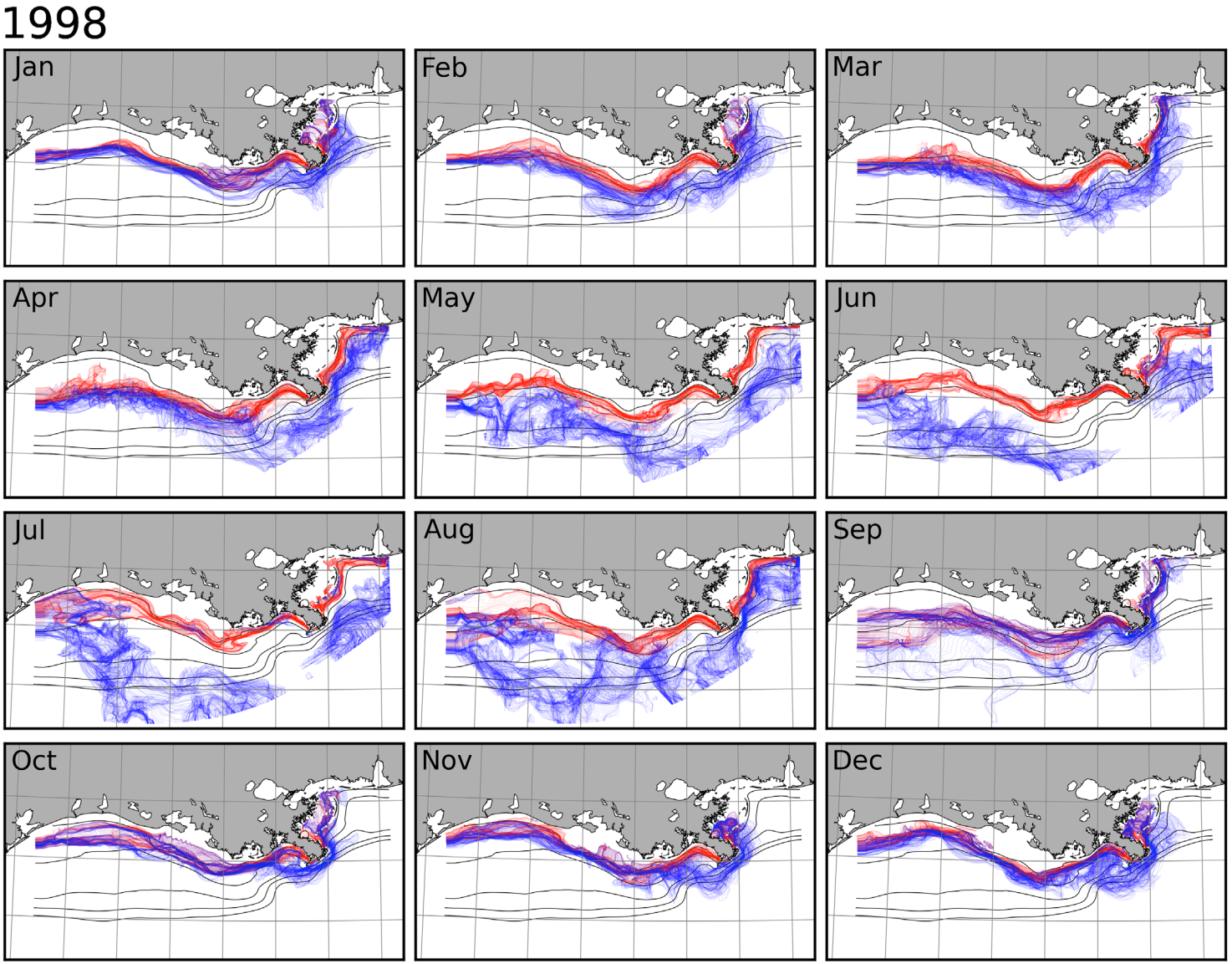

Figure D-7: Surface (blue) and bottom (red) contours of the 33 psu isohaline displayed at four hour intervals for each month in 1998.

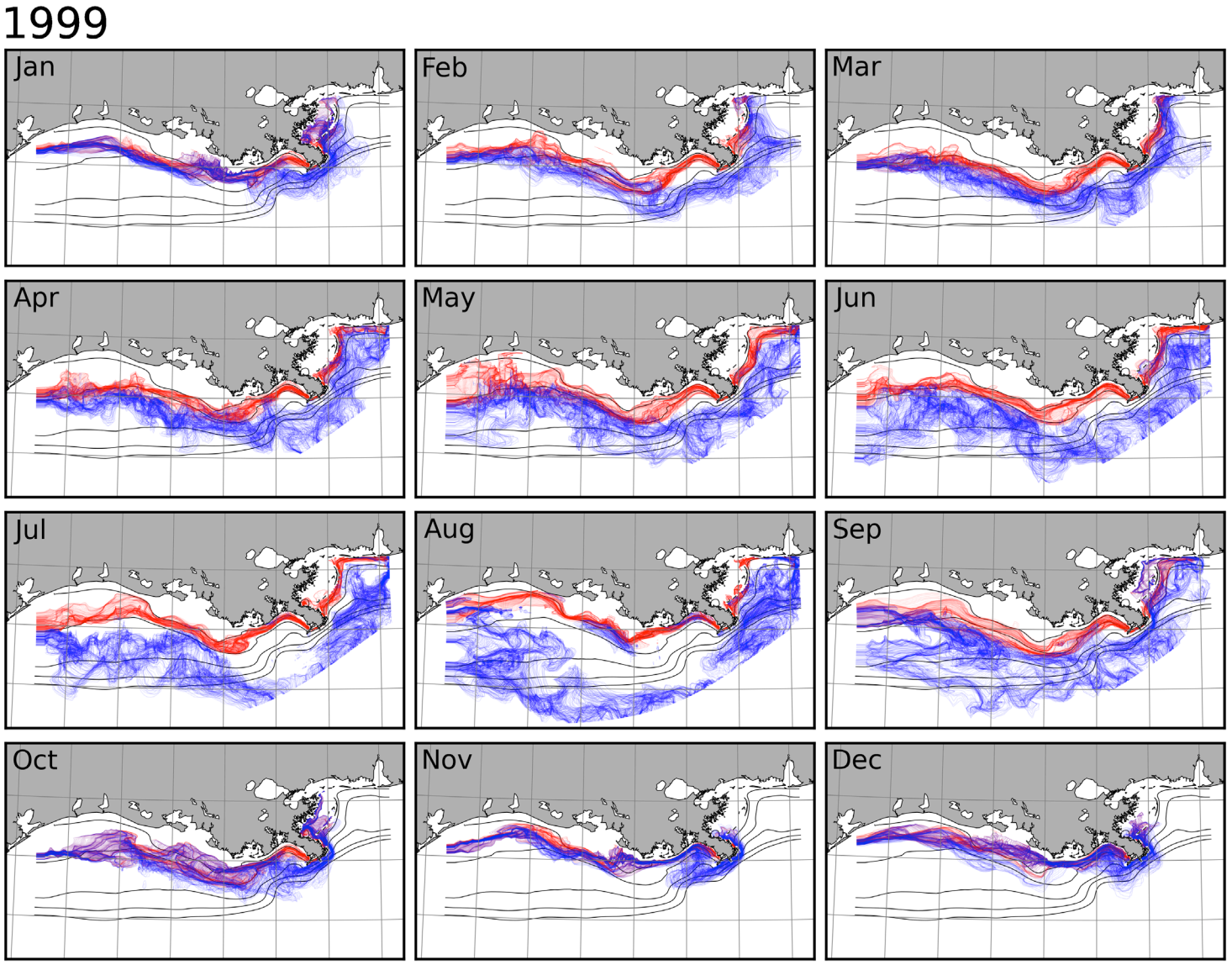

Figure D-8: Surface (blue) and bottom (red) contours of the 33 psu isohaline displayed at four hour intervals for each month in 1999.

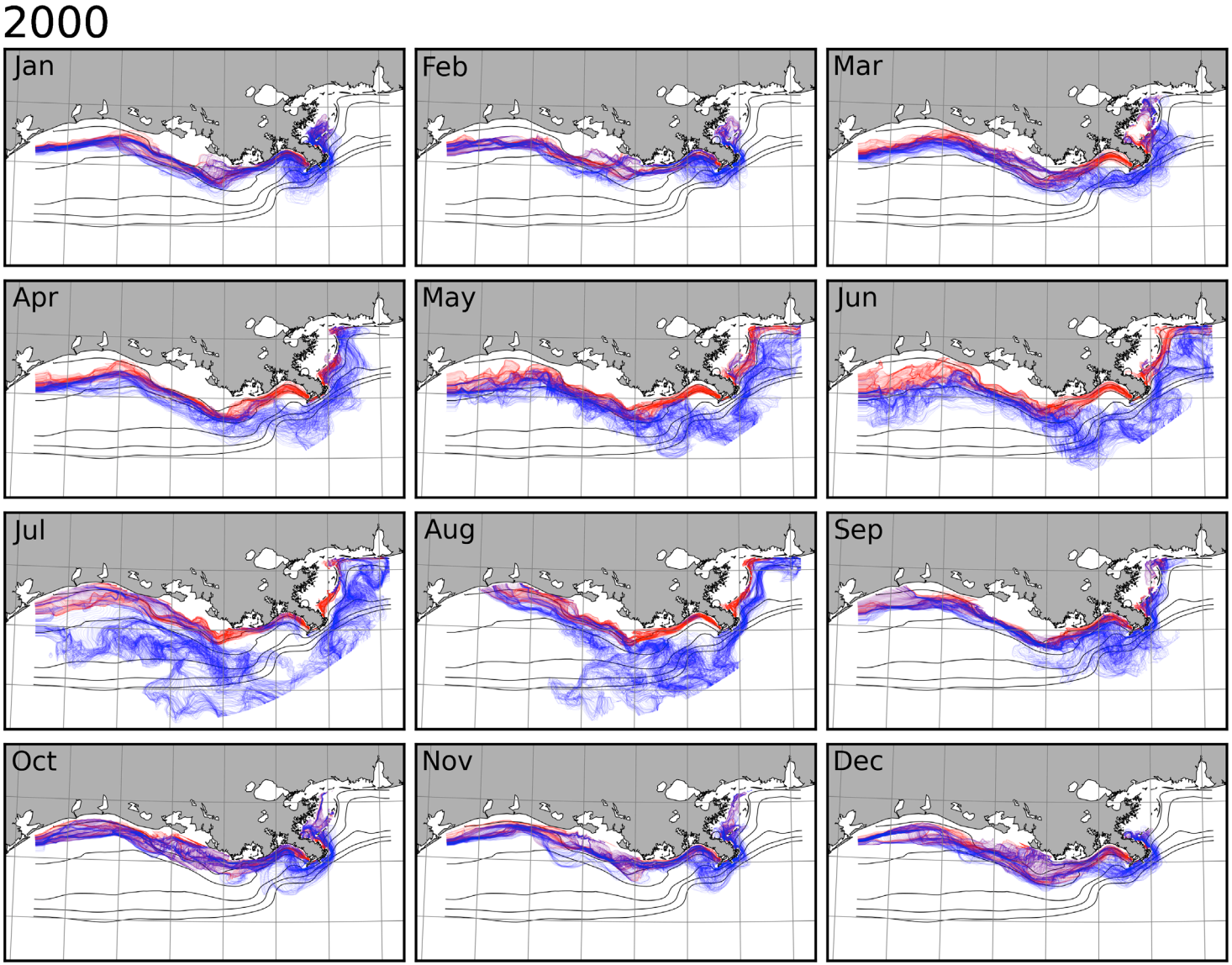

Figure D-9: Surface (blue) and bottom (red) contours of the 33 psu isohaline displayed at four hour intervals for each month in 2000.

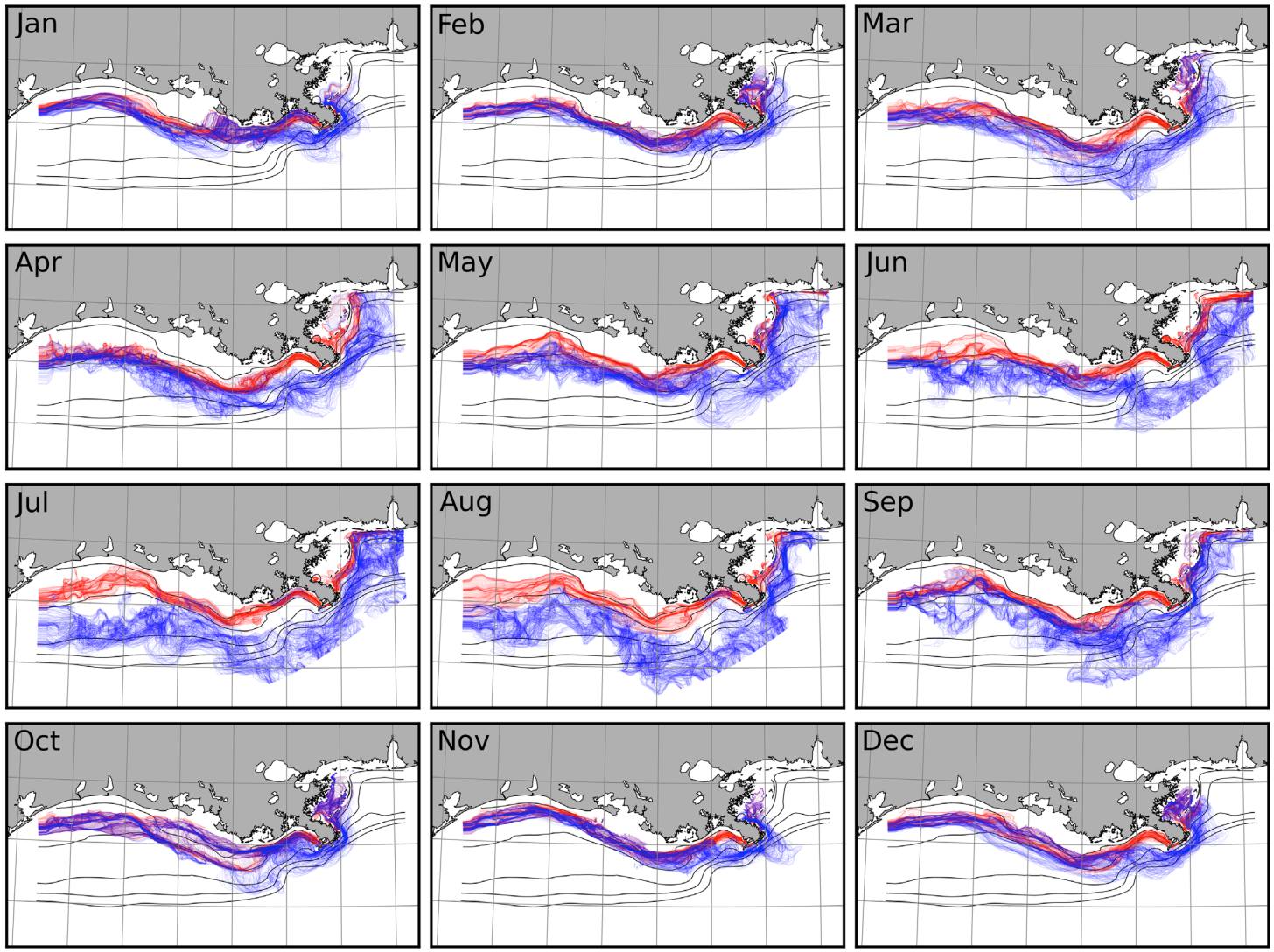

Figure D-10: Surface (blue) and bottom (red) contours of the 33 psu isohaline displayed at four hour intervals for each month in 2001.

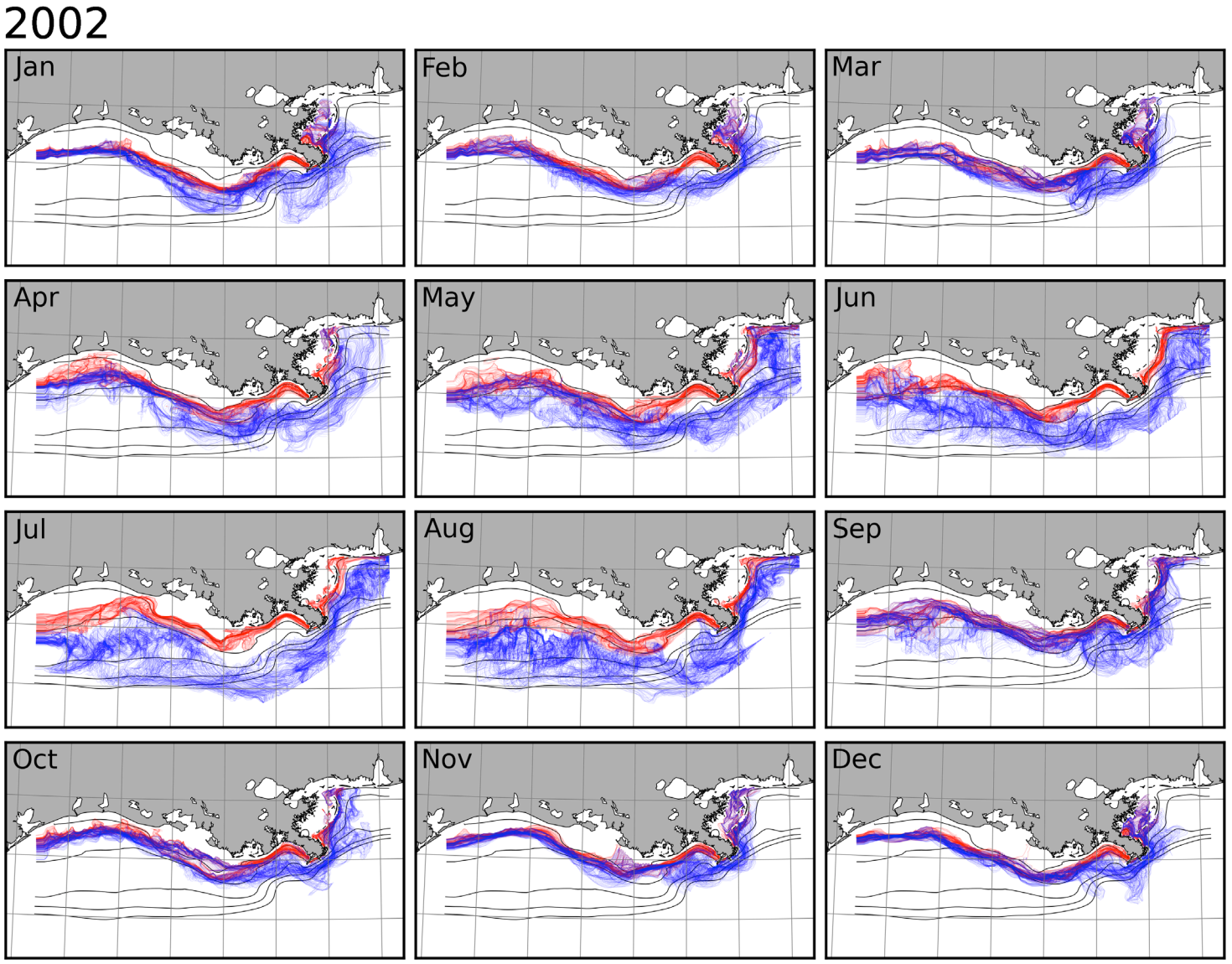

Figure D-11: Surface (blue) and bottom (red) contours of the 33 psu isohaline displayed at four hour intervals for each month in 2002.

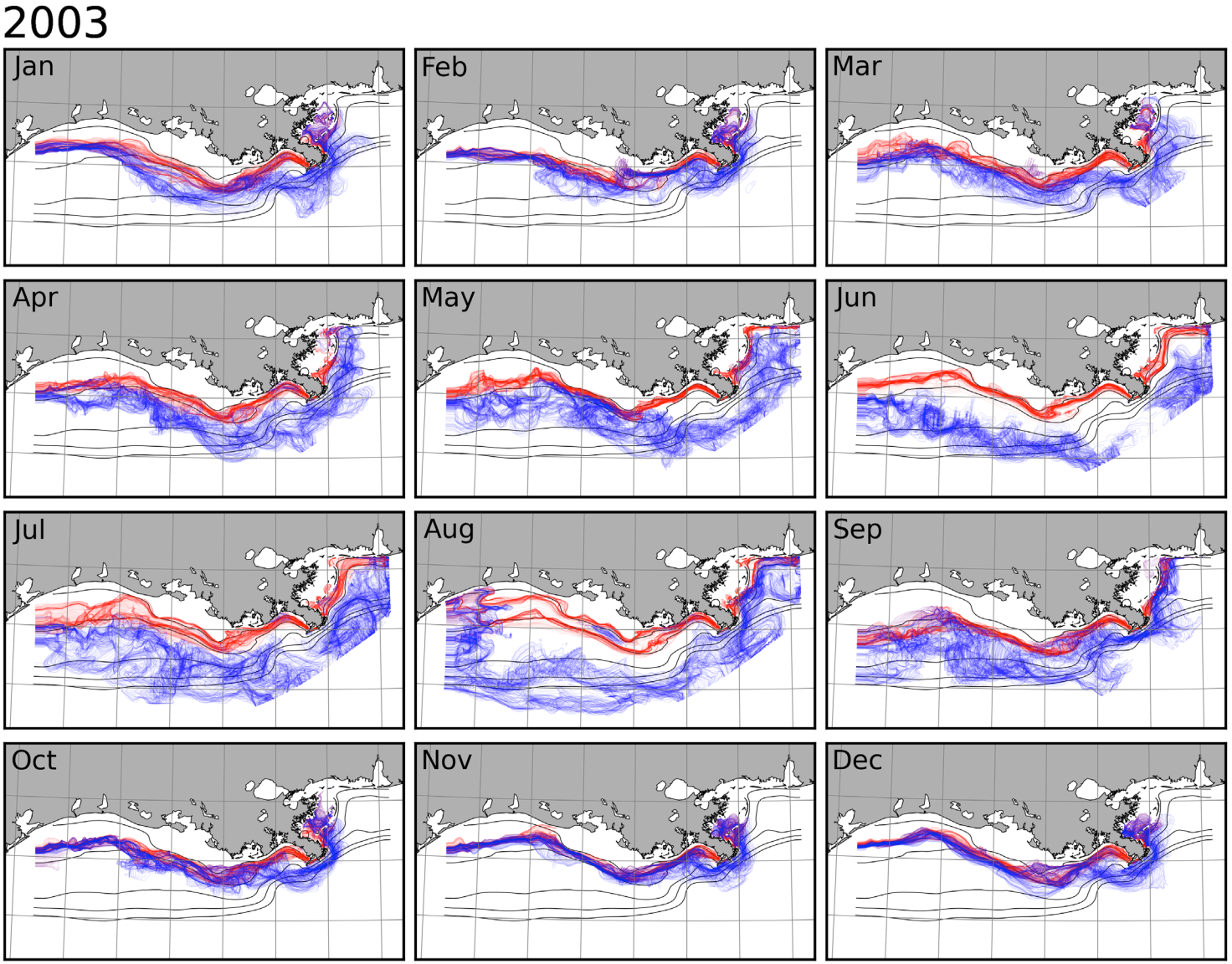

Figure D-12: Surface (blue) and bottom (red) contours of the 33 psu isohaline displayed at four hour intervals for each month in 2003.

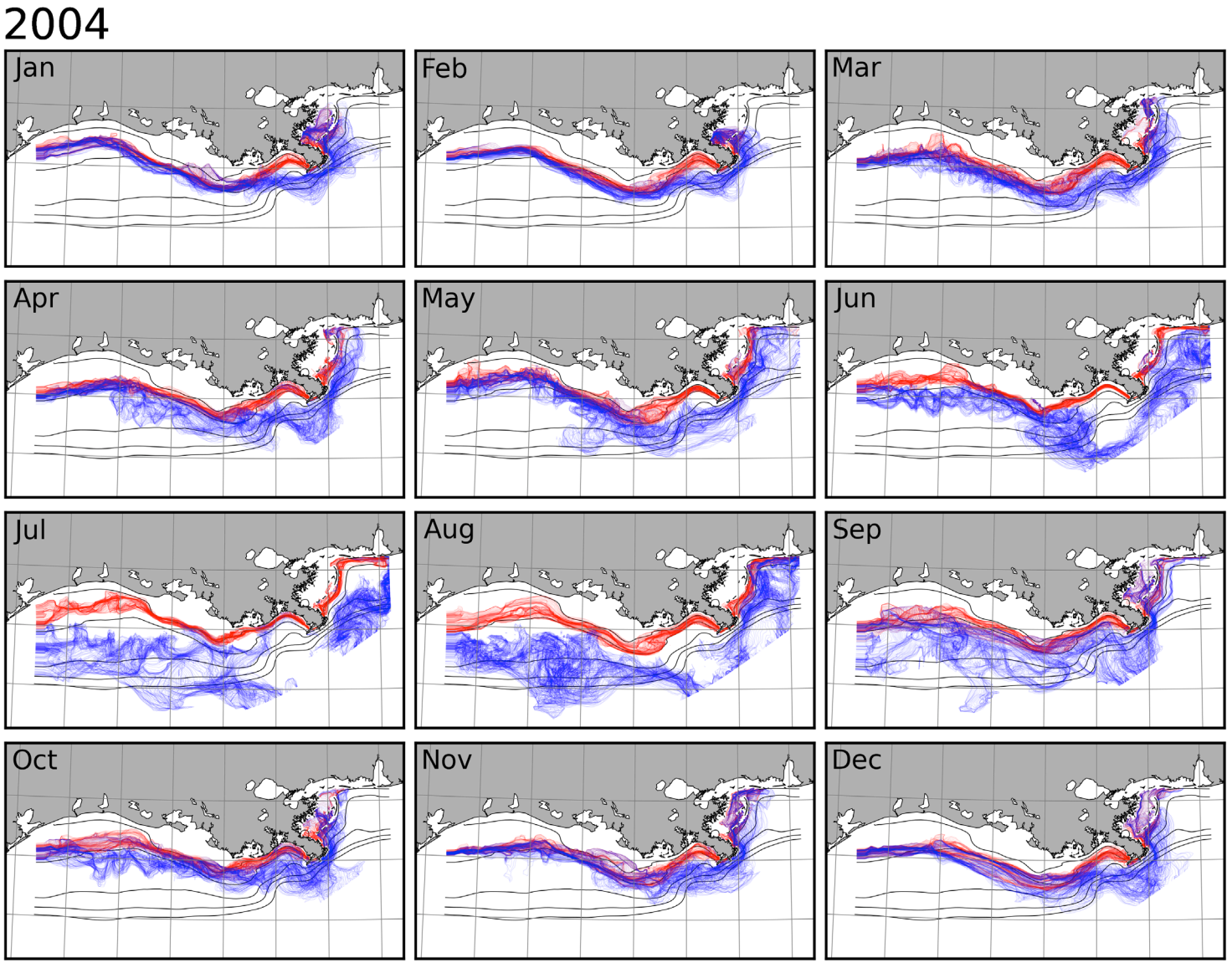

Figure D-13: Surface (blue) and bottom (red) contours of the 33 psu isohaline displayed at four hour intervals for each month in 2004.

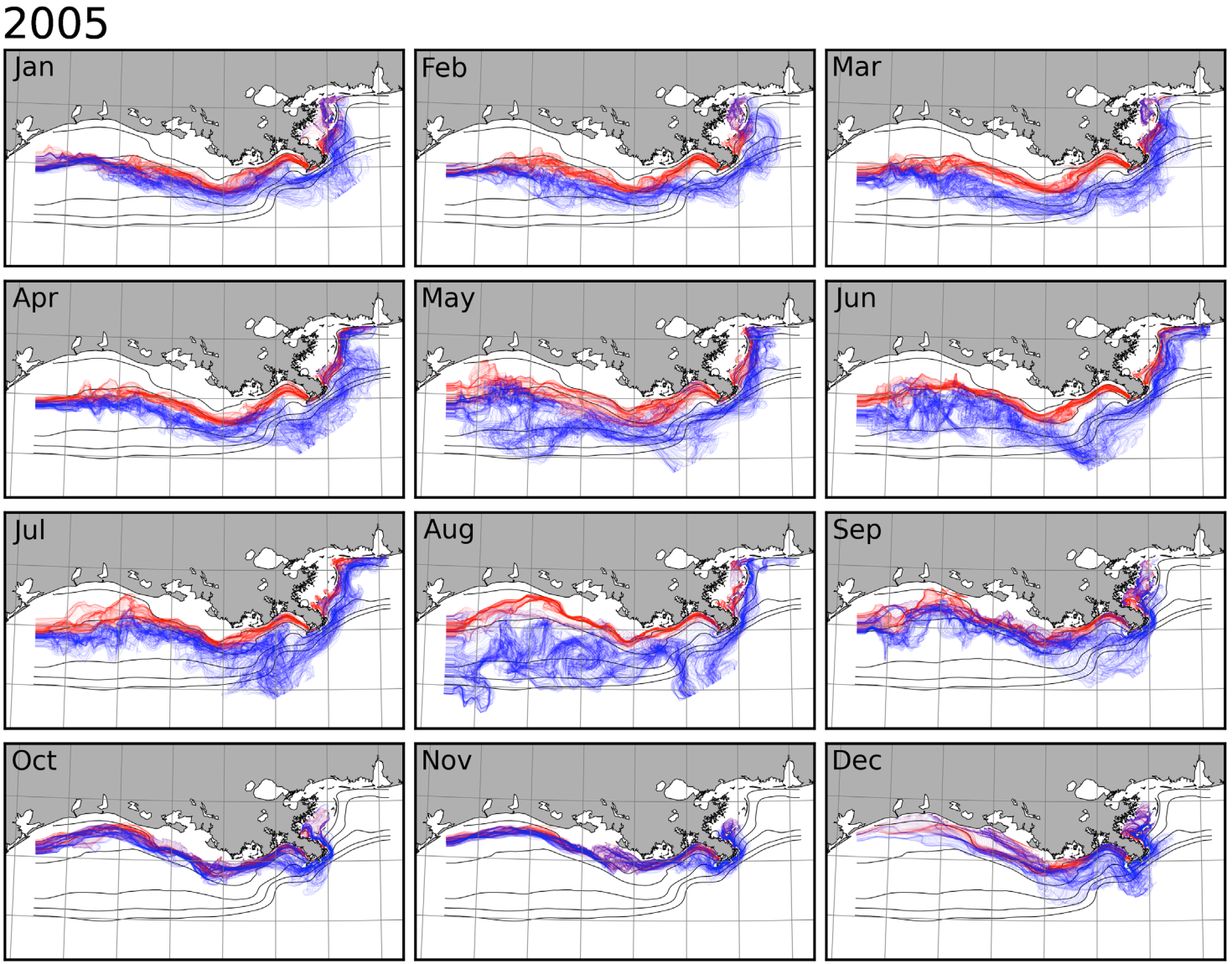

Figure D-14: Surface (blue) and bottom (red) contours of the 33 psu isohaline displayed at four hour intervals for each month in 2005.

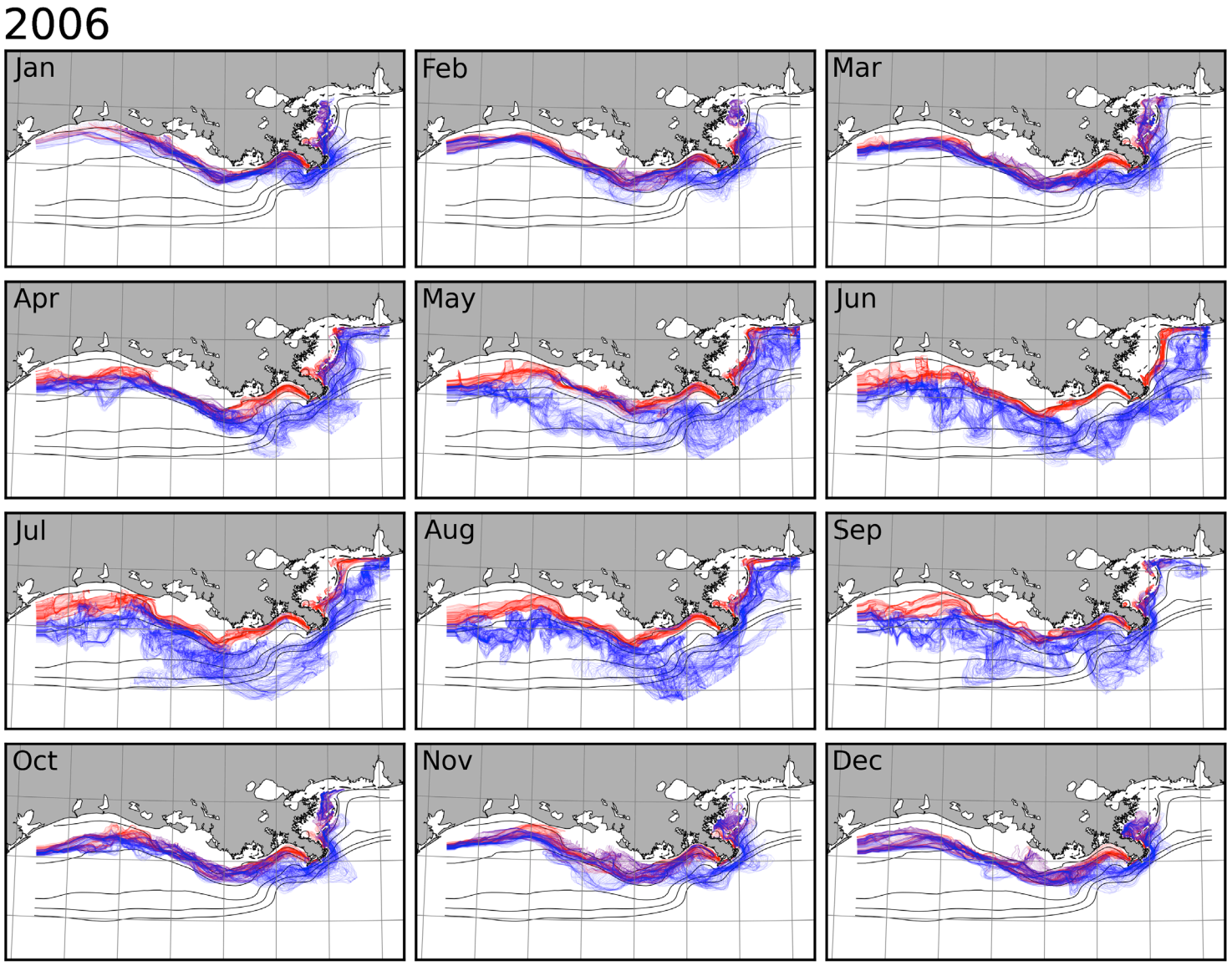

Figure D-15: Surface (blue) and bottom (red) contours of the 33 psu isohaline displayed at four hour intervals for each month in 2006.

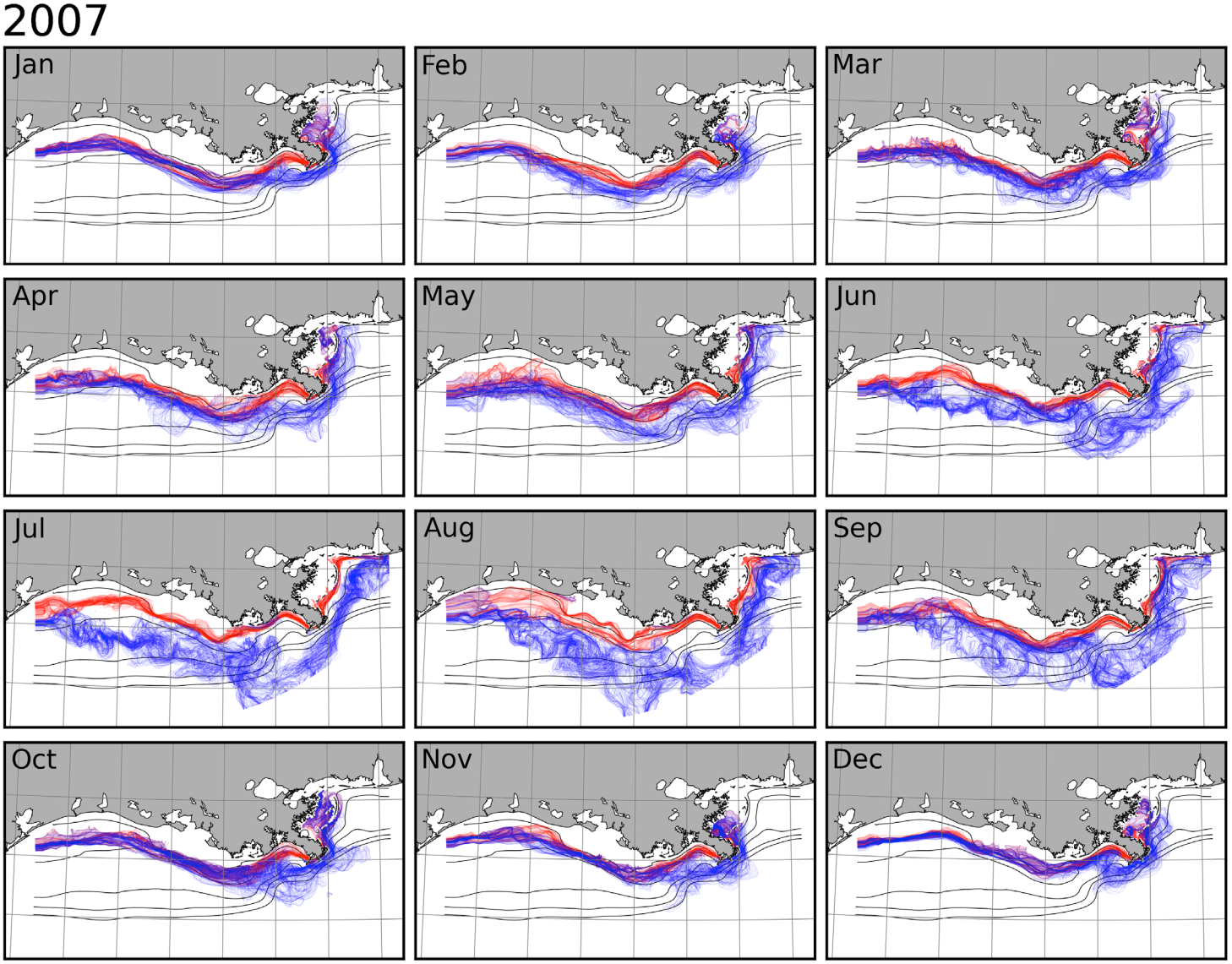

Figure D-16: Surface (blue) and bottom (red) contours of the 33 psu isohaline displayed at four hour intervals for each month in 2007

The Department of the Interior Mission

As the Nation's principal conservation agency, the Department of the Interior has responsibility for most of our nationally owned public lands and natural resources. This includes fostering the sound use of our land and water resources; protecting our fish, wildlife, and biological diversity; preserving the environmental and cultural values of our national parks and historical places; and providing for the enjoyment of life through outdoor recreation. The Department assesses our energy and mineral resources and works to ensure that their development is in the best interests of all our people by encouraging stewardship and citizen participation in their care. The Department also has a major responsibility for American Indian reservation communities and for people who live in island communities.

The Bureau of Ocean Energy Management Mission

The Bureau of Ocean Energy Management (BOEM) promotes energy independence, environmental protection, and economic development through responsible, science-based management of offshore conventional and renewable energy.